SELF-ADAPTIVE *hp* FINITE-ELEMENT SIMULATION OF MULTI-COMPONENT INDUCTION MEASUREMENTS ACQUIRED IN DIPPING, INVADED, AND ANISOTROPIC FORMATIONS

M. J. Nam, D. Pardo, and C. Torres-Verdín,
The University of Texas at Austin

***hp*-FEM team: D. Pardo, M. J. Nam, L. Demkowicz, C. Torres-Verdín,
V. M. Calo, M. Paszynski, and P. J. Matuszik**

Presentation at Korean Institute of Geoscience and Minerals (KIGAM), September 8, 2008.

Overview

1. Main Lines of Research and Applications
   - Previous work
   - Main features of our technology

2. Application 1: Tri-Axial Induction Instruments (M. J. Nam)

3. Application 2: Dual-Laterolog Instruments (M. J. Nam)

4. Multi-Physics Inversion (D. Pardo)

5. Sonic Instruments (L. Demkowicz)

Outline

- Introduction to Tri-Axial Induction
- Method
- Numerical Results:
  - Verification of 3D Method for Tri-Axial Induction Tool
  - Dipping, Invaded, Anisotropic Formations
- Conclusions

Tri-Axial Induction Tool

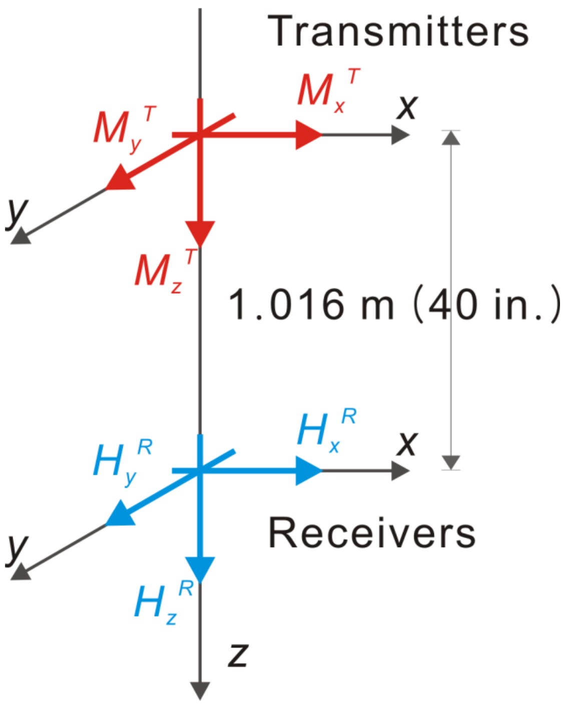

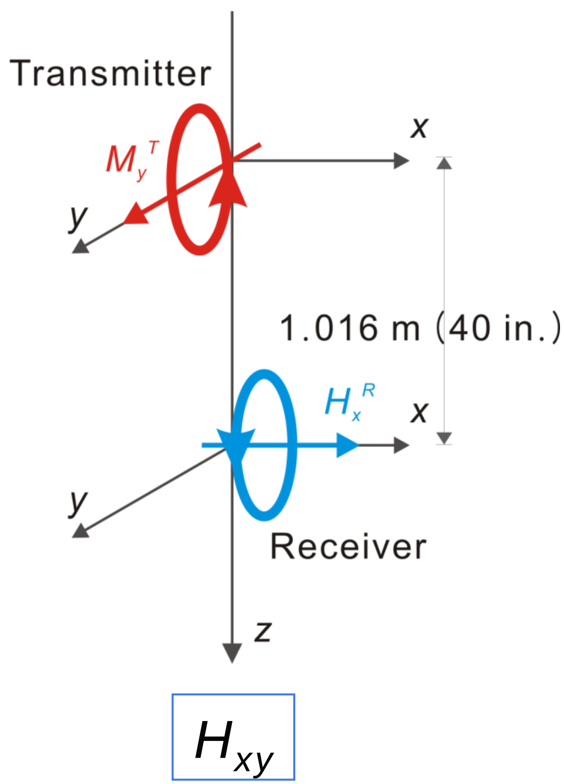

L = 1.016 m (40 In.)

Operating frequency: 20 kHz

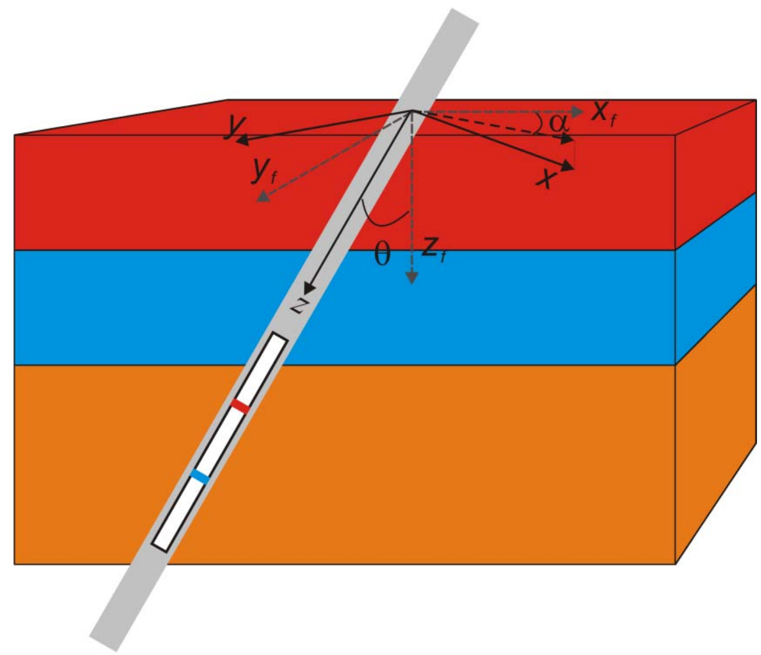

θ: dip angle

α: tool orientation angle

3D Source Implementation

1. Solenoidal Coil (J_ϕ) for M_z

→ ***becoming a 2D source in (ρ, ϕ, z)***

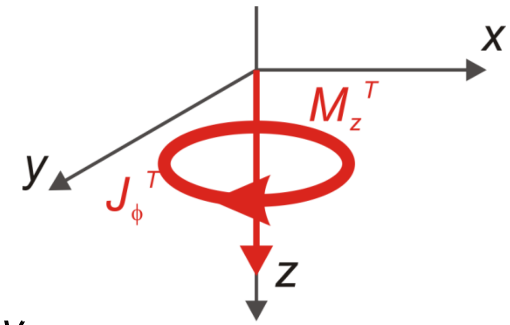

2. Delta Function for 3D source M_x or M_y

$$f(\phi) = \delta(\phi - \phi_0)$$

ϕ_0: the position of the center of the peak (0° for M_x; 90° for M_y)

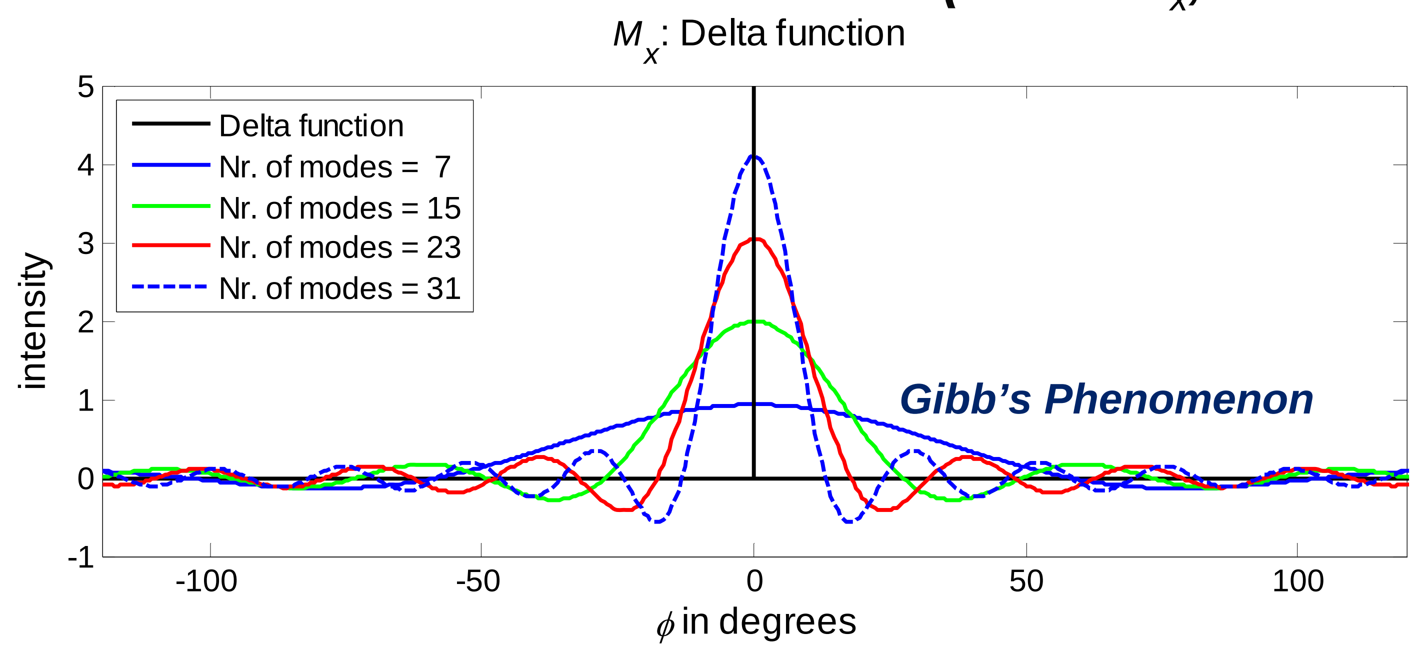

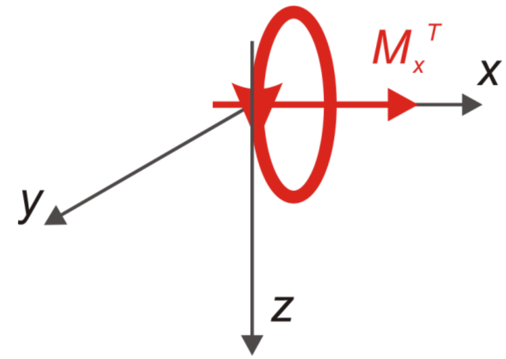

3D Source and Receiver (Delta Functions)

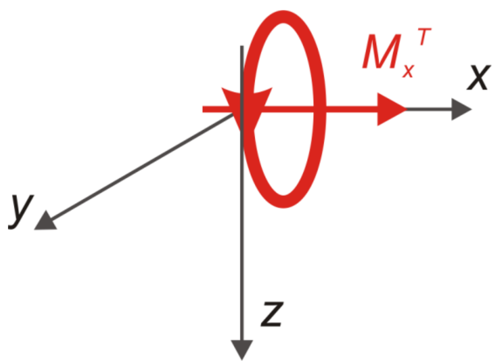

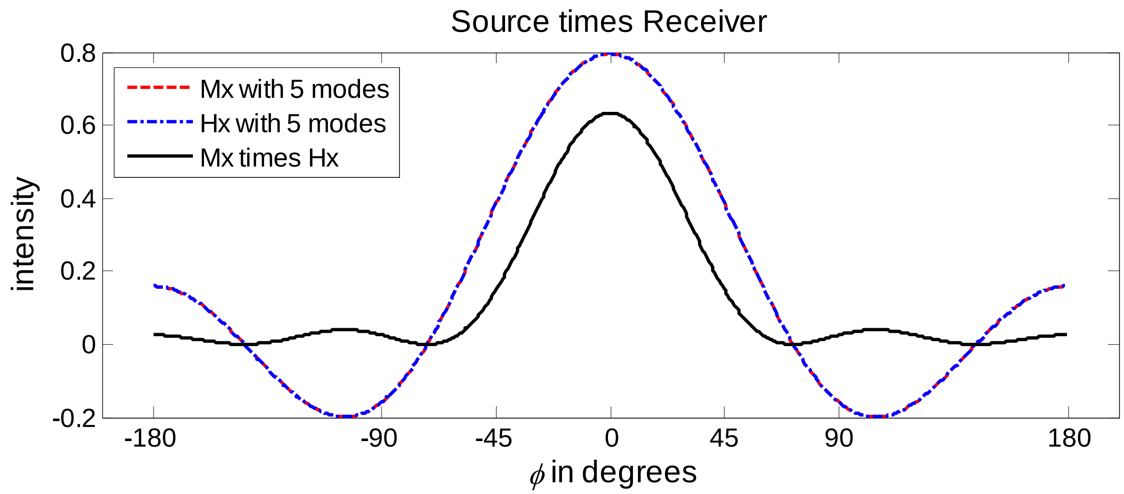

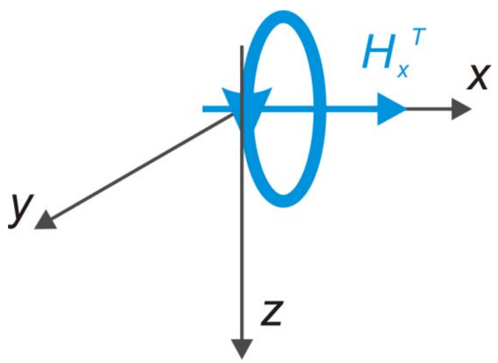

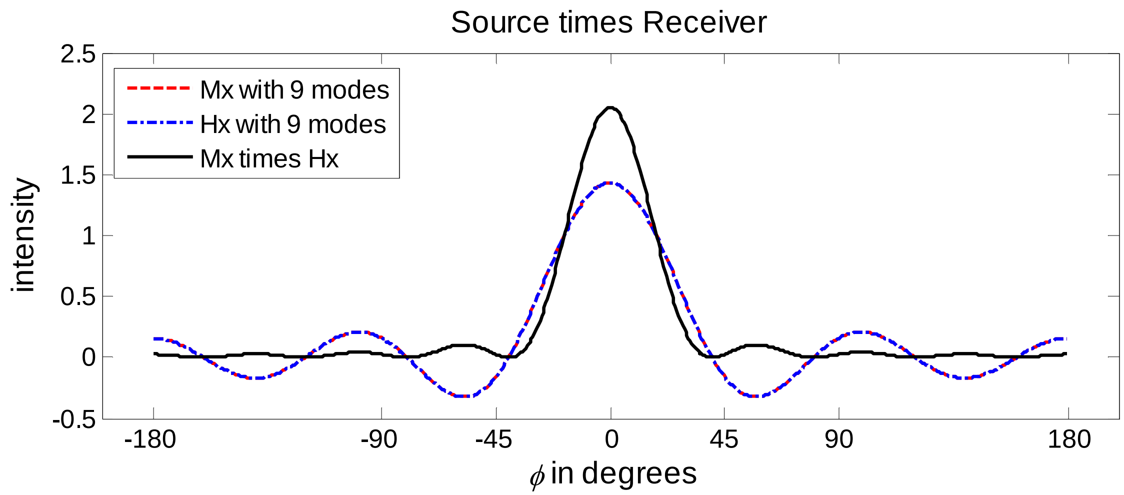

Coupling between source and receiver:
less Gibb's phenomenon

Method

Combination of:

1. **A Self-Adaptive Goal-Oriented *hp*-FEM for AC problems**

2. **A Fourier Series Expansion in a Non-Orthogonal System of Coordinates**

3. **Parallel Implementation**

Verification of 2.5D Simulation ($H_{xx} = H_{yy}$)

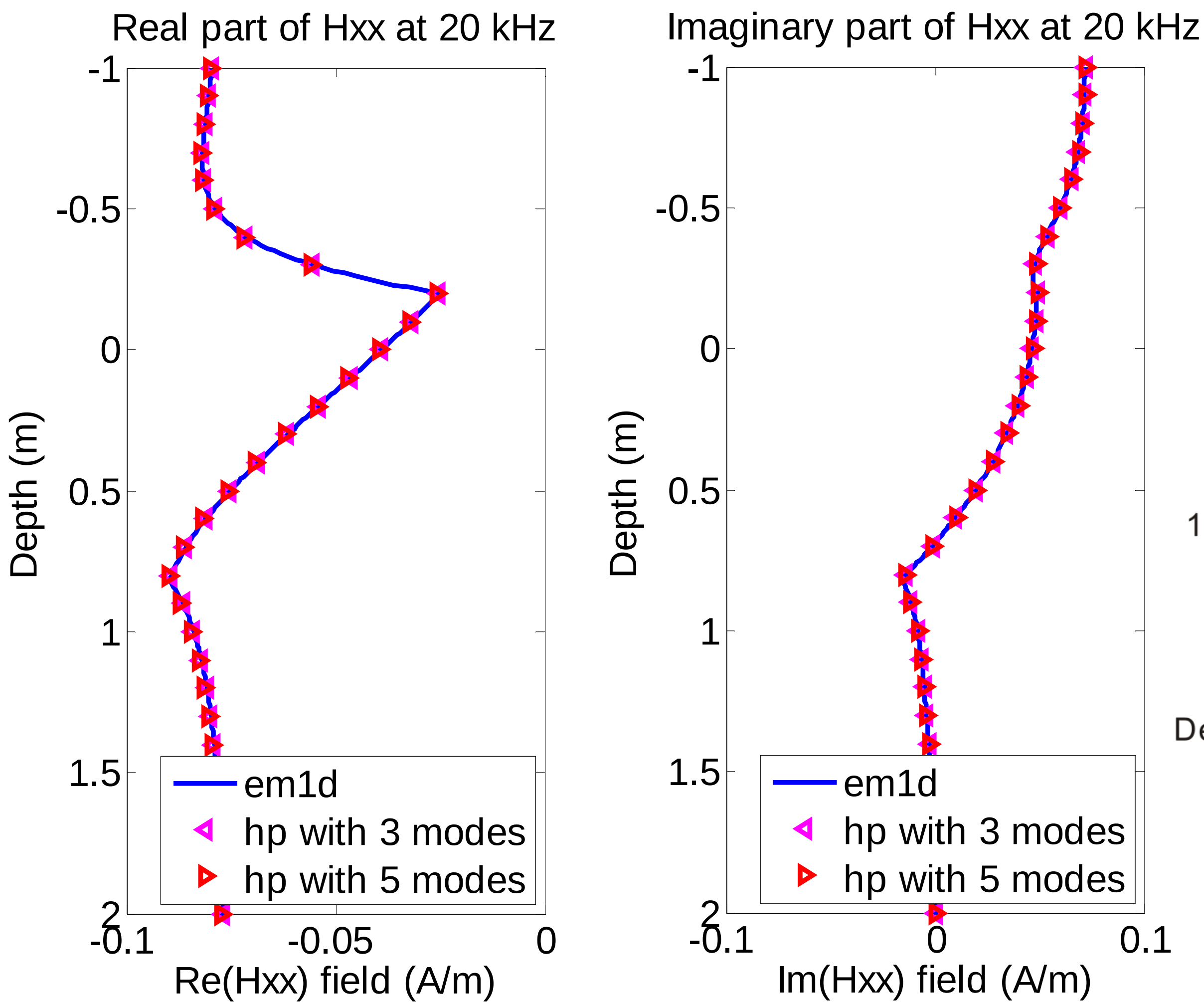

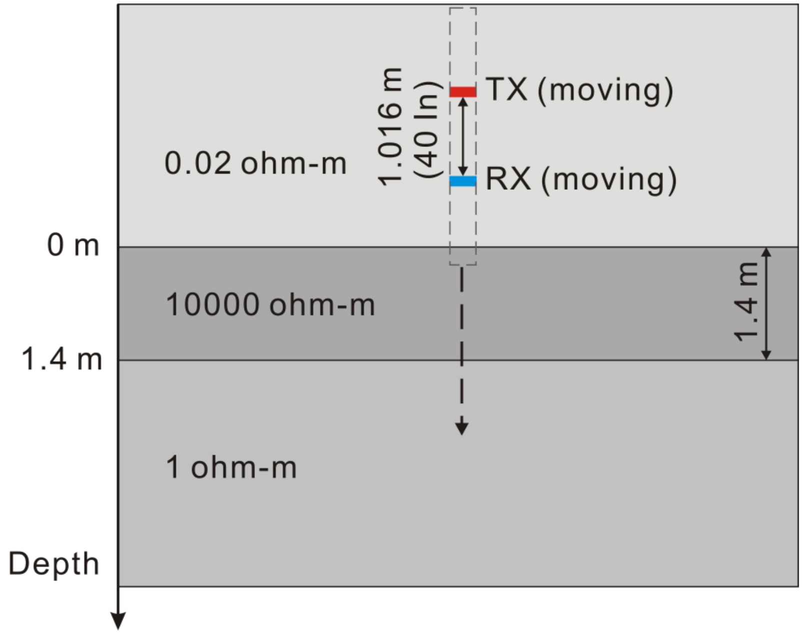

Converged solutions with 3 Fourier modes

em1D: K. H. Lee 1984, pers. comm.

Verification of 2.5D Simulation (H_{zz})

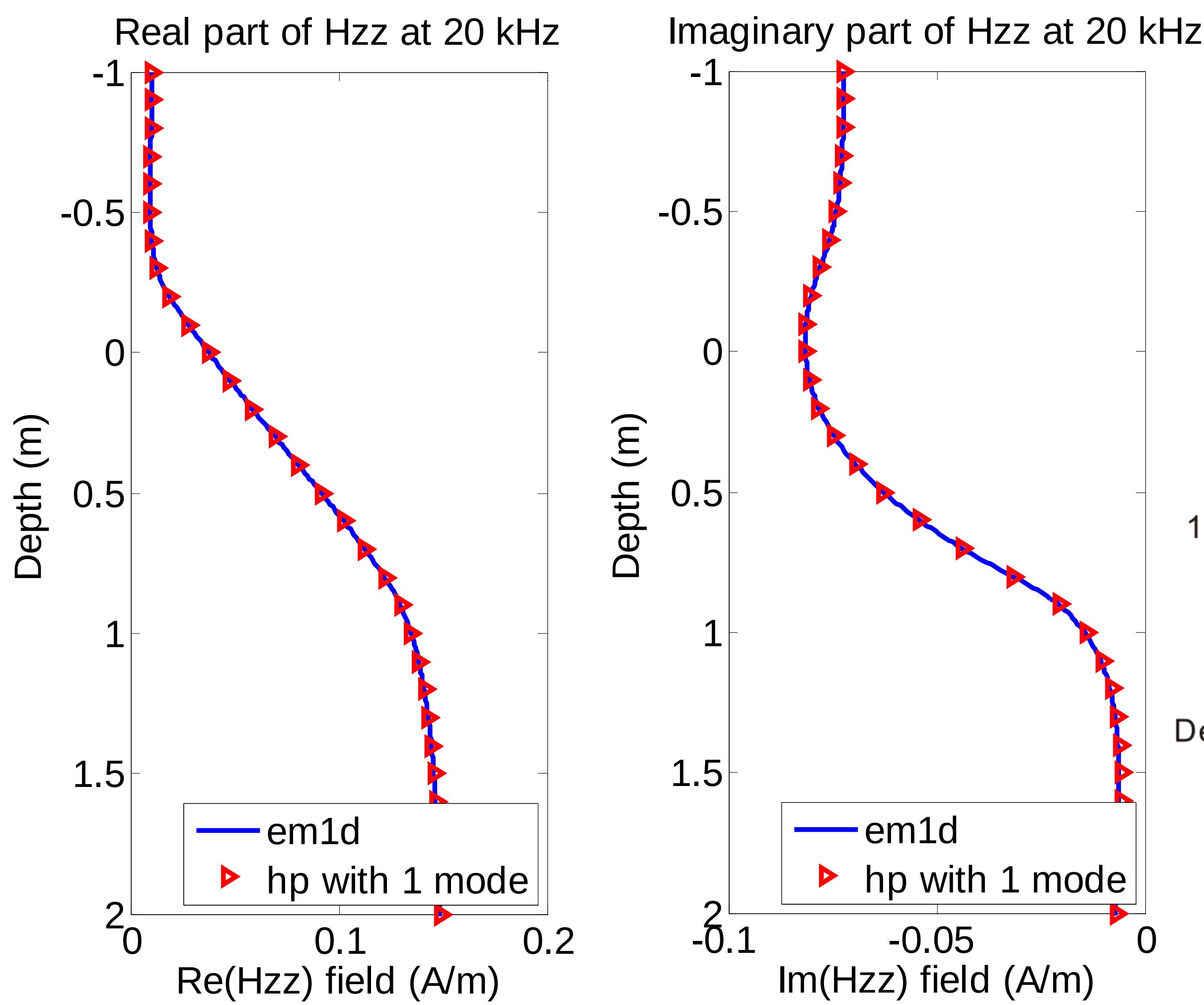

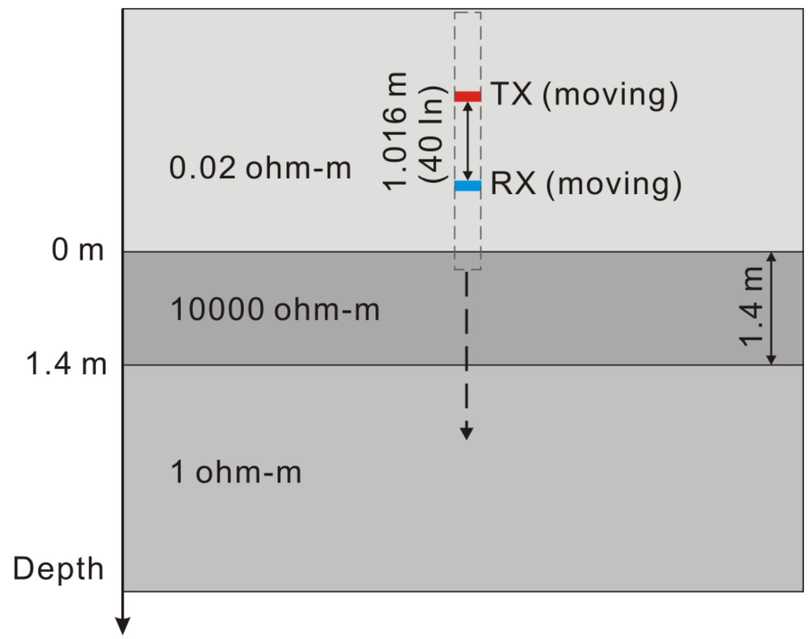

The same solutions with 1 Fourier mode

Verification of 2.5D Simulation ($H_{xy} = H_{yx}$)

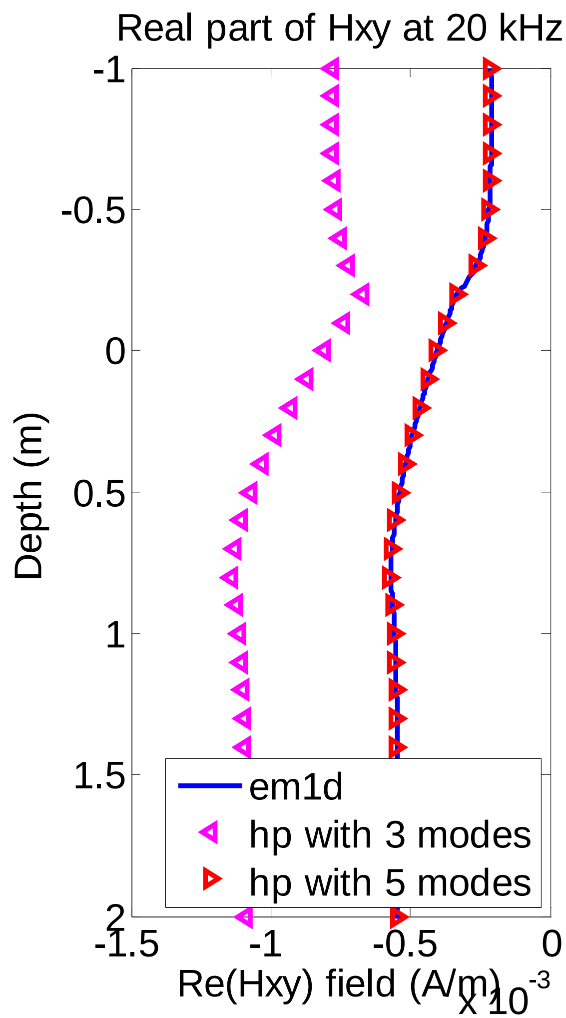

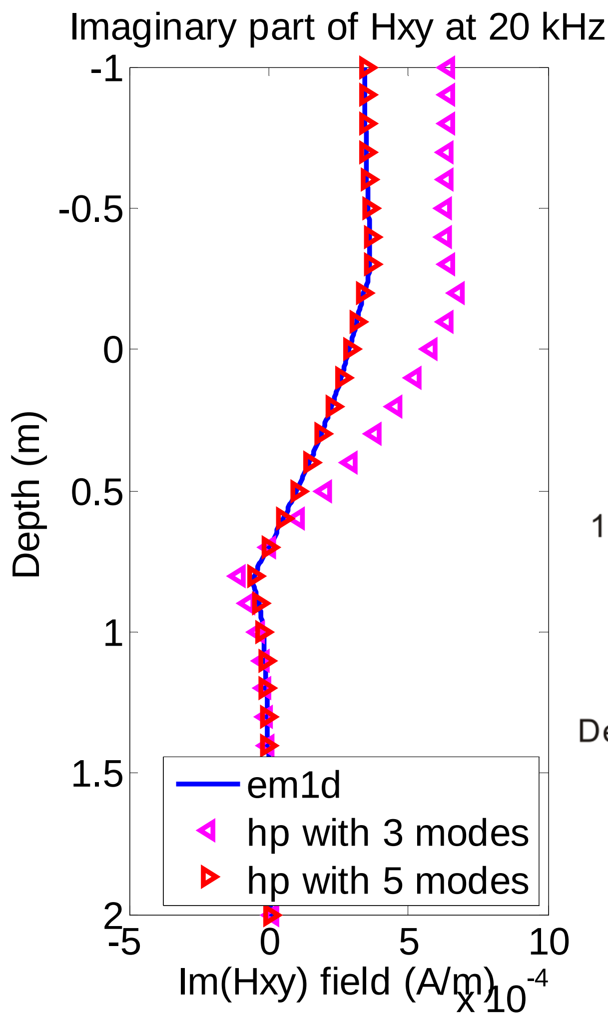

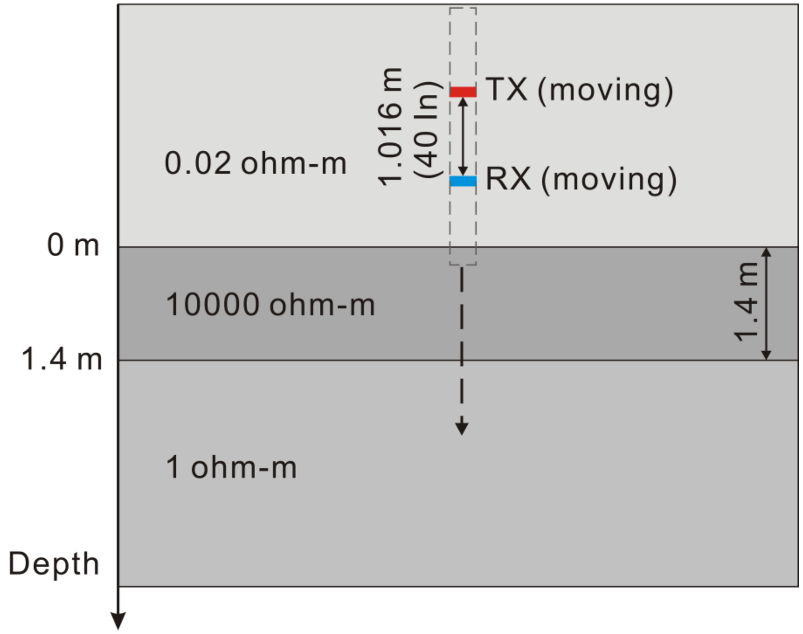

Converged solutions with 5 Fourier modes

Verification of 2.5D Simulation ($H_{xz} = H_{zx}$)

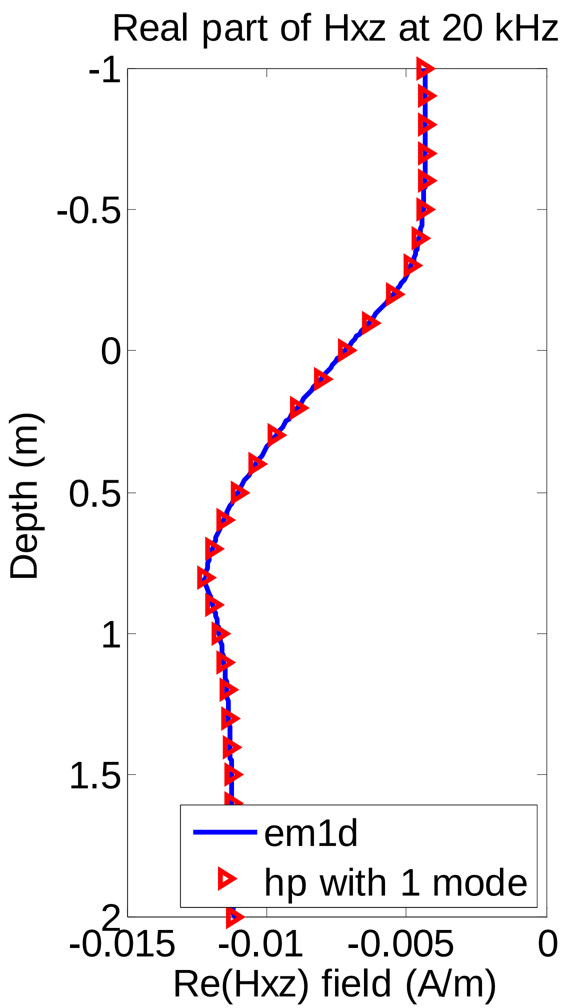

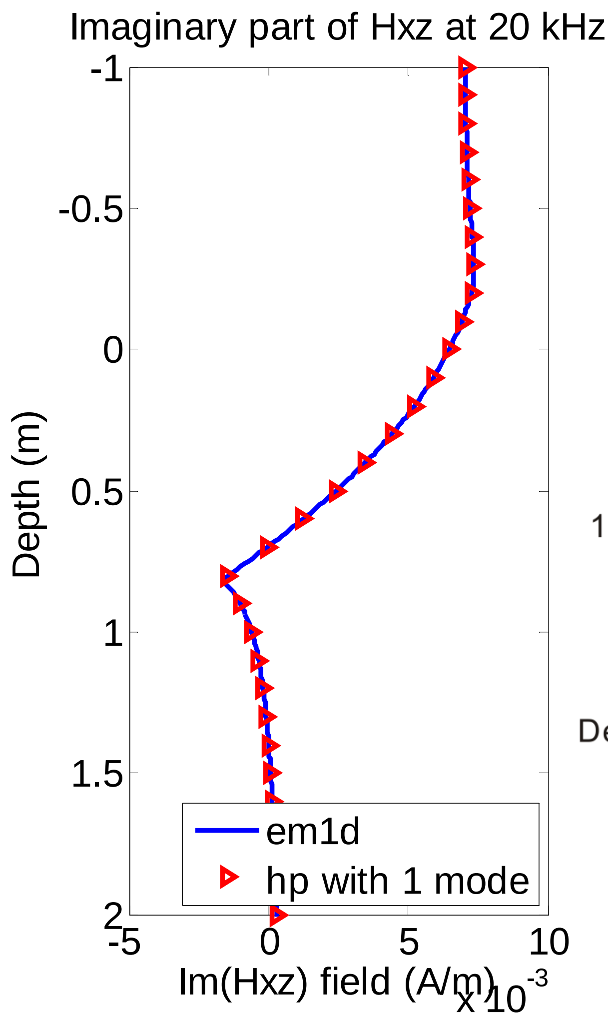

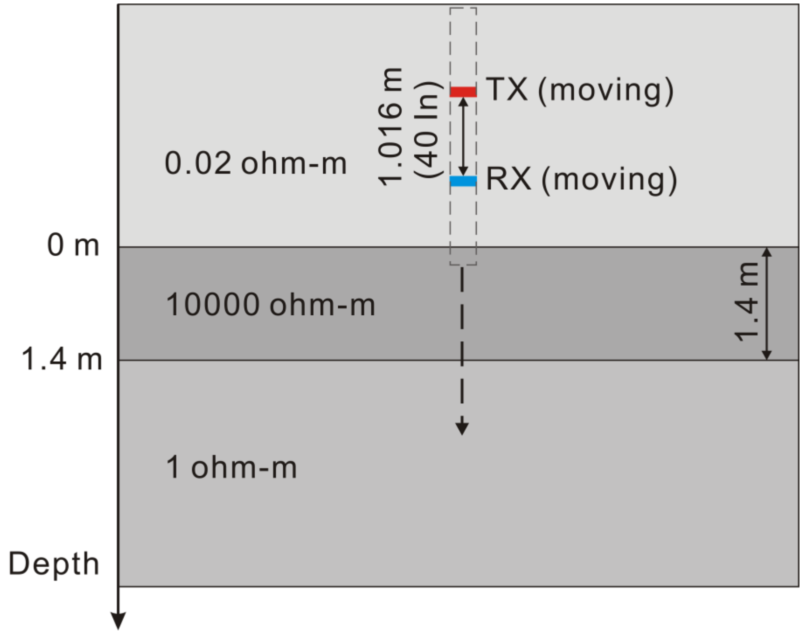

The same solutions with 1 Fourier mode

Verification of 3D Simulation ($H_{xx} = H_{yy}$)

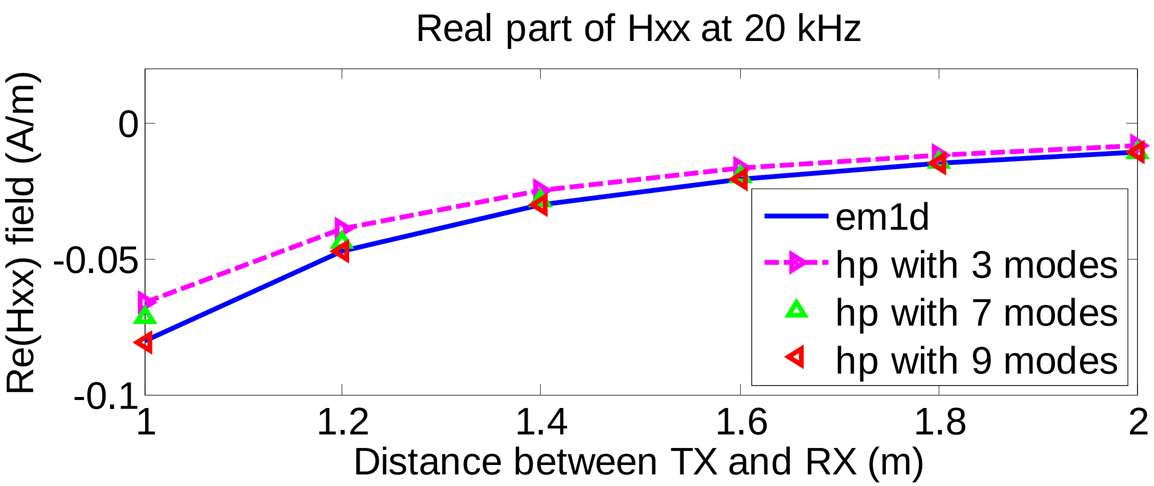

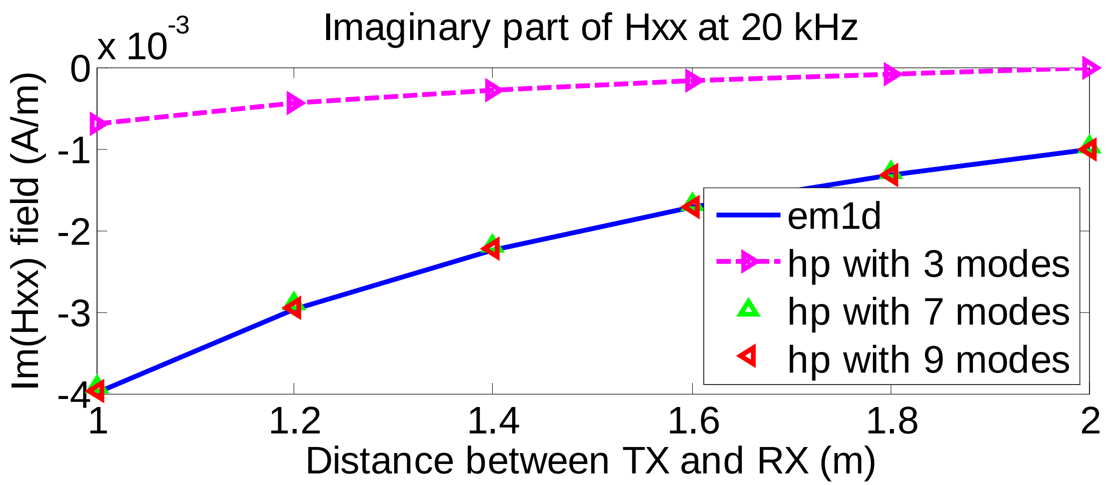

Dip angle: 60 degrees

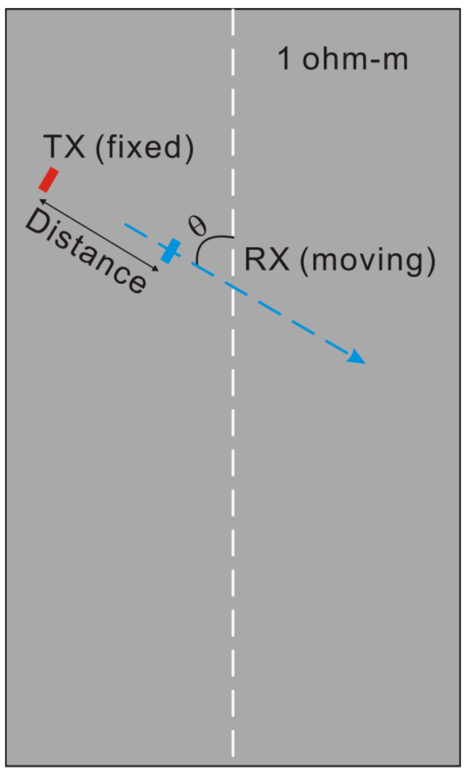

Converged solutions with 9 Fourier mode

Verification of 3D Simulation (H_{zz})

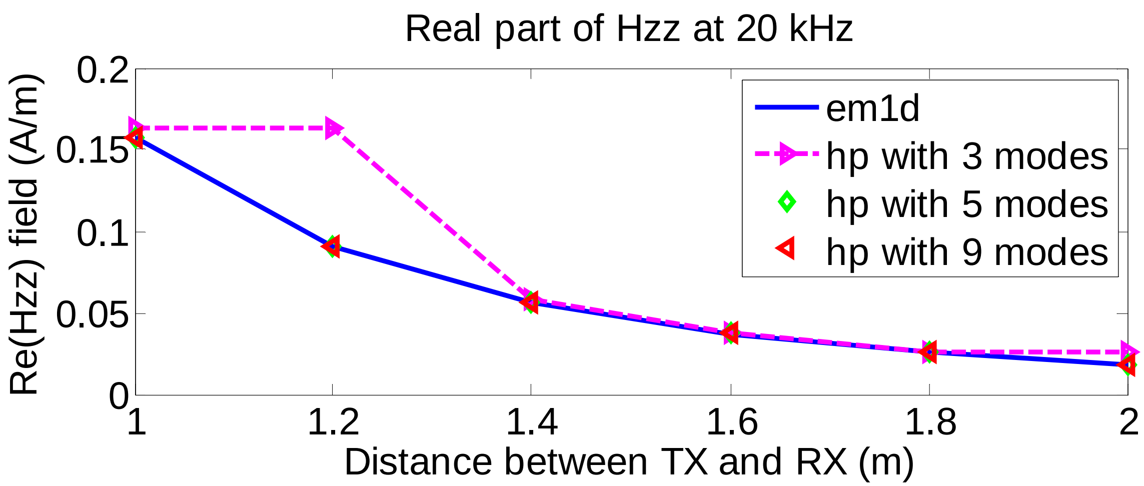

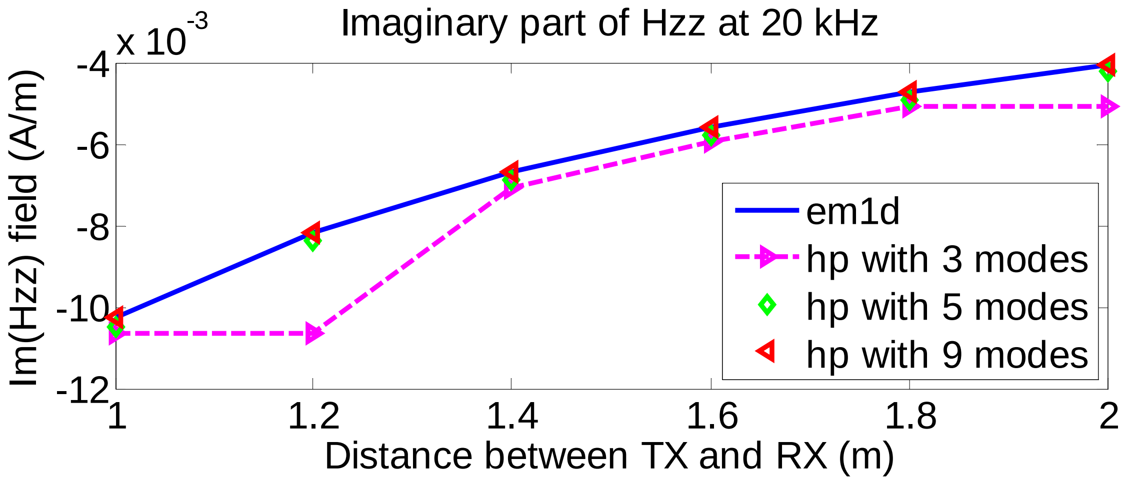

Dip angle: 60 degrees

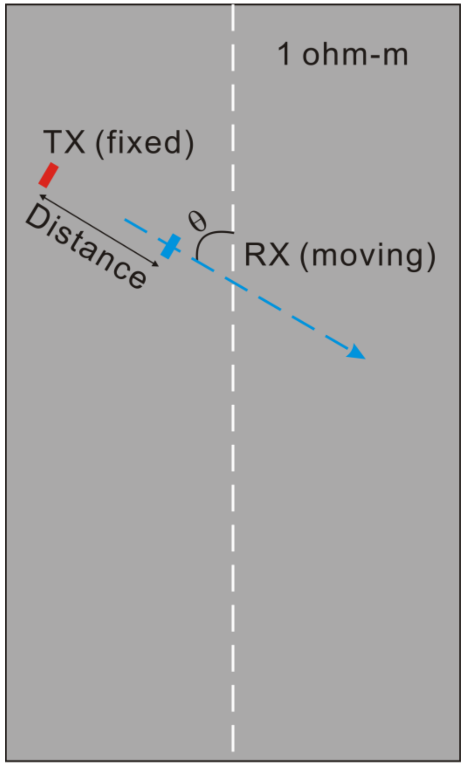

Converged solutions with 5 Fourier mode

Description of the Tri-Axial Tool

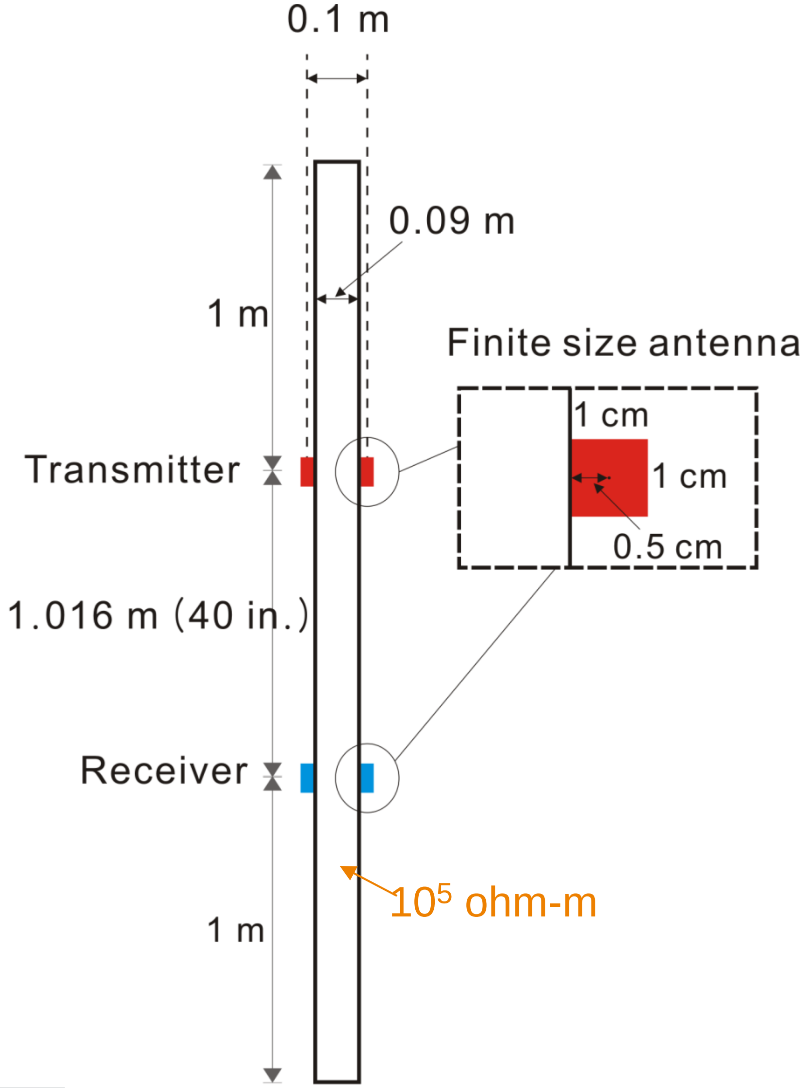

Operating frequency: 20 kHz

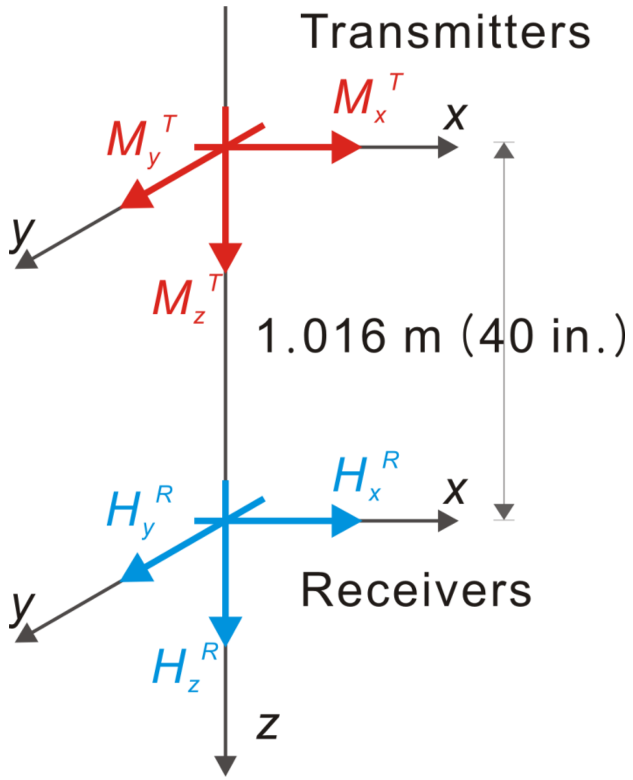

Verification of 2.5D Simulation (H_{xx})

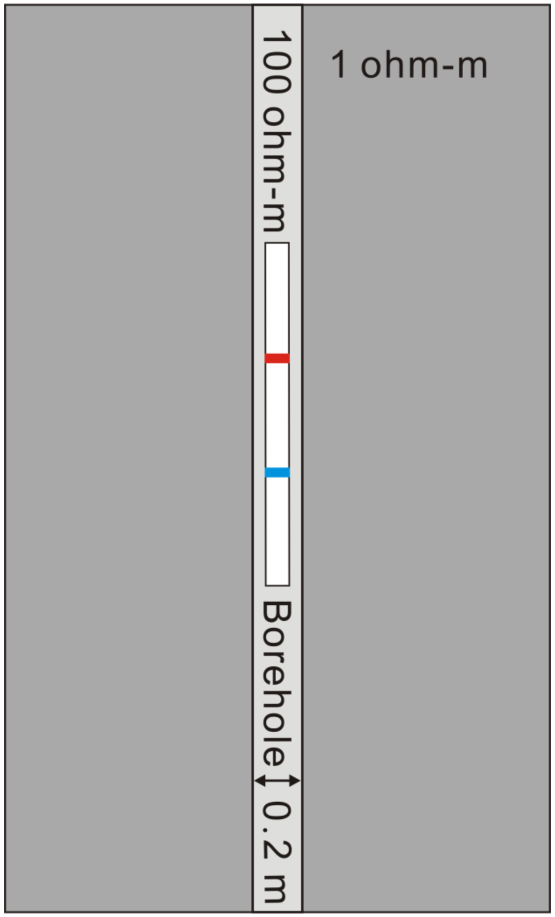

Relative errors of tri-axial induction solutions with respect to the solution with 9 Fourier modes

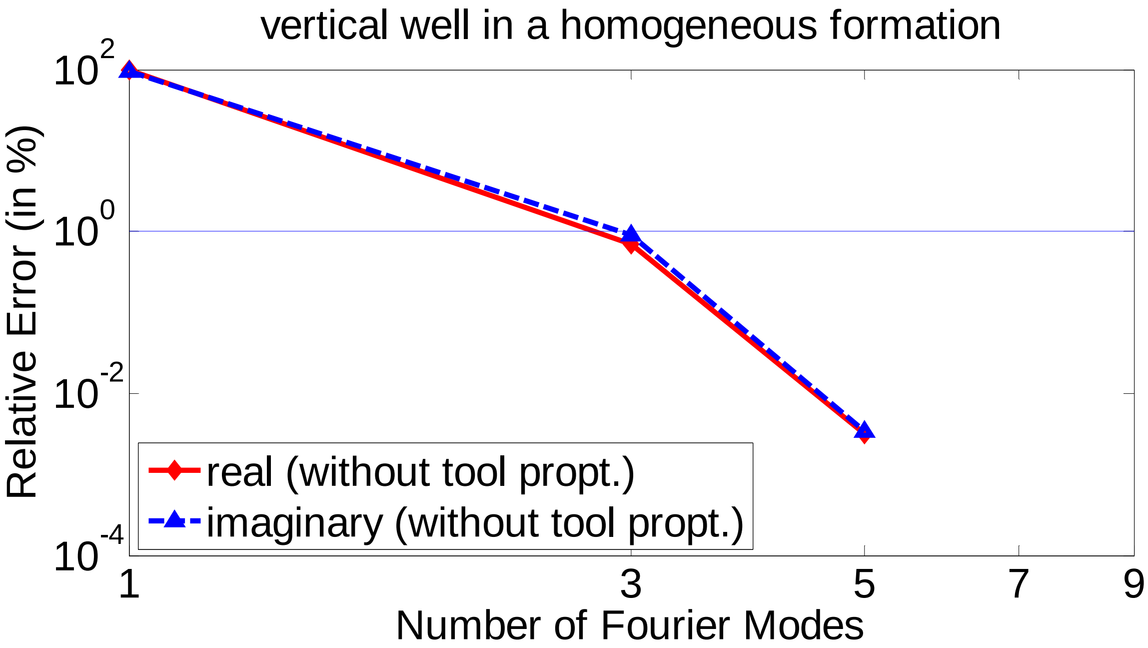

Verification of 3D Simulation (H_{xx})

θ = 60 degrees

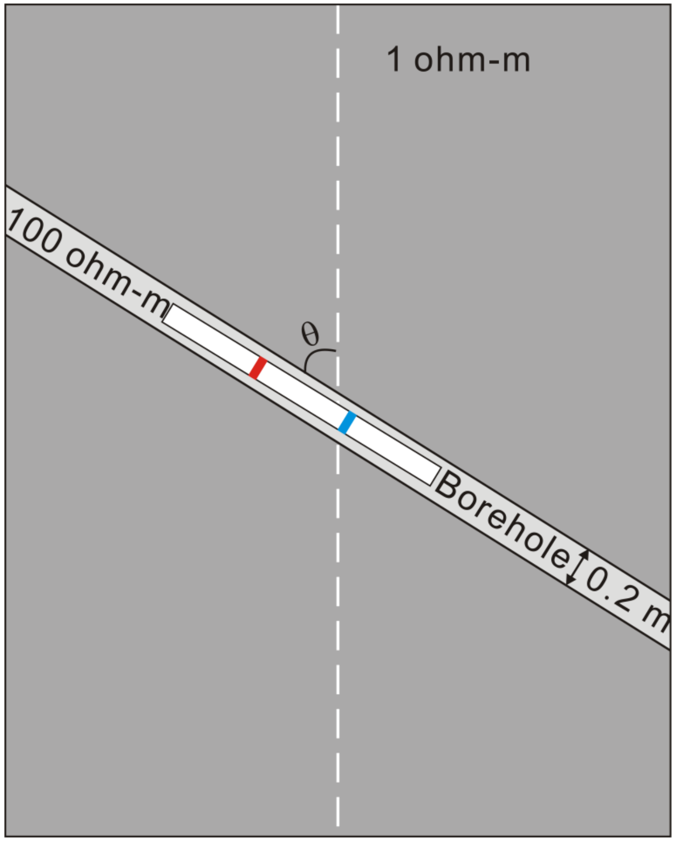

Relative errors of tri-axial Induction solutions with respect to the solution for the vertical well

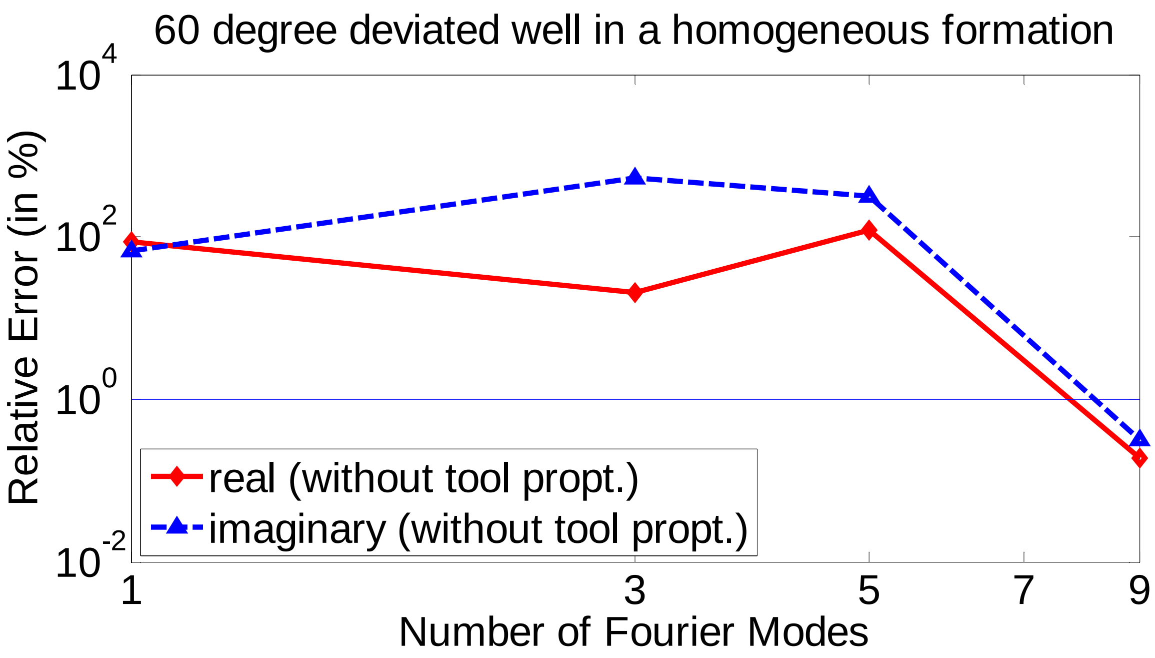

Model for Numerical Experiments

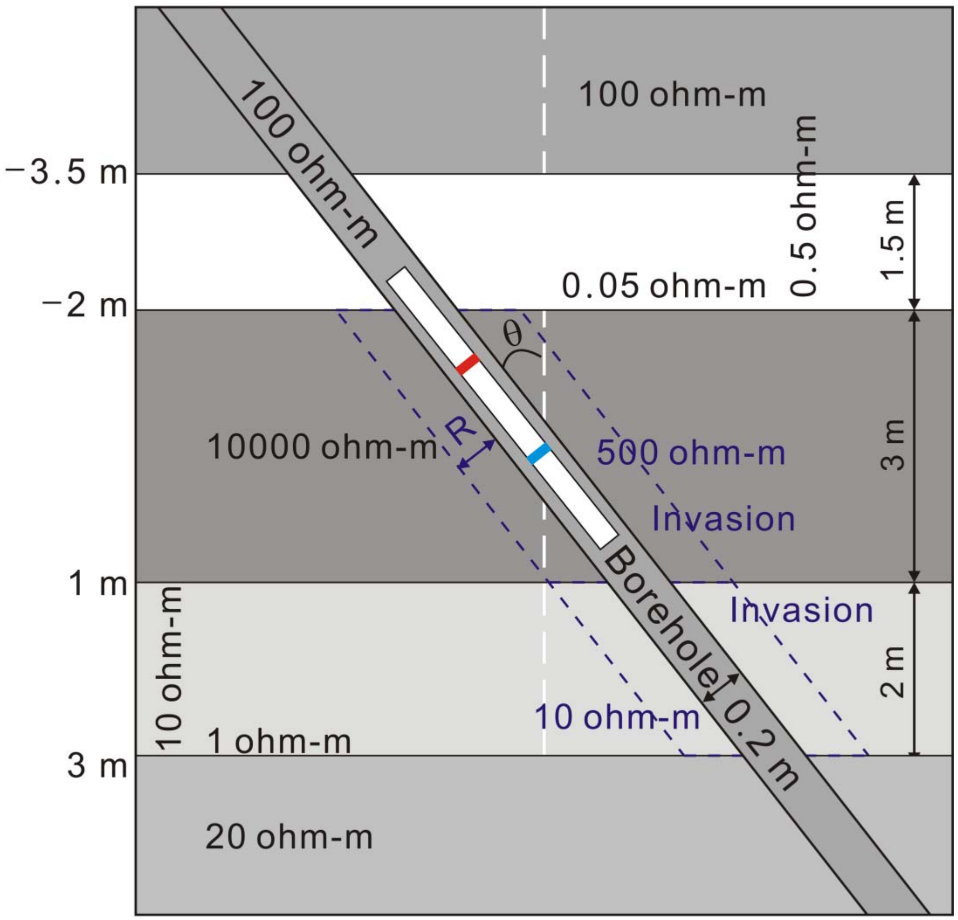

Five layers: 100, 0.05, 10000, 1 and 20 ohm-m from top to bottom

Borehole: 0.1 m in radius
100 ohm-m in resistivity

Invasion in the third and fourth layers

Anisotropy in the second and fourth layers

θ = 0, 30 and 60 degrees

Convergence History of H_{xx} in Vertical Well

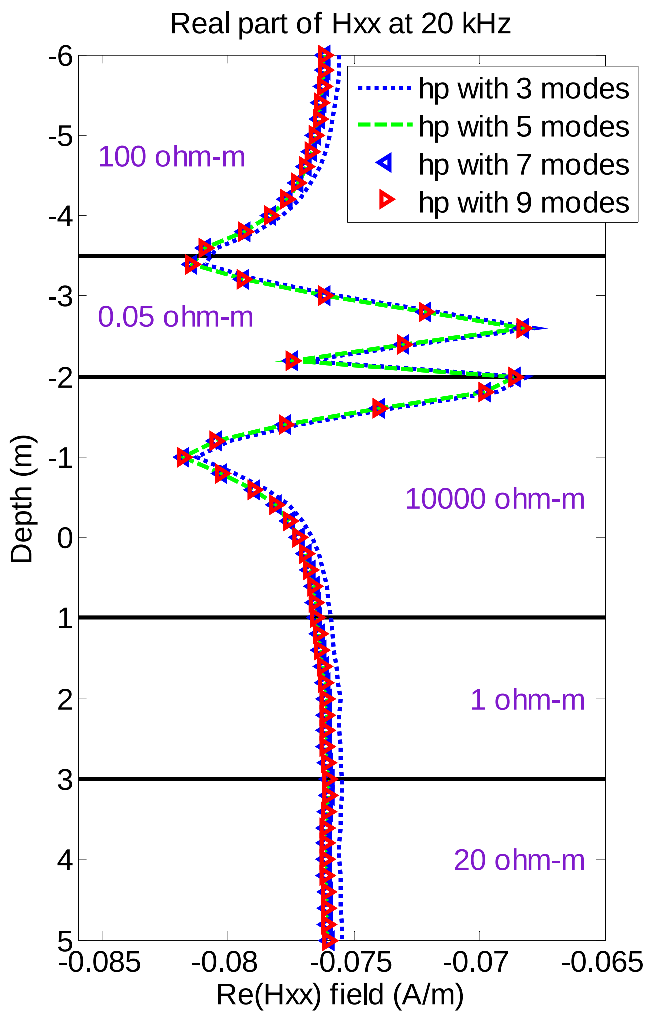

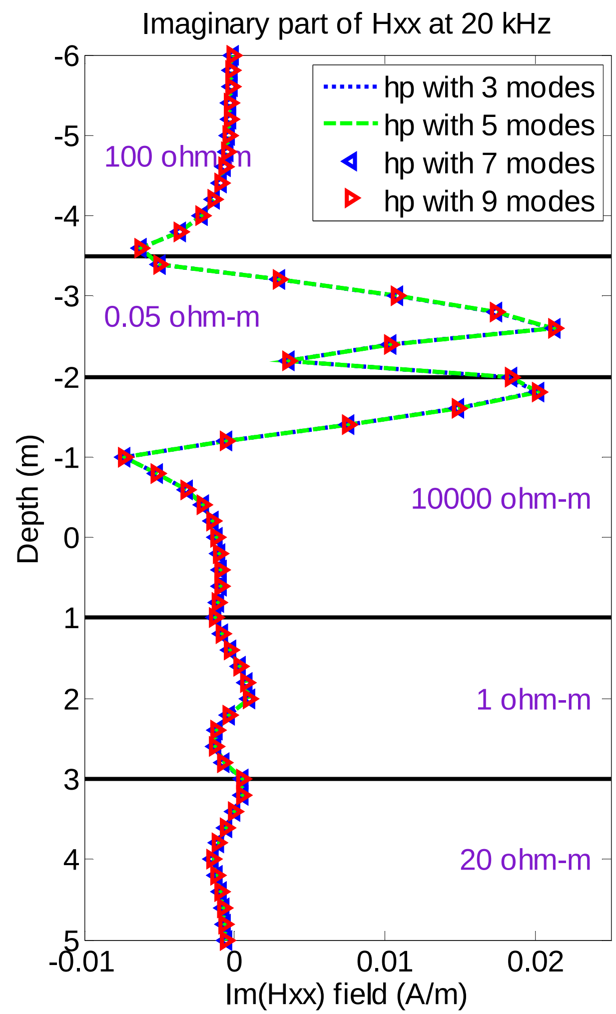

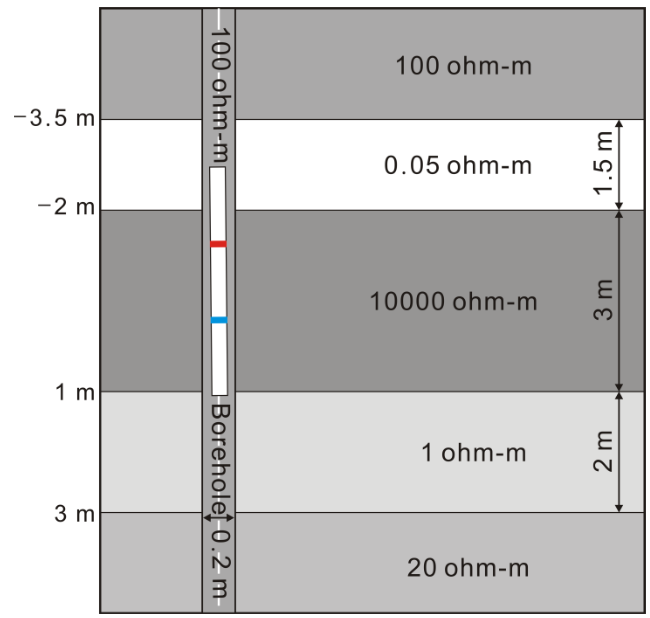

Converged solutions with 5 Fourier modes

Convergence History of H_{xx} in Deviated Well

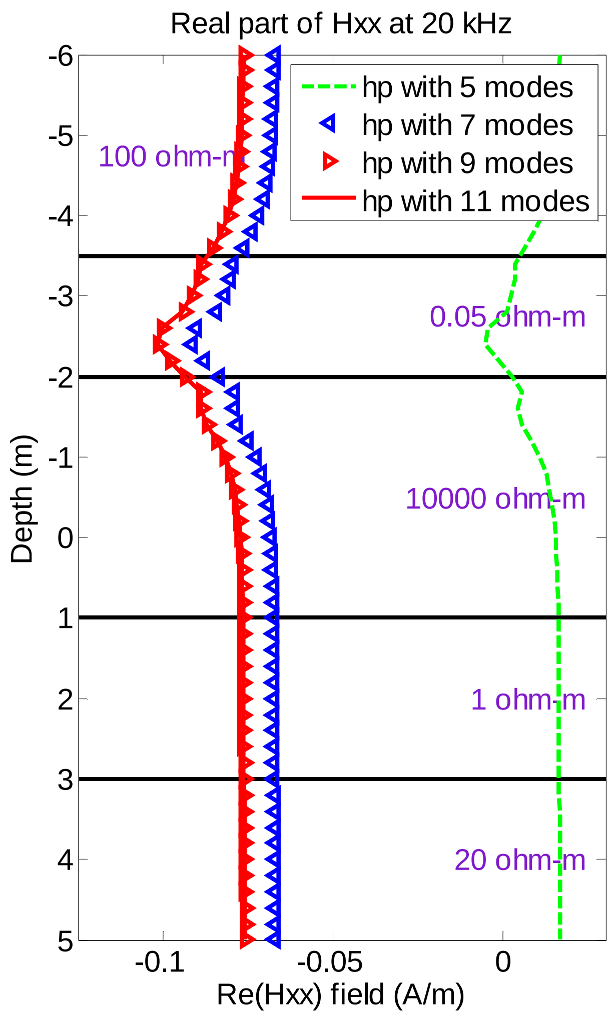

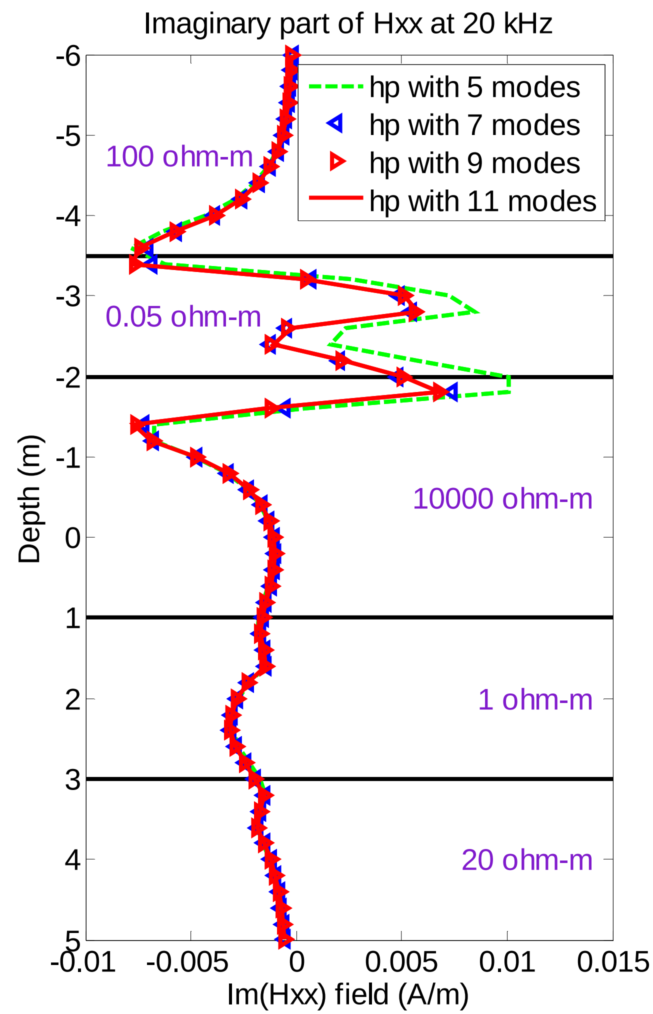

θ = 60 degrees

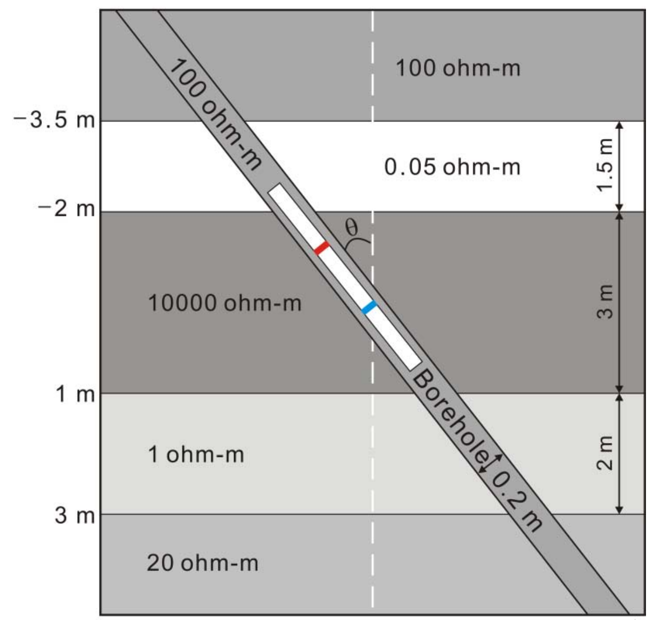

Converged solutions with 9 Fourier modes

Deviated Wells (0, 30 & 60 degrees)

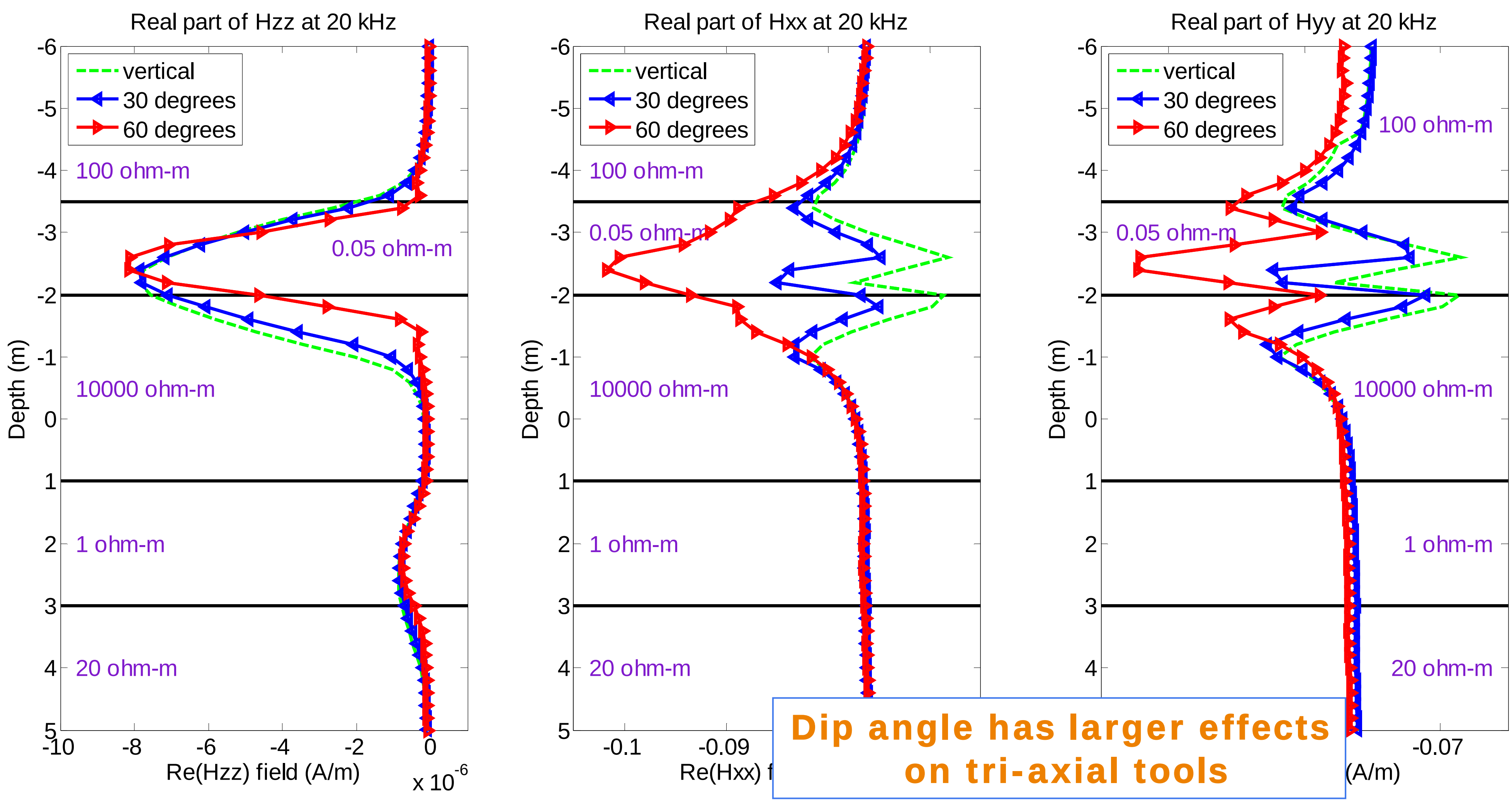

Dip angle has larger effects on tri-axial tools

Deviated Wells (0, 30 & 60 degrees)

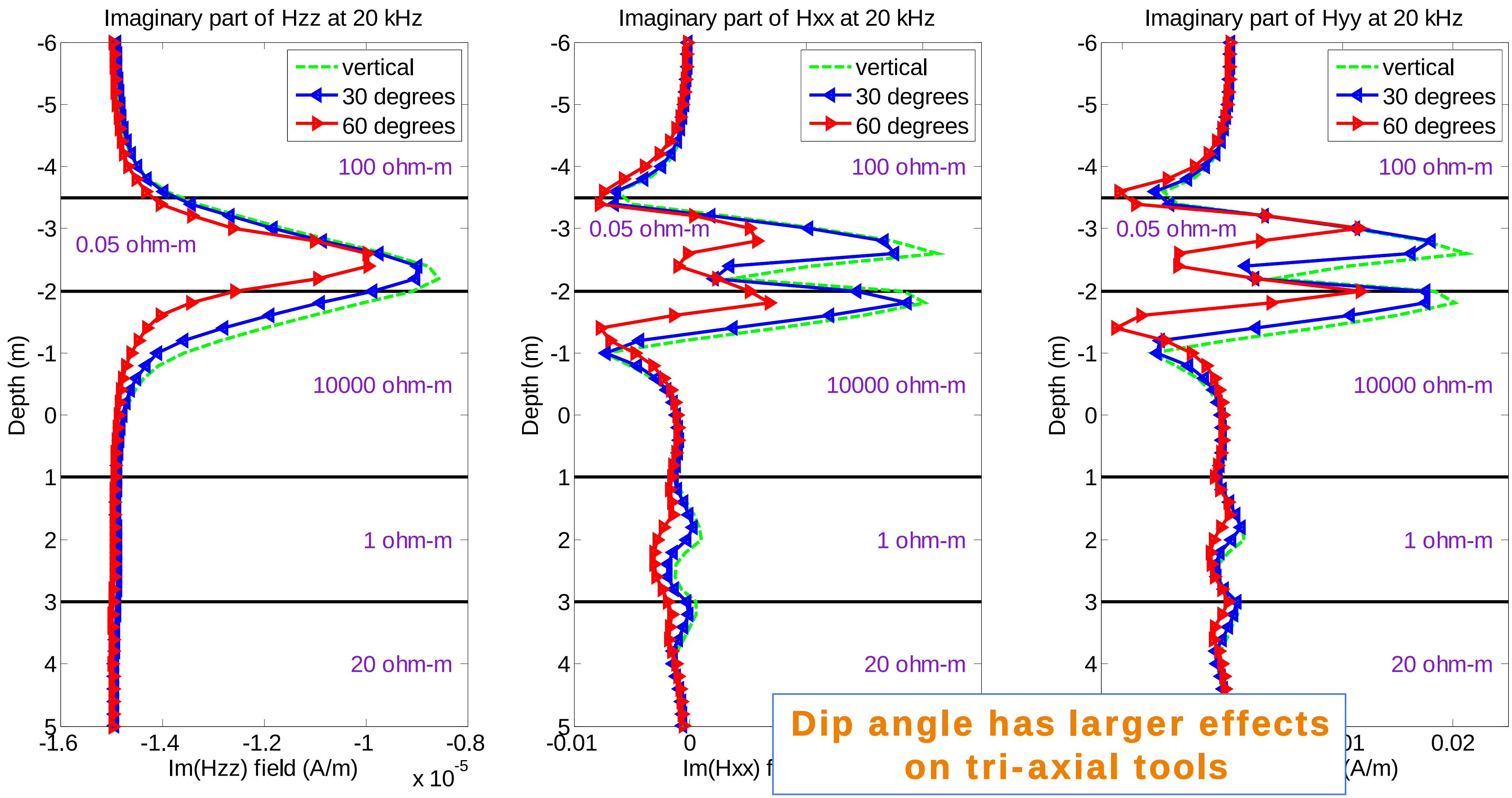

Dip angle has larger effects on tri-axial tools

H_{zz} in Deviated Wells with Invasion (Re.)

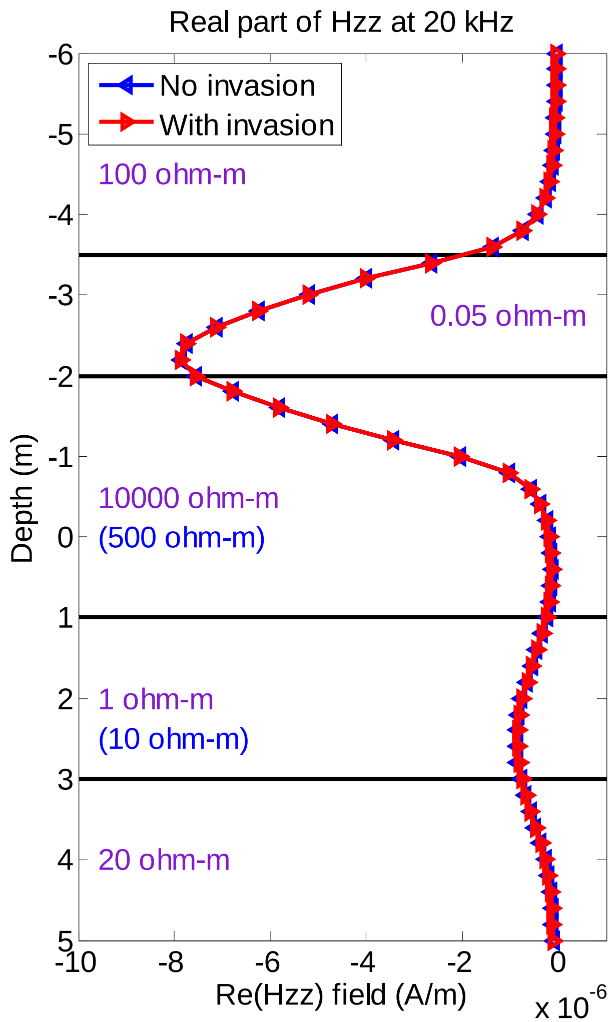

vertical

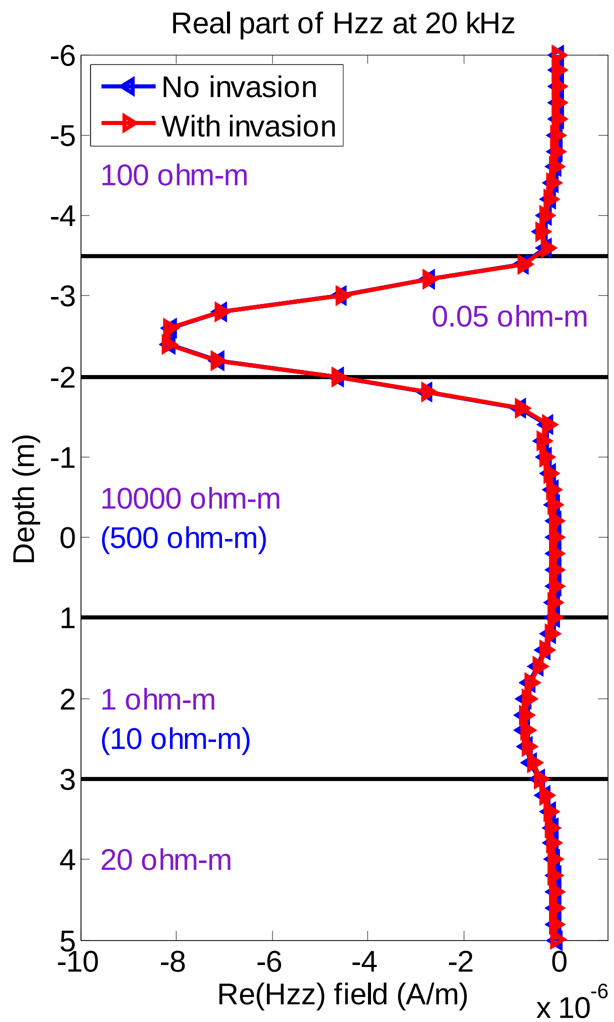

60 degrees

Shallow invasion with R = 0.1 m

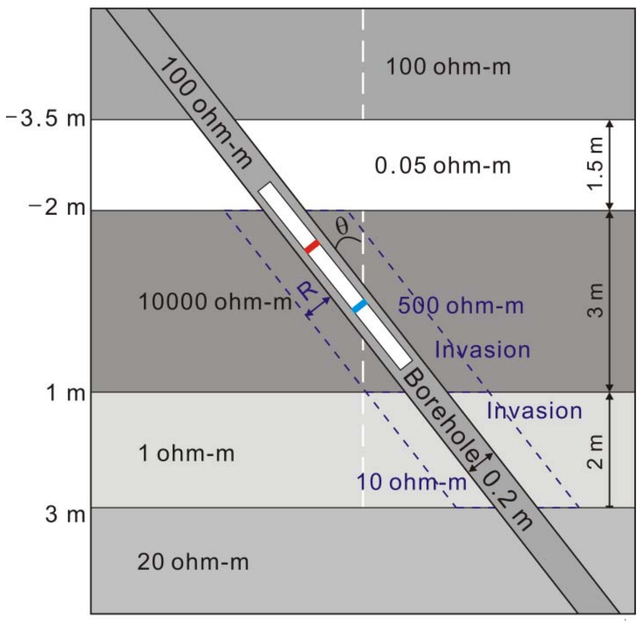

H_{zz} in Deviated Wells with Invasion (Im.)

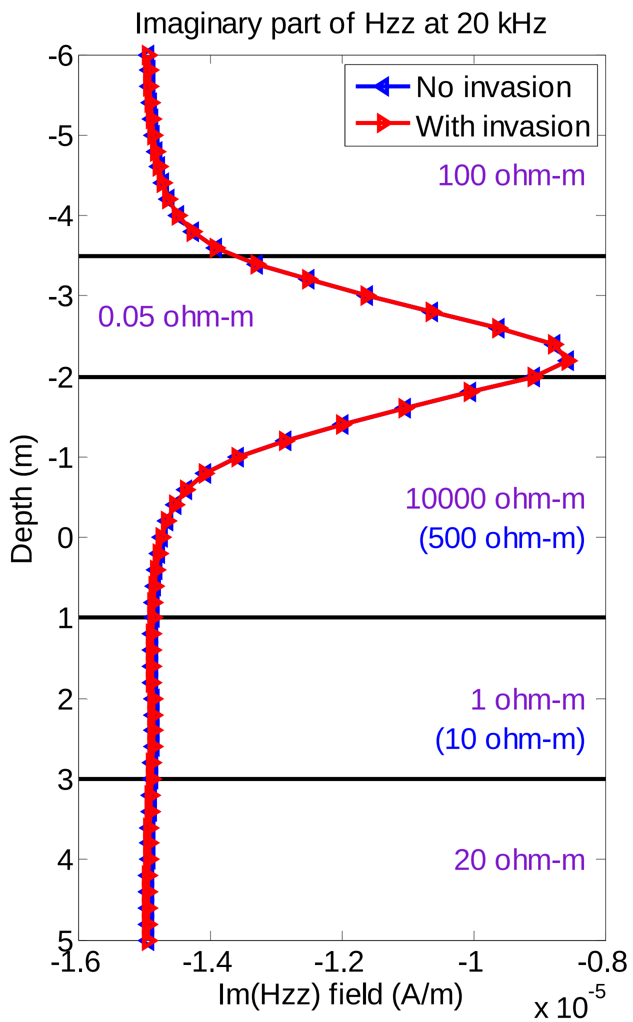

vertical

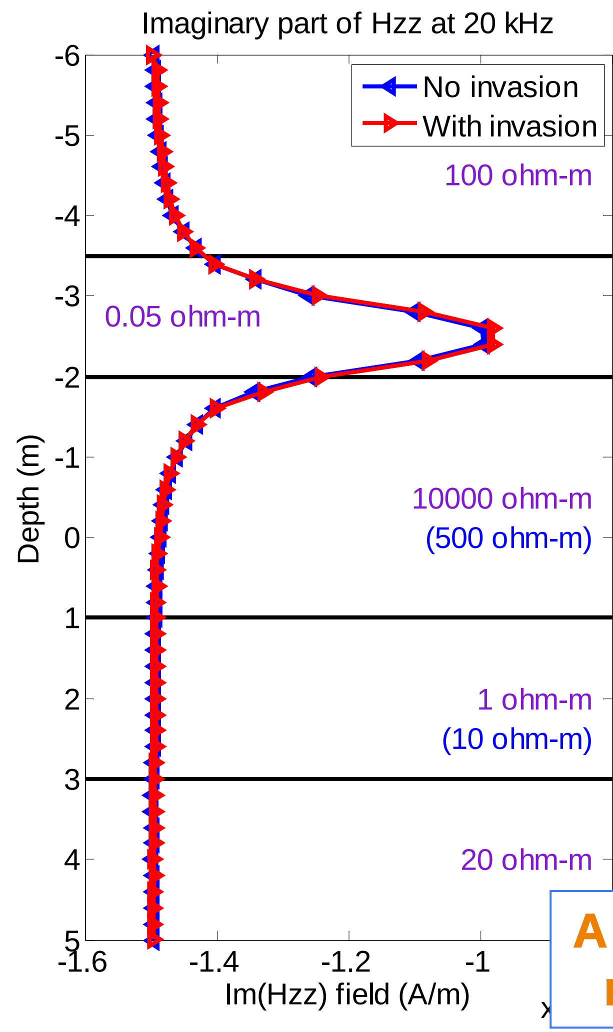

60 degrees

Shallow invasion with R = 0.1 m

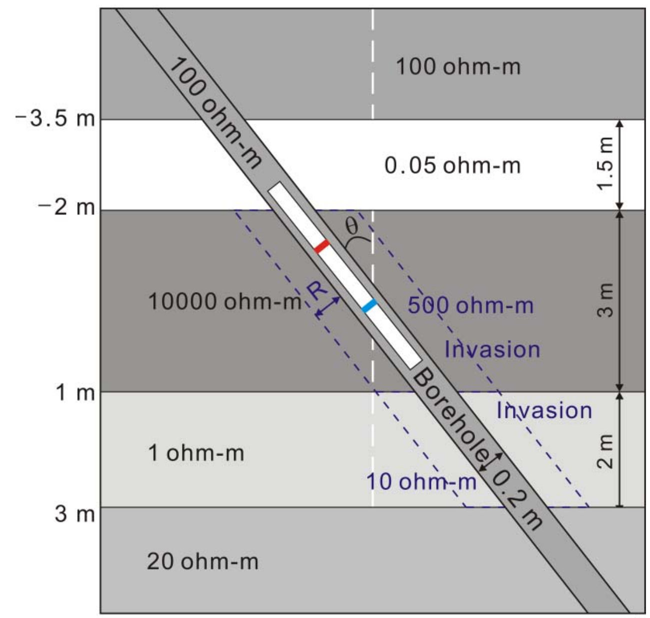

Almost no effects of invasion regardless of the dip angle

H_{xx} in Deviated Wells with Invasion (Re.)

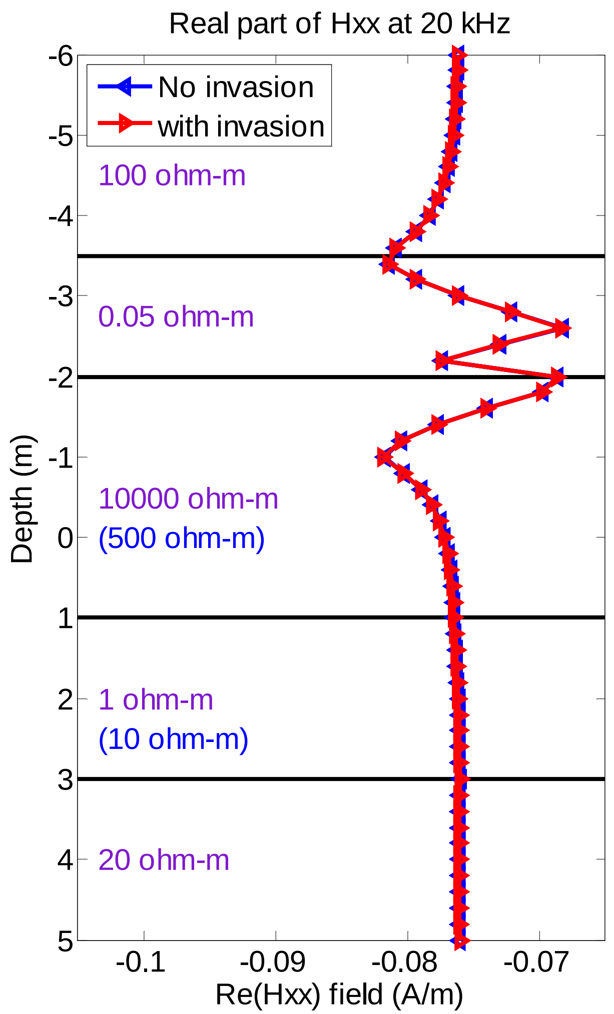

vertical

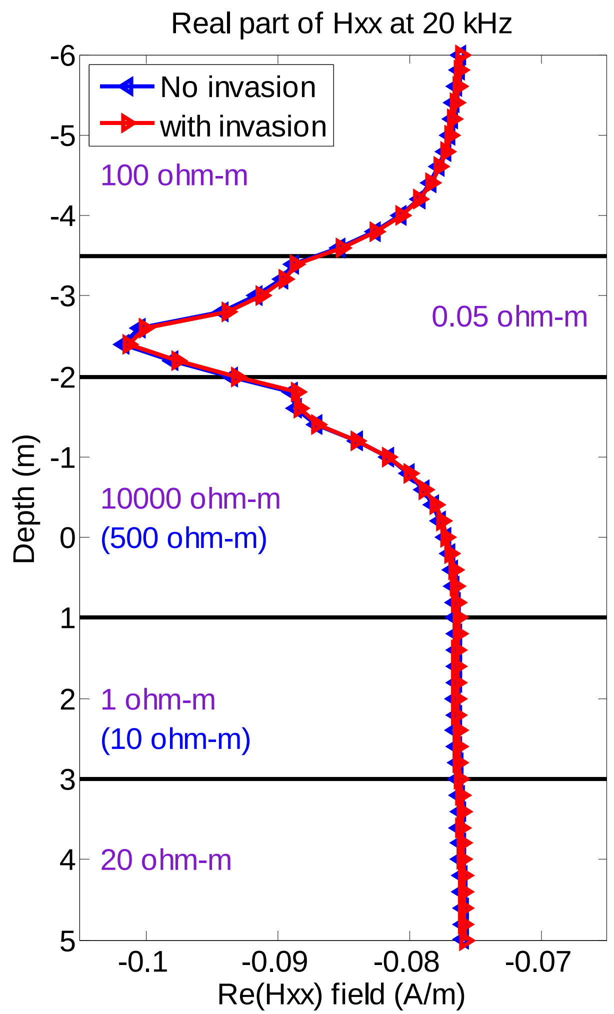

60 degrees

Shallow invasion with R = 0.1 m

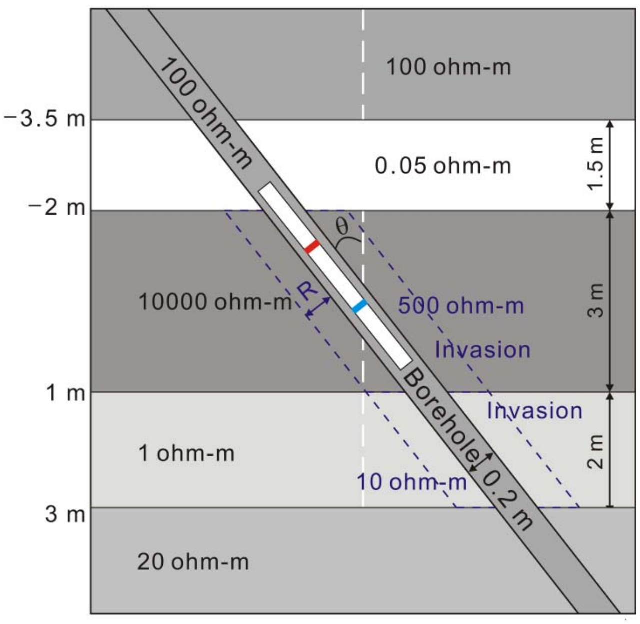

H_{xx} in Deviated Wells with Invasion (Im.)

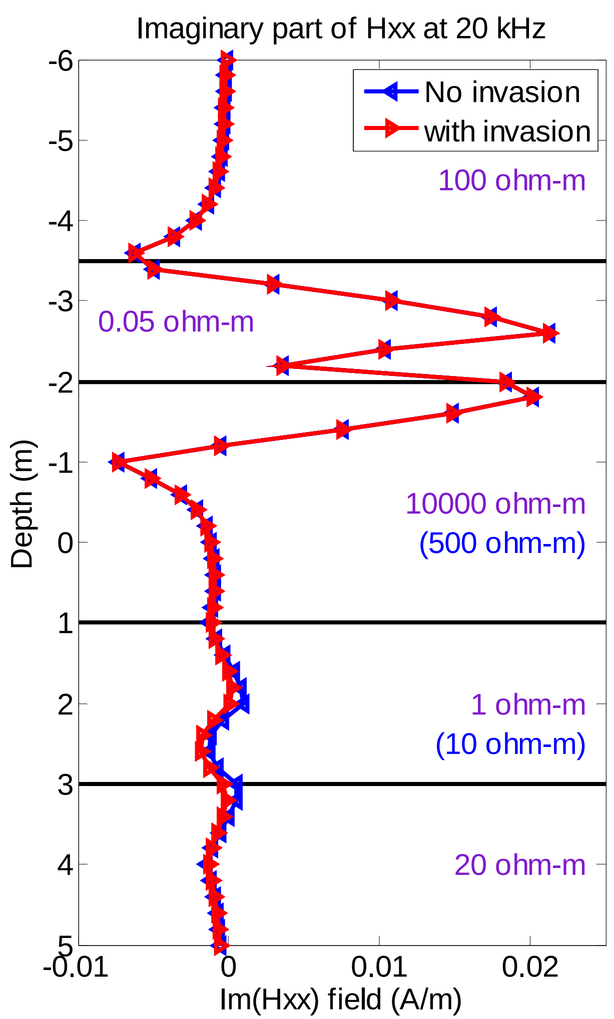

vertical

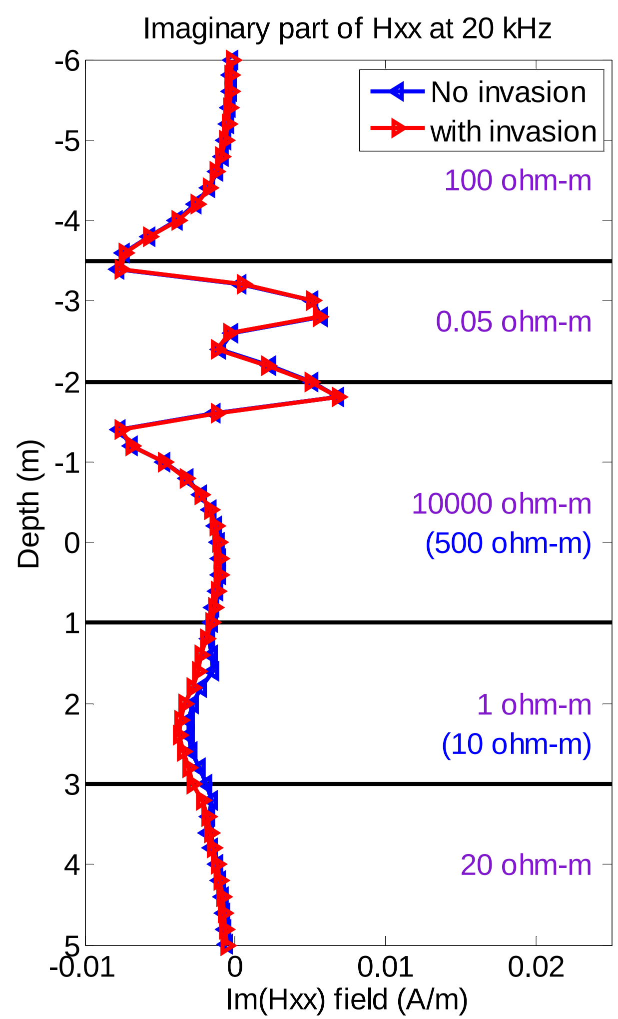

60 degrees

Shallow invasion with R = 0.1 m

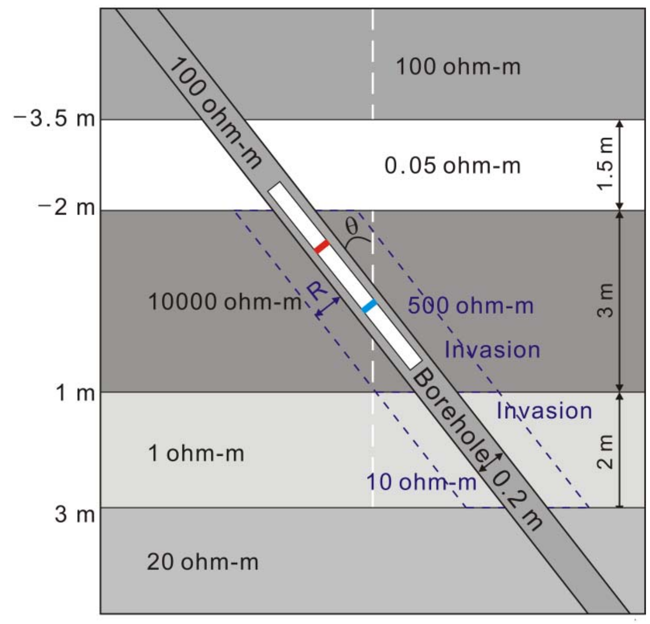

Small effects of invasion

H_{yy} in Deviated Wells with Invasion (Re.)

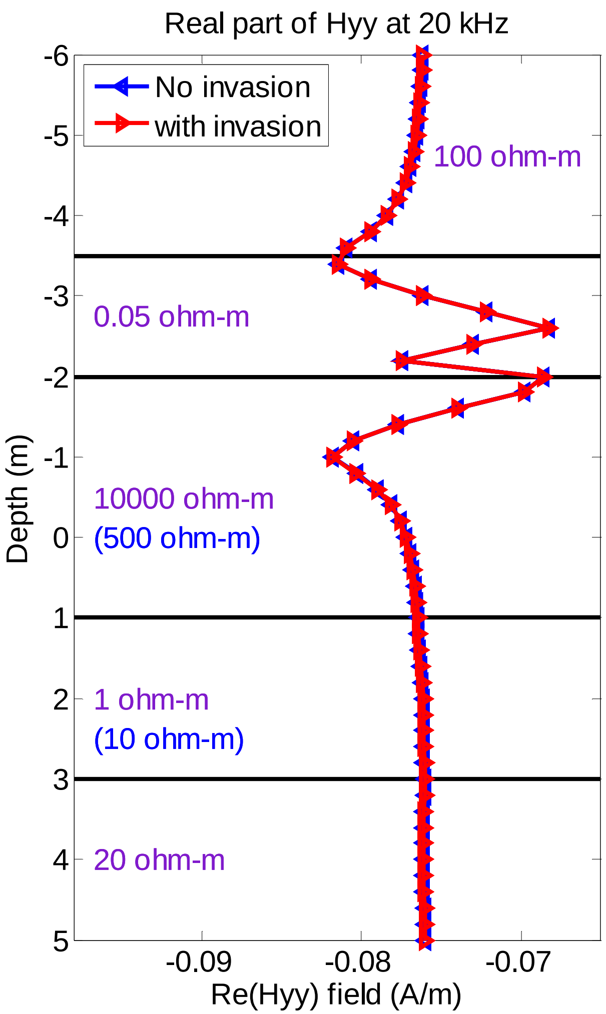

vertical

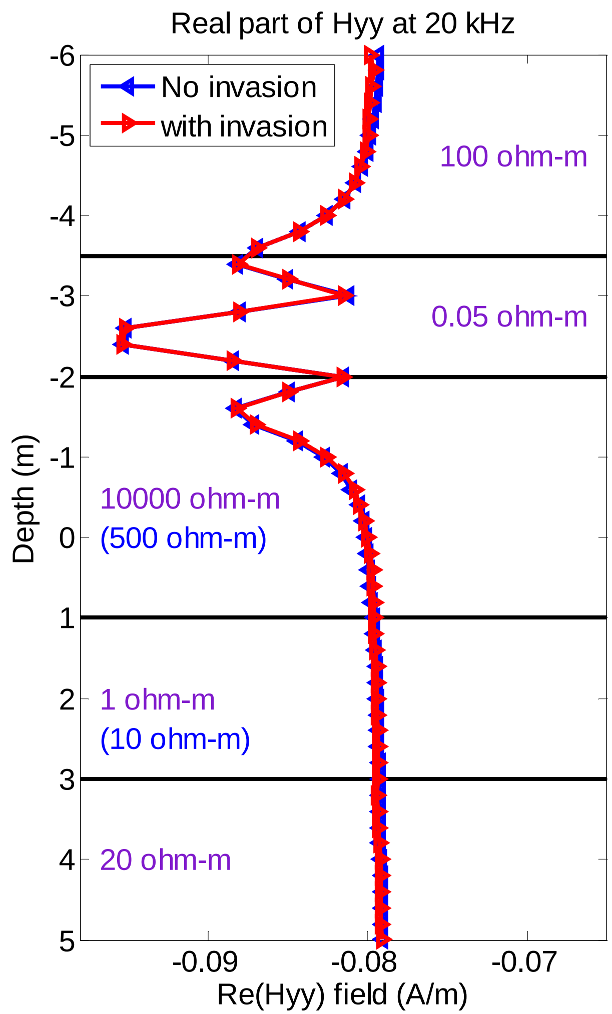

60 degrees

Shallow invasion with R = 0.1 m

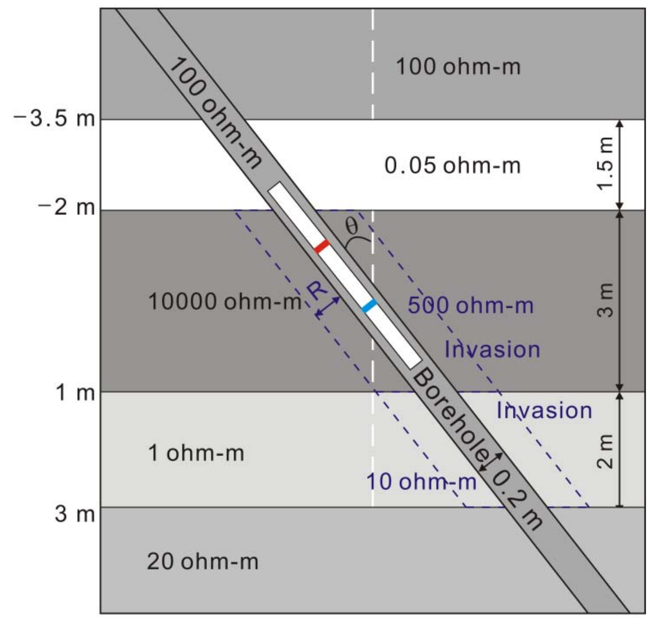

H_{yy} in Deviated Wells with Invasion (Im.)

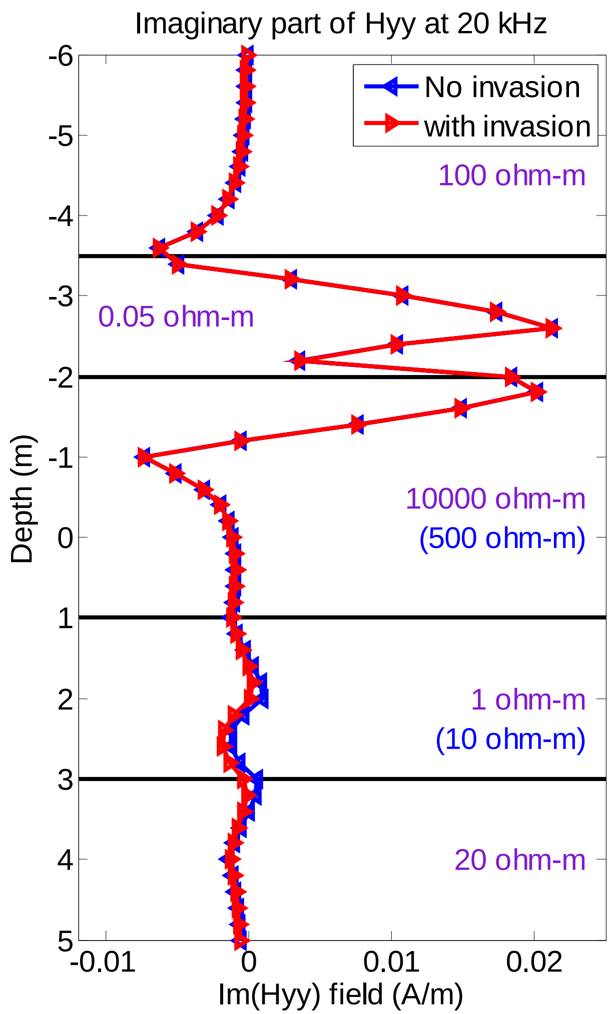

vertical

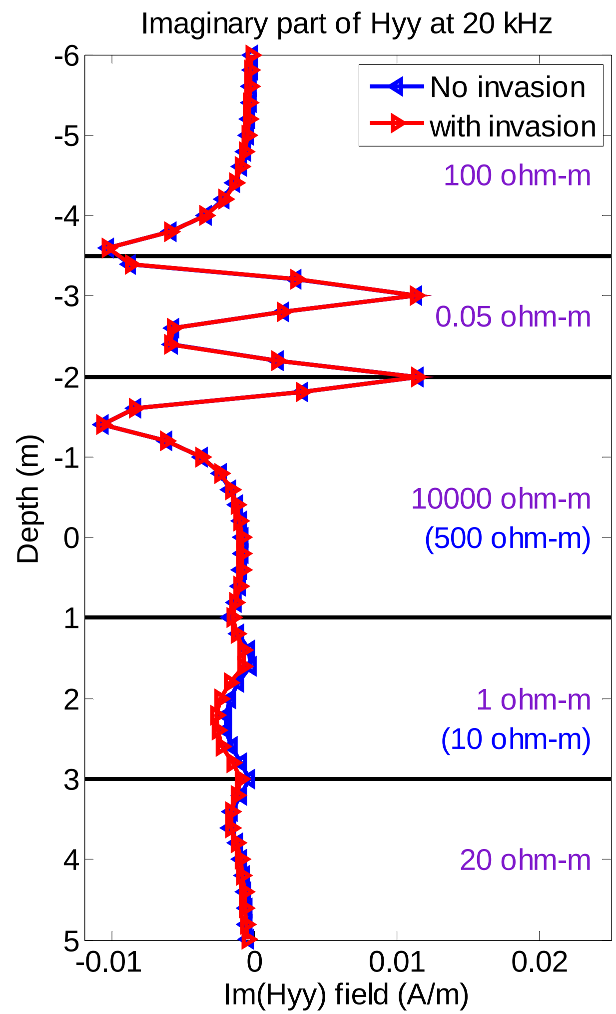

60 degrees

Shallow invasion with R = 0.1 m

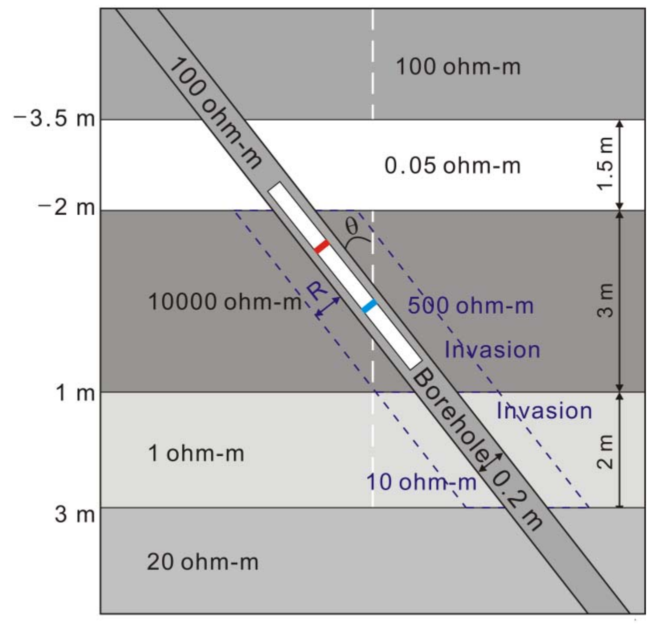

Small effects of invasion

H_{zz} in Deviated Wells with Anisotropy (Re.)

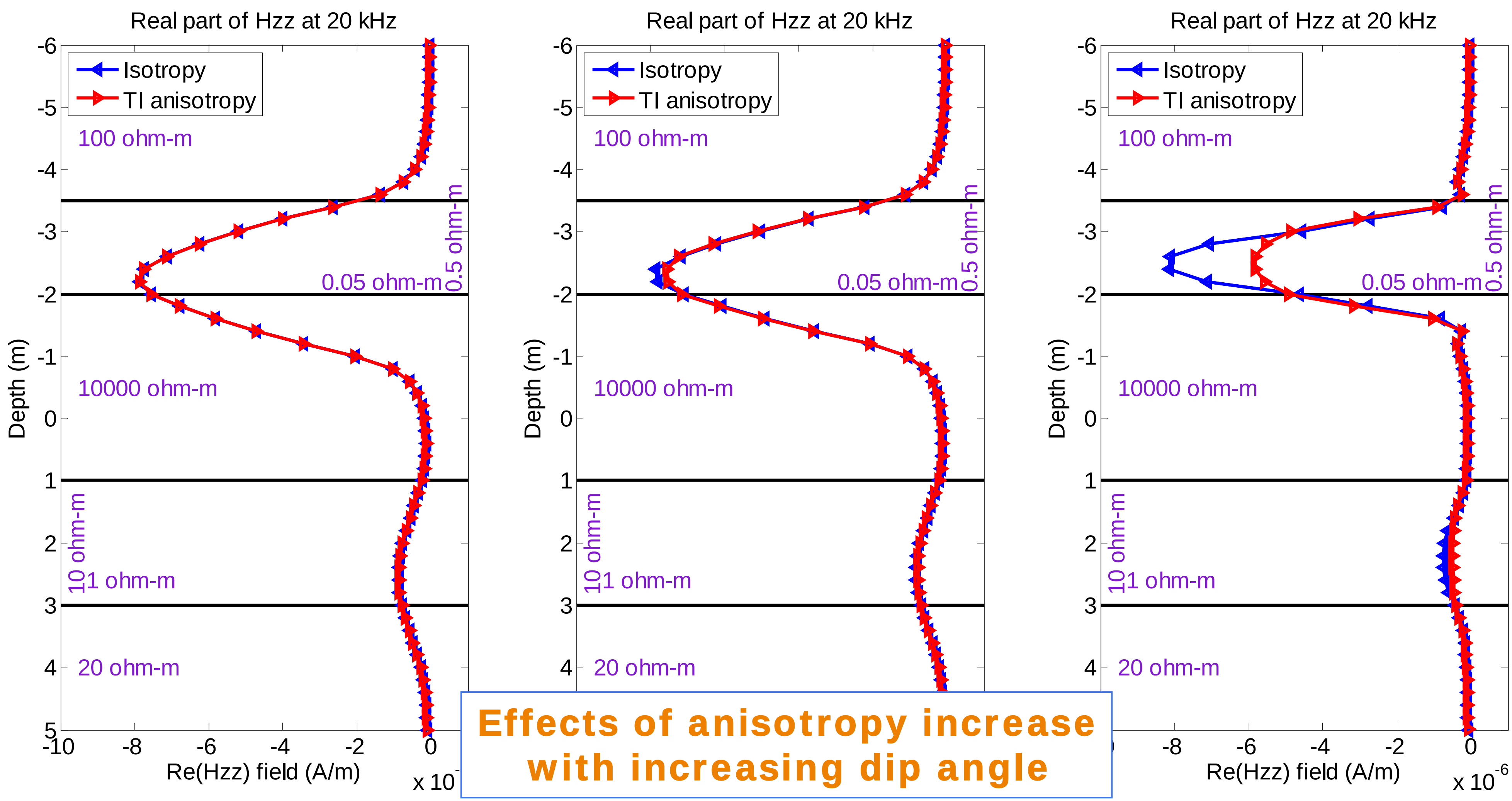

Effects of anisotropy increase with increasing dip angle

vertical **30 degrees** **60 degrees**

H_{zz} in Deviated Wells with Anisotropy (Im.)

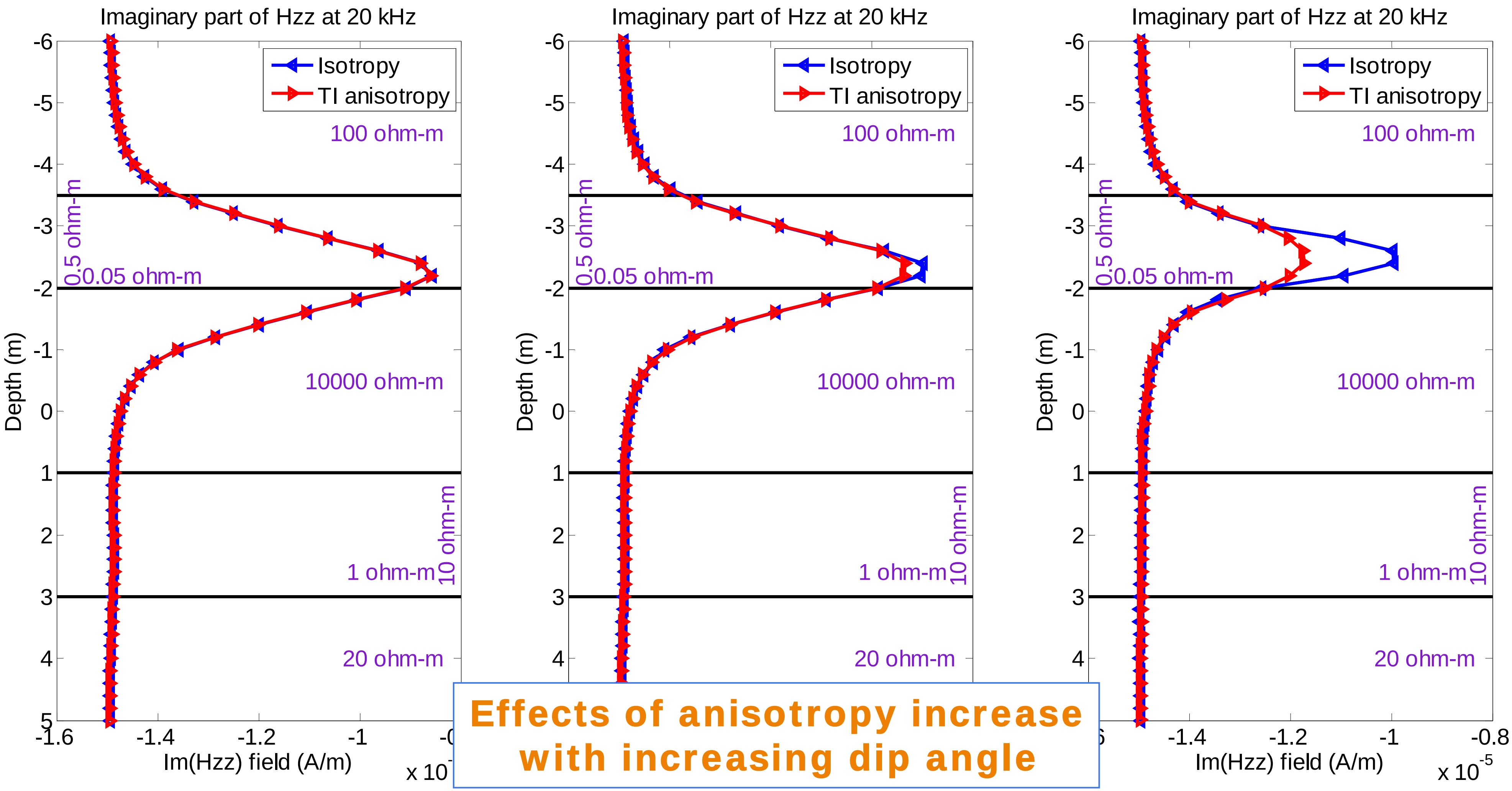

Effects of anisotropy increase with increasing dip angle

vertical | **30 degrees** | **60 degrees**

H_{xx} in Deviated Wells with Anisotropy (Re.)

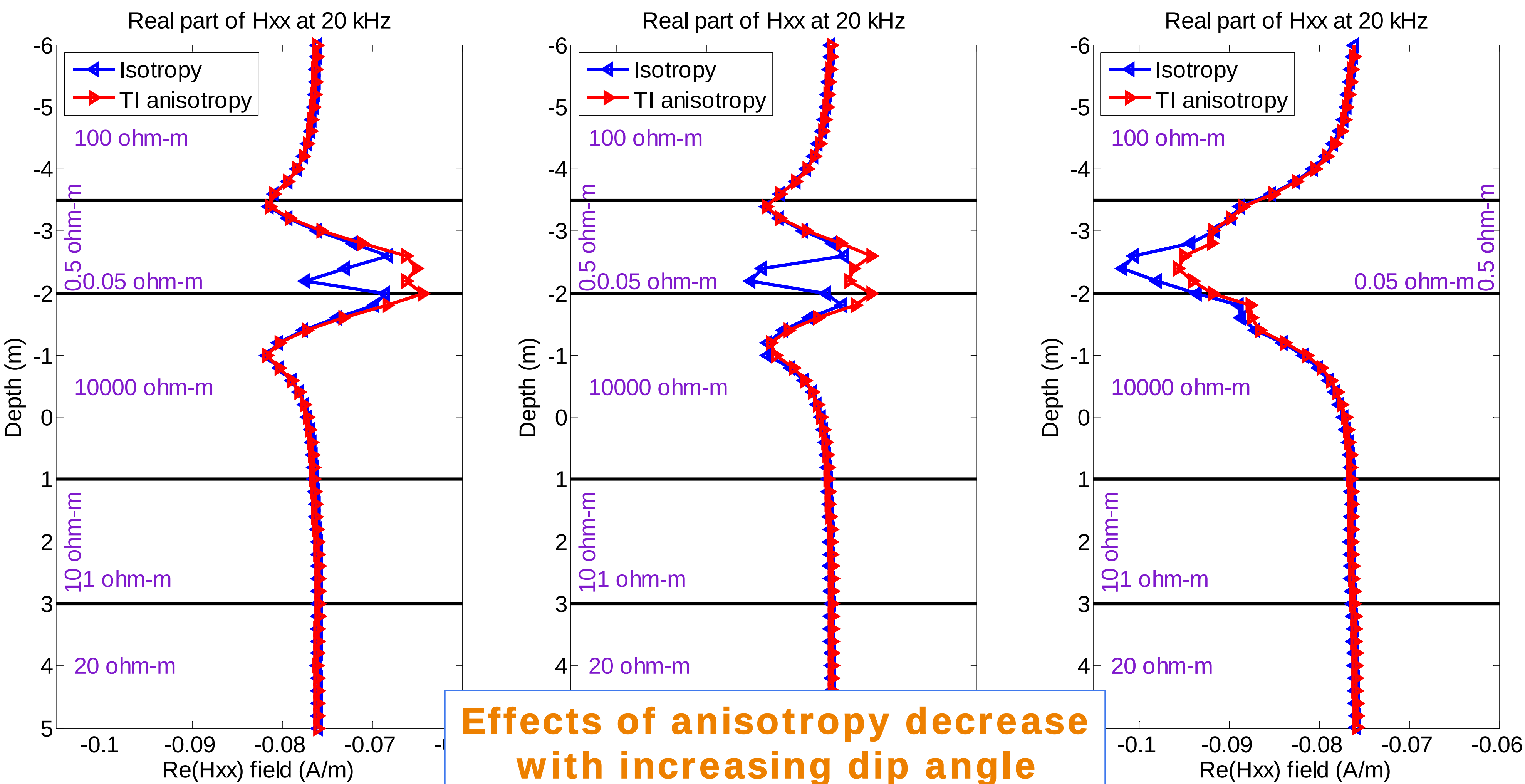

Effects of anisotropy decrease with increasing dip angle

vertical **30 degrees** **60 degrees**

H_{xx} in Deviated Wells with Anisotropy (Im.)

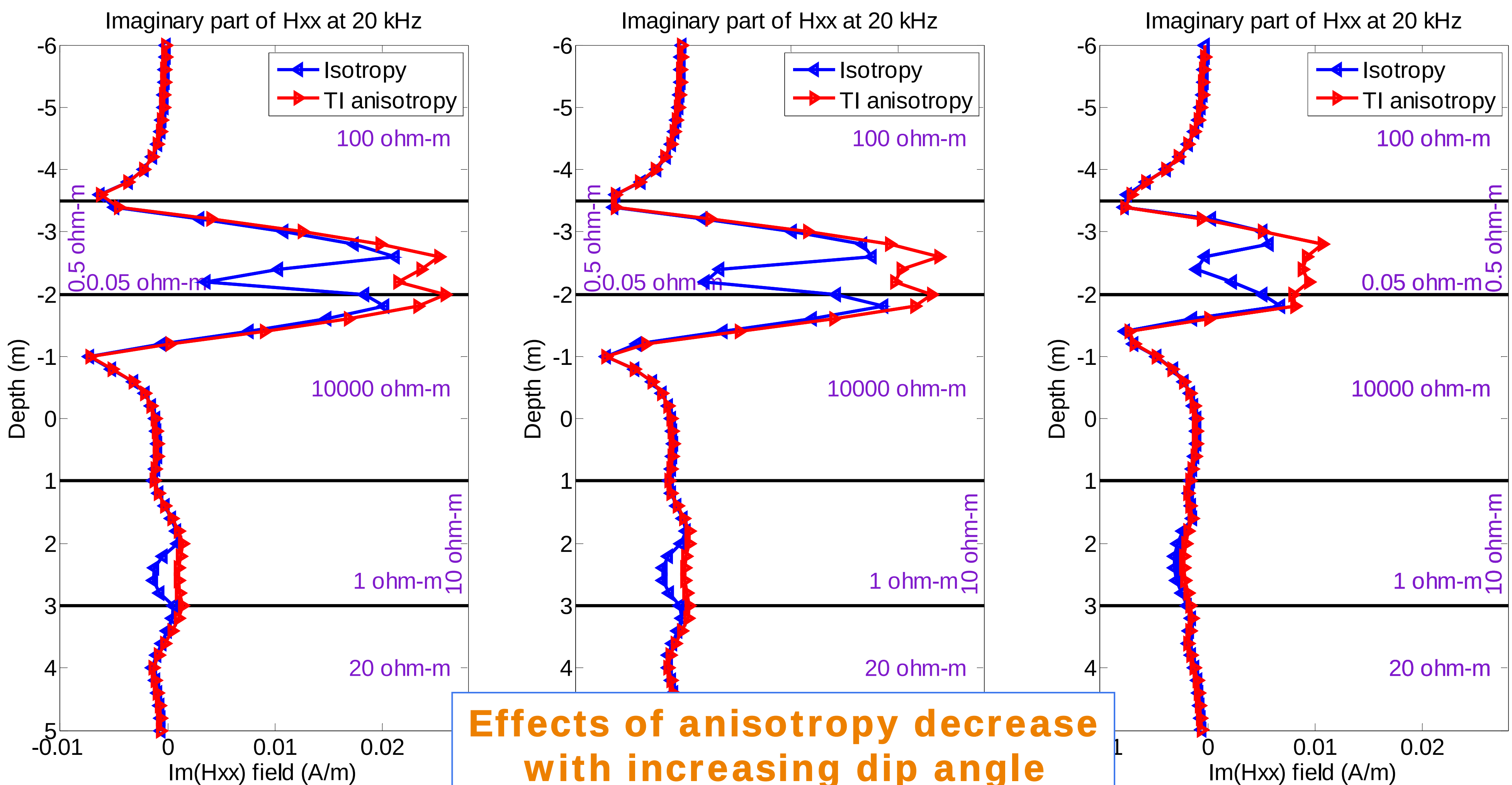

Effects of anisotropy decrease with increasing dip angle

vertical **30 degrees** **60 degrees**

H_{yy} in Deviated Wells with Anisotropy (Re.)

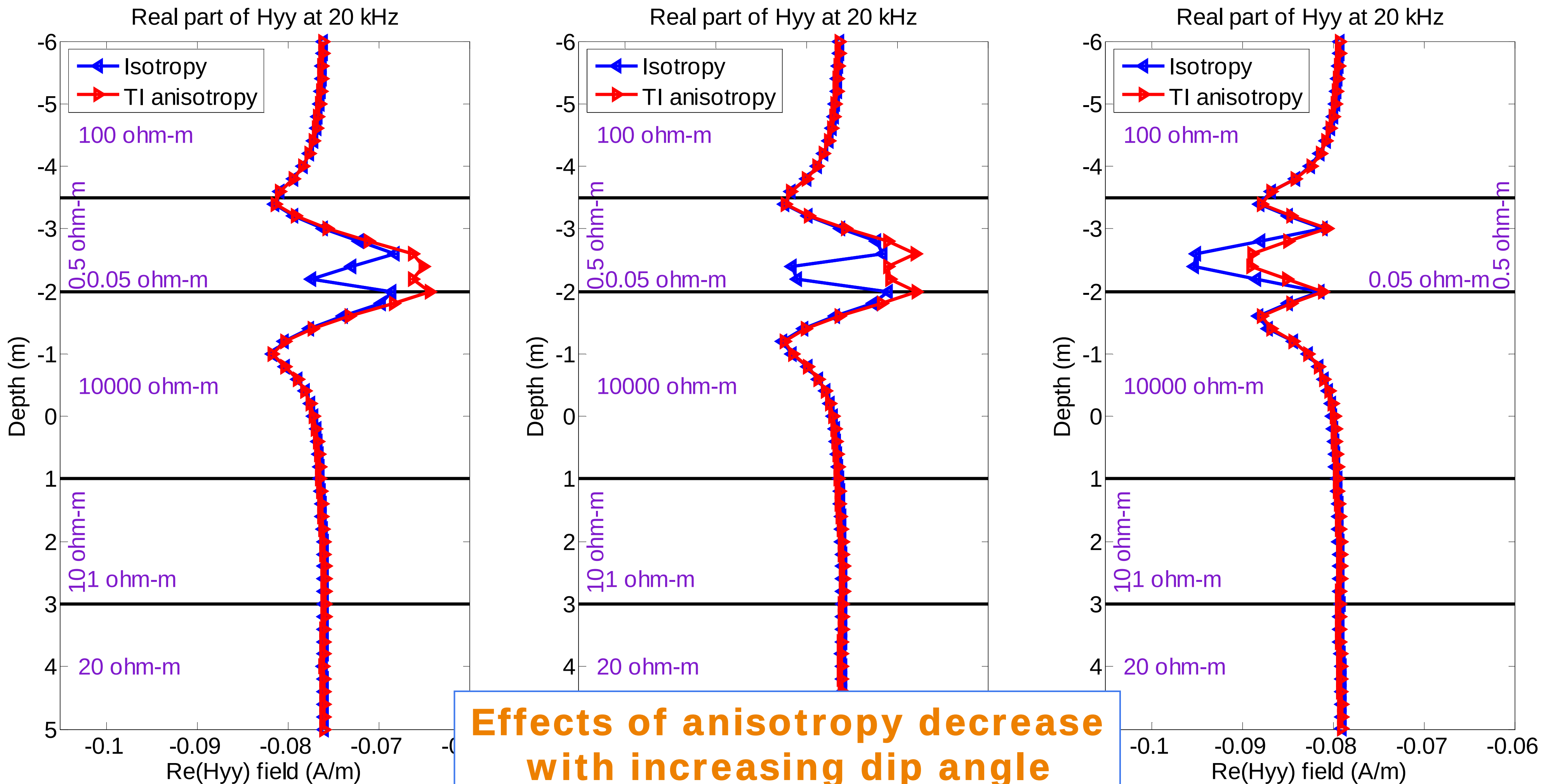

Effects of anisotropy decrease with increasing dip angle

vertical **30 degrees** **60 degrees**

H_{yy} in Deviated Wells with Anisotropy (Im.)

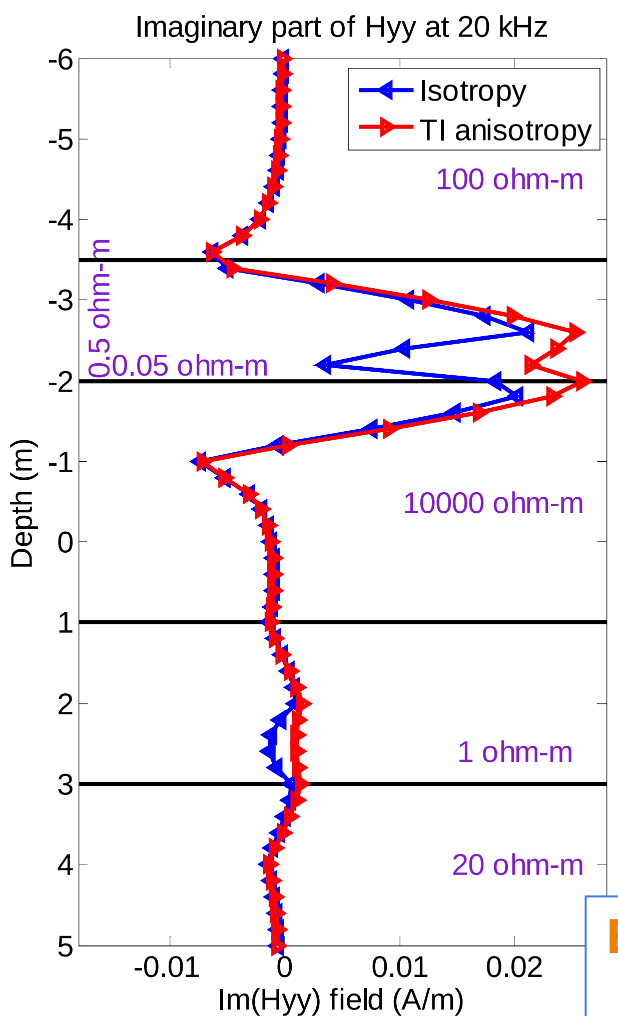

vertical

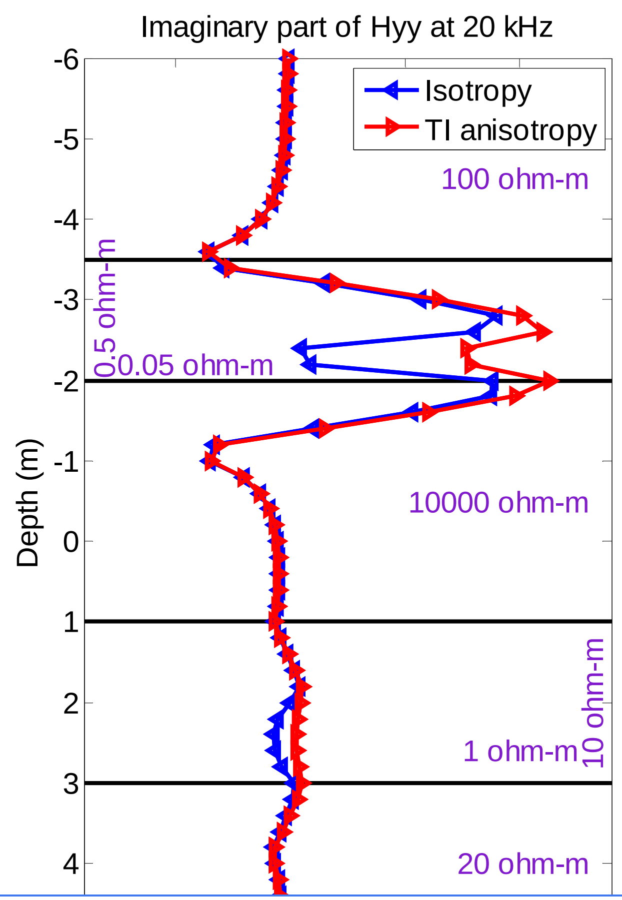

Effects of anisotropy decrease with increasing dip angle

30 degrees

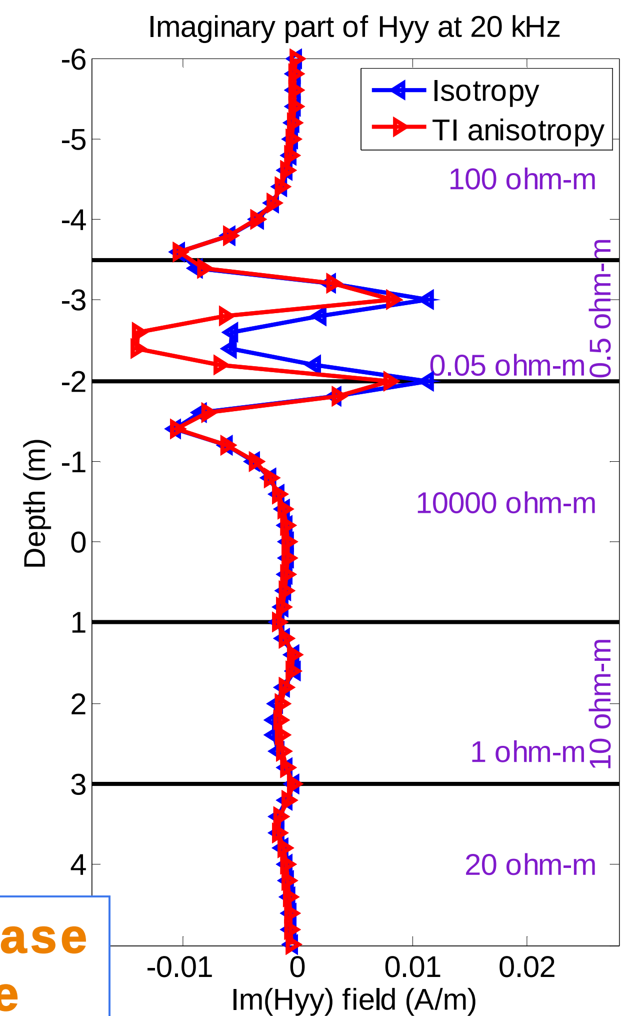

60 degrees

H_{xx} at 20 KHz and 2 MHz in Vertical Well

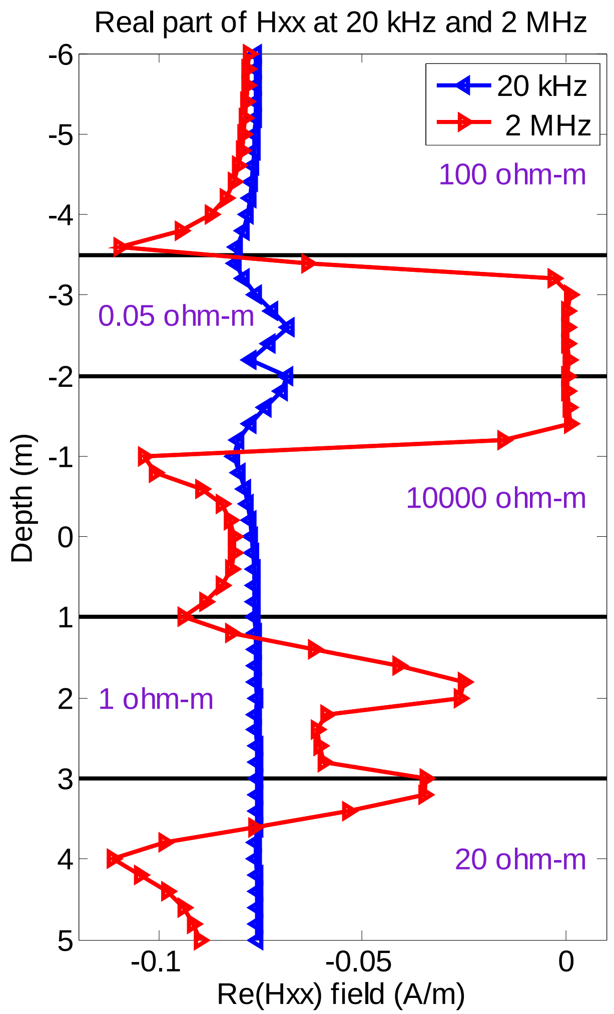

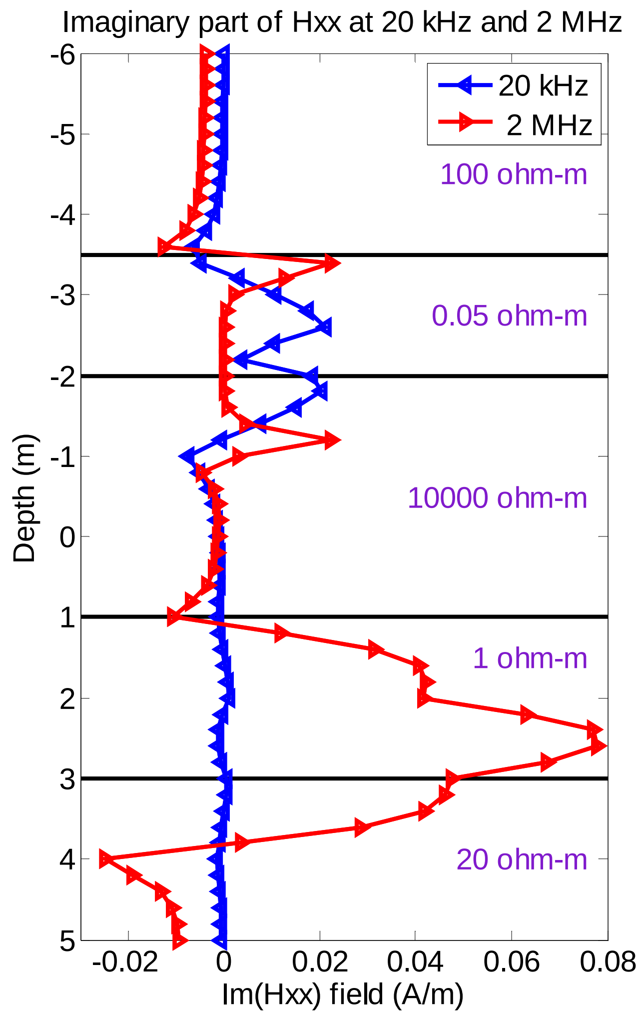

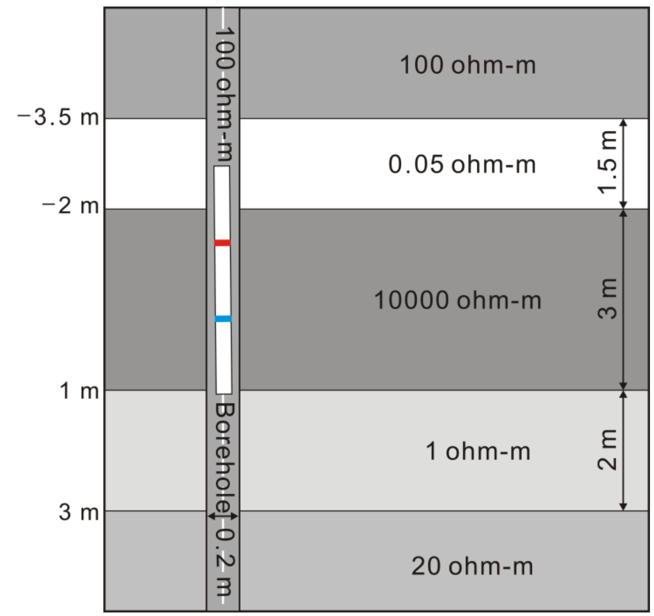

Larger variations at 2 MHz than at 20 kHz

Conclusions

- We successfully simulated 3D tri-axial induction measurements by combining the use of a Fourier series expansion in a non-orthogonal system of coordinates with a 2D high-order, self-adaptive *hp* finite-element method.

- Dip angle effects on tri-axial tools are larger than on more traditional induction logging instruments.

- Anisotropy effects on H_{xx} and H_{yy} decrease with increasing dip angle, while those on H_{zz} increase.

- H_{xx} at 20 kHz exhibits smaller variations than at 2 MHz.

Acknowledgements

Sponsors of UT Austin's consortium on Formation Evaluation:

Anadarko Petroleum Corporation
ارامكو السعودية Saudi Aramco
Baker Hughes Baker Atlas
bhpbilliton
bp
Chevron
ConocoPhillips
Agip Eni
ExxonMobil
HALLIBURTON
IMP Innovar INSTITUTO MEXICANO DEL PETRÓLEO
Marathon Marathon Oil Corporation
BR PETROBRAS
Schlumberger
Shell
StatoilHydro
TOTAL
Weatherford

SELF-ADAPTIVE *hp* FINITE-ELEMENT SIMULATION OF DC/AC DUAL-LATEROLOG MEASUREMENTS IN DIPPING, INVADED, AND ANISOTROPIC FORMATIONS

M. J. Nam, D. Pardo, and C. Torres-Verdín,
The University of Texas at Austin

***hp*-FEM team: D. Pardo, M. J. Nam, L. Demkowicz, C. Torres-Verdín, V. M. Calo, M. Paszynski, and P. J. Matuszyk**

Presentation at Korean Institute of Geoscience and Minerals (KIGAM), September 8, 2008.

THE UNIVERSITY OF TEXAS AT AUSTIN

Overview

1. **Main Lines of Research and Applications**
   - **Previous work**
   - **Main features of our technology**

2. **Application 1: Tri-Axial Induction Instruments (M. J. Nam)**

3. **Application 2: Dual-Laterolog Instruments (M. J. Nam)**

4. **Multi-Physics Inversion (D. Pardo)**

5. **Sonic Instruments (L. Demkowicz)**

Outline

- Introduction to Dual Laterolog
- Previous Work
- Method
- Numerical Results:
  - Groningen Effects on AC DLL
  - Dipping, Invaded, Anisotropic Formations (DC)
  - Eccentricity (DC)
- Conclusions

Dual Laterolog (DLL)

- **Determination of Intensities (W_j) of Bucking Currents**

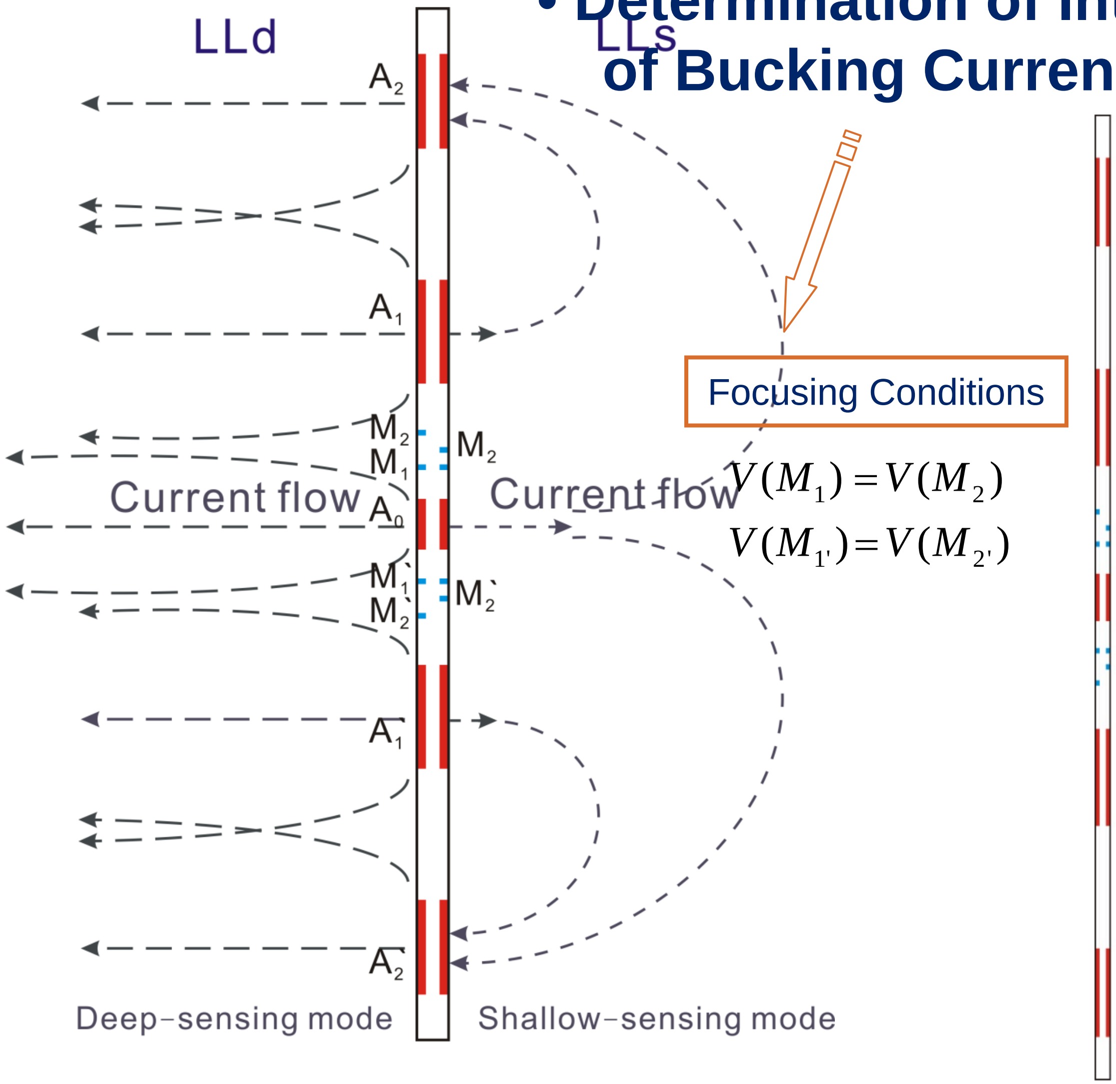

Focusing Conditions

$$V(M_1) = V(M_2)$$

$$V(M_{1'}) = V(M_{2'})$$

Summary from Last Year

Post-Processing Method

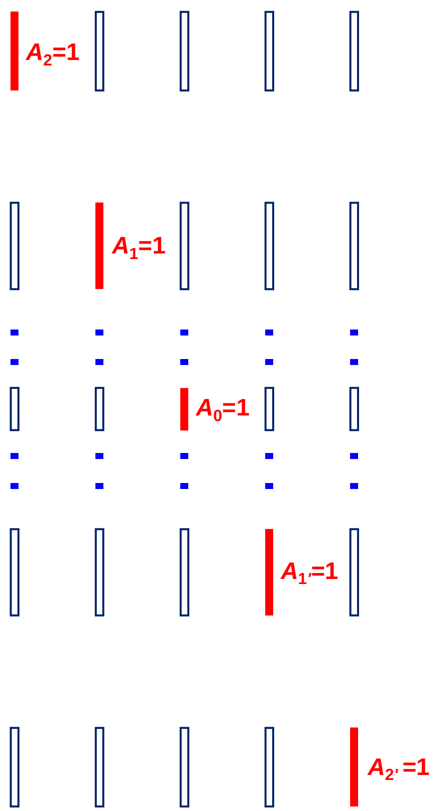

(1) Focusing conditions

$$V(M_1) = V(M_2)$$
$$V(M_{1'}) = V(M_{2'})$$

(2) Relationships between W_j

$$W_2 = (W_1 + c), \quad W_{2'} = (W_{1'} + c) \quad for\ \text{LLd}$$
$$W_2 = -(W_1 + c), \quad W_{2'} = -(W_{1'} + c) \quad for\ \text{LLs}$$

with $c = 0.5$

Total potential on M_i

→ Superposition principle

$$V(M_2) = W_2 V_{2,2} + W_1 V_{2,1} + V_{2,0} + W_{1'} V_{2,1'} + W_{2'} V_{2,2'}$$
$$V(M_1) = W_2 V_{1,2} + W_1 V_{1,1} + V_{1,0} + W_{1'} V_{1,1'} + W_{2'} V_{1,2'}$$
$$V(M_{1'}) = W_2 V_{1',2} + W_1 V_{1',1} + V_{1',0} + W_{1'} V_{1',1'} + W_{2'} V_{1',2'}$$
$$V(M_{2'}) = W_2 V_{2',2} + W_1 V_{2',1} + V_{2',0} + W_{1'} V_{2',1'} + W_{2'} V_{2',2'}$$

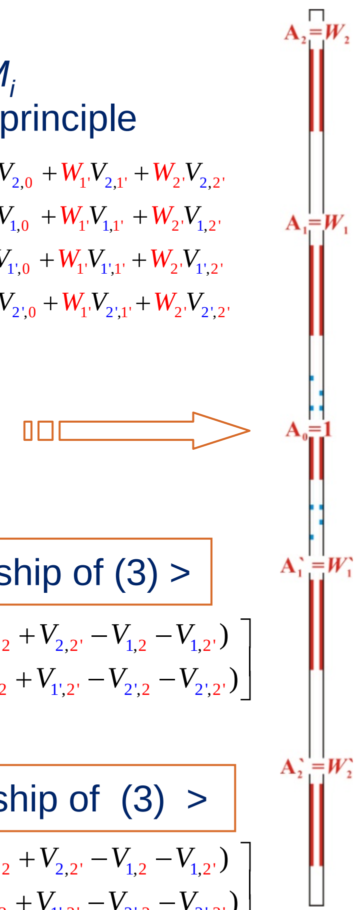

W_j for LLd: < from (1) and (2) with the LLd relationship of (3) >

$$\begin{bmatrix} V_{1,2}+V_{1,1}-V_{2,2}-V_{2,1} & V_{1,1'}+V_{1,2'}-V_{2,1'}-V_{2,2'} \\ V_{2',2}+V_{2',1}-V_{1',2}-V_{1',1} & V_{2',1'}+V_{2',2'}-V_{1',1'}-V_{1',2'} \end{bmatrix} \begin{bmatrix} W_1 \\ W_{1'} \end{bmatrix} = \begin{bmatrix} V_{2,0}-V_{1,0}+c(V_{2,2}+V_{2,2'}-V_{1,2}-V_{1,2'}) \\ V_{1',0}-V_{2',0}+c(V_{1',2}+V_{1',2'}-V_{2',2}-V_{2',2'}) \end{bmatrix}$$

W_j for LLs: < from (1) and (2) with the LLs relationship of (3) >

$$\begin{bmatrix} V_{2,2}+V_{1,1}-V_{2,1}-V_{1,2} & V_{2,2'}+V_{1,1'}-V_{1,2'}-V_{2,1'} \\ V_{1',2}+V_{2',1}-V_{1',1}-V_{2',2} & V_{1',2'}+V_{2',1'}-V_{2',2'}-V_{1',1'} \end{bmatrix} \begin{bmatrix} W_1 \\ W_{1'} \end{bmatrix} = \begin{bmatrix} V_{2,0}-V_{1,0}+c(V_{2,2}+V_{2,2'}-V_{1,2}-V_{1,2'}) \\ V_{1',0}-V_{2',0}+c(V_{1',2}+V_{1',2'}-V_{2',2}-V_{2',2'}) \end{bmatrix}$$

One problem with several RHSs

Summary from Last Year

Embedded Post-Processing Method

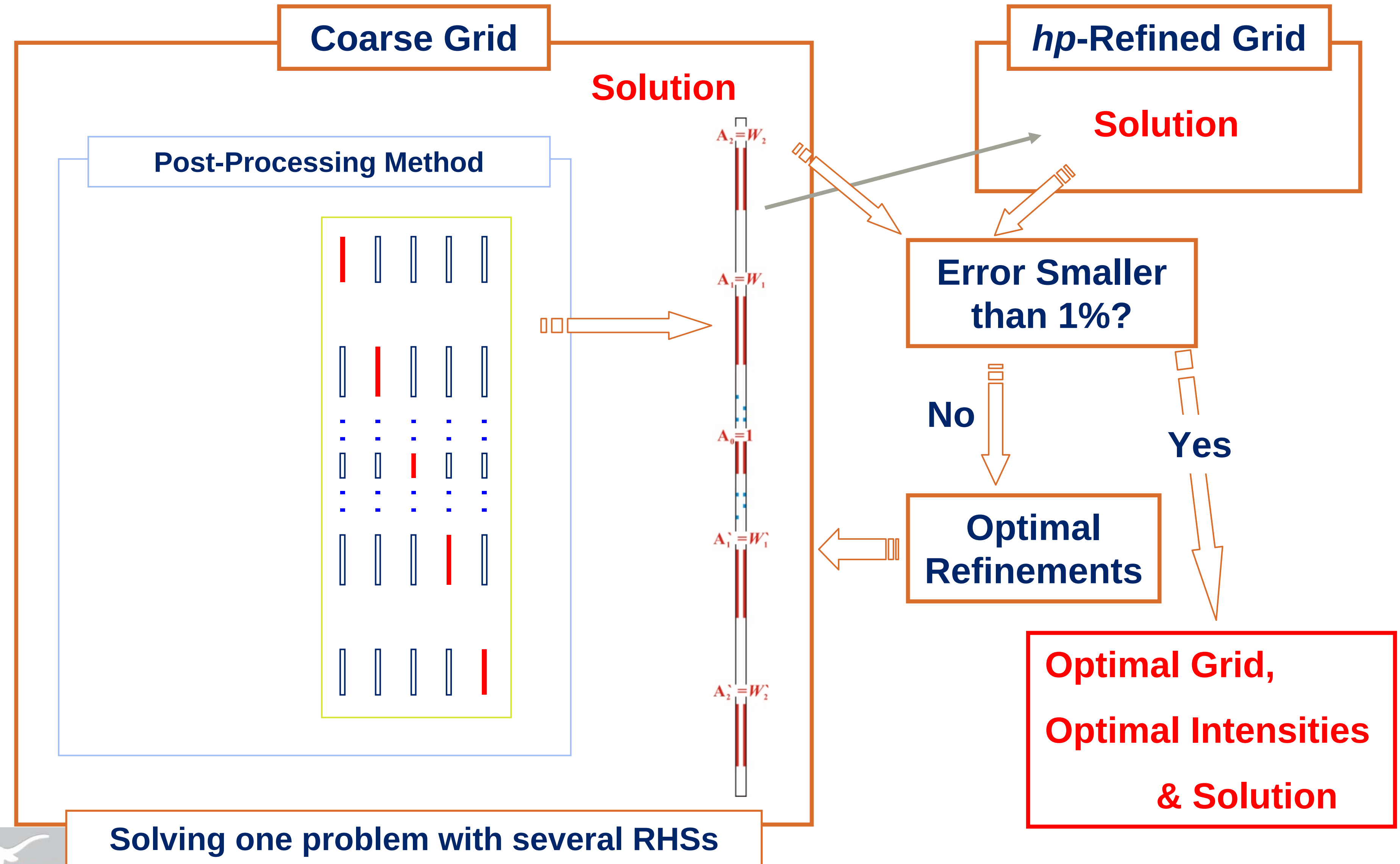

Summary from Last Year

What we modeled in simulating the DLL tool

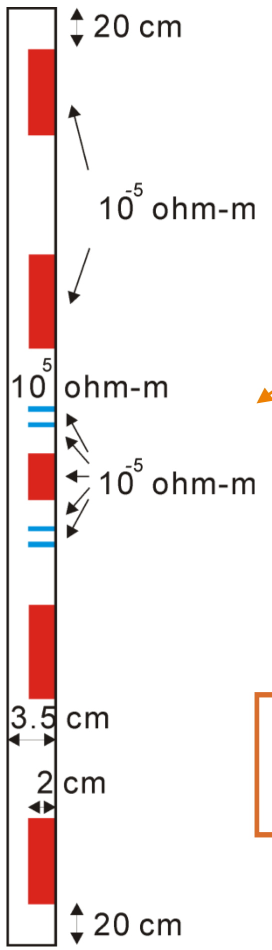

The resistivities and radial lengths of electrode and mandrel.

The vertical dimensions and locations of each electrode:
We followed the vertical tool configuration of a commercial tool

Summary from Last Year

Deviated Wells (0, 10, 45, and 60 degrees) at DC

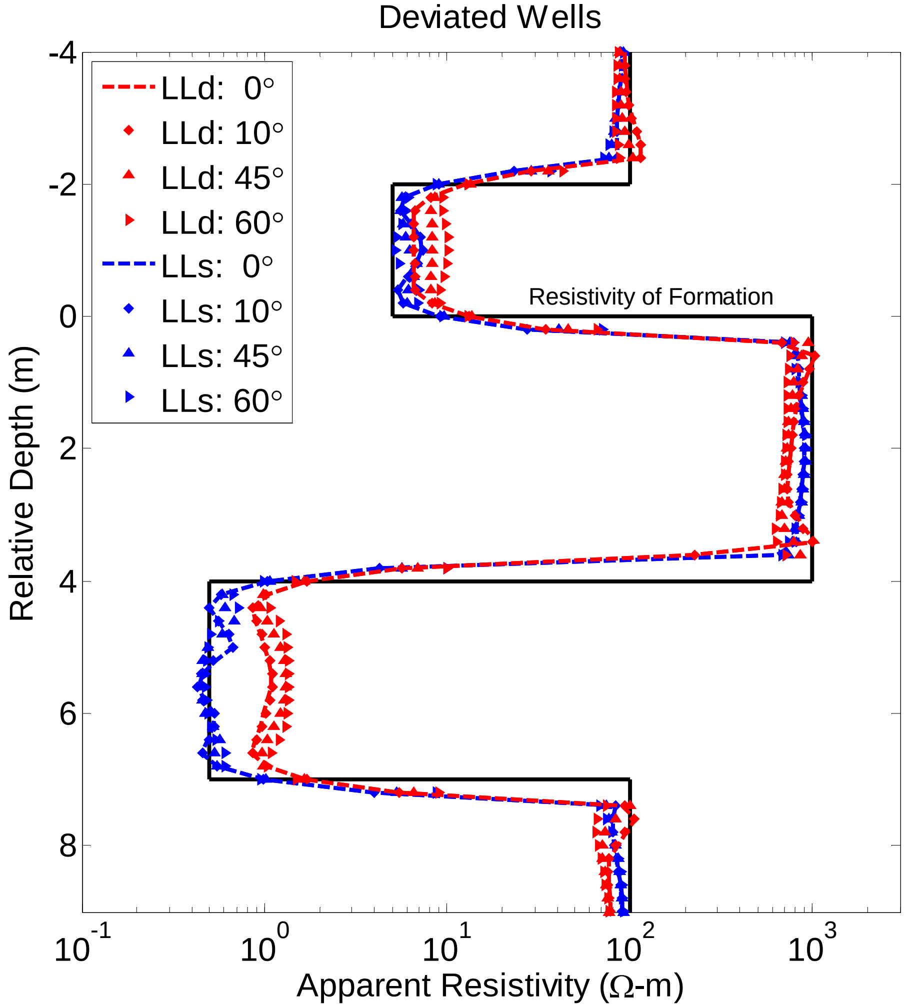

Effects of dip angle:

Thin layer ↑

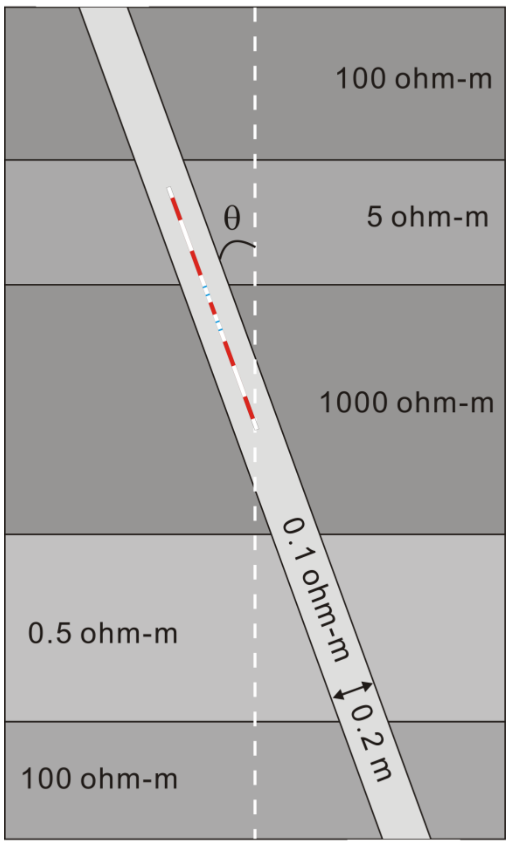

Summary from Last Year

Anisotropic Formation (60- and 0-degree Deviated Wells) at DC

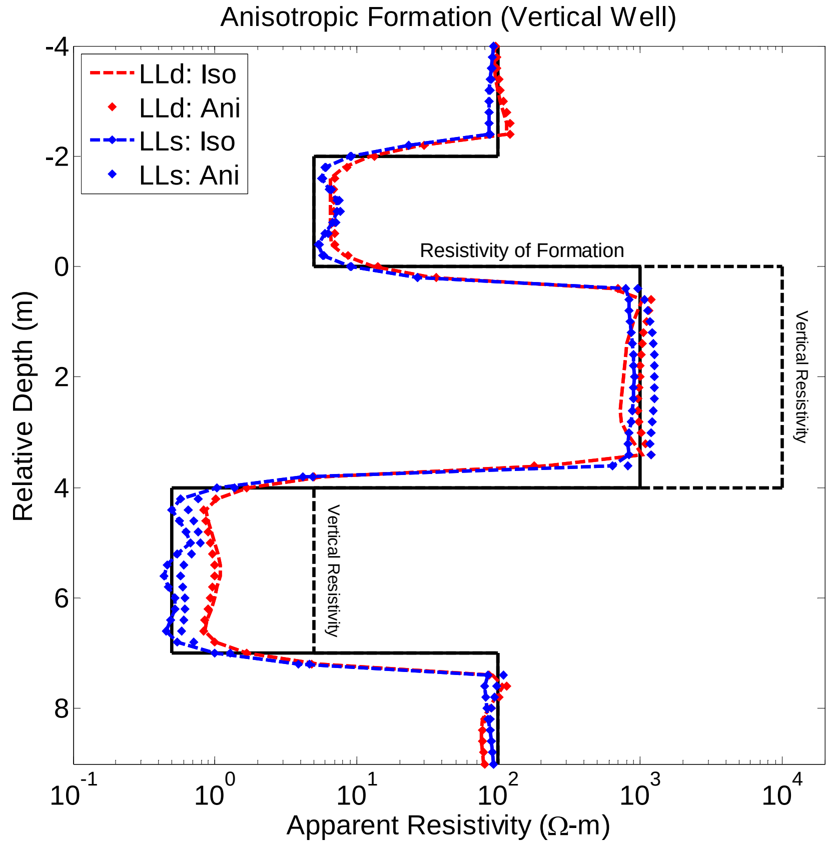

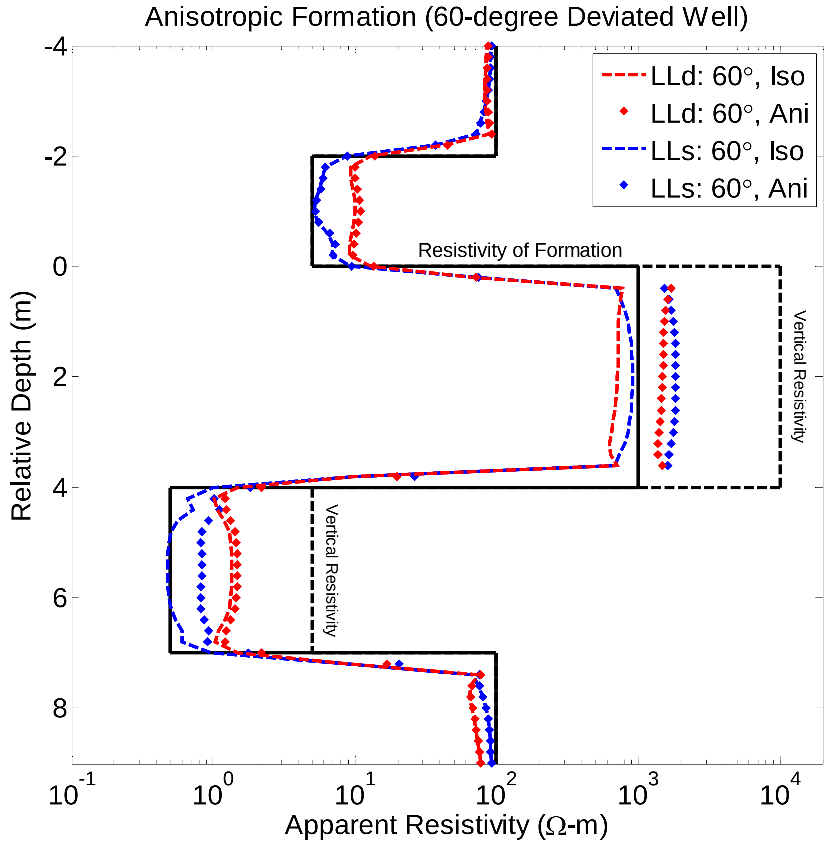

Effects of anisotropy increase with increase of dip angle

Method for Simulating AC DLL Measurements

Combination of:

1. **A Self-Adaptive Goal-Oriented *hp*-FEM for AC problems**

2. **Embedded Post-Processing Method (EPPM)**

3. **Parallel Implementation**

Simulating AC DLL Measurements 1

Main challenges when simulating AC DLL measurements 1:

Introducing in the AC formulation a source equivalent to $\nabla \cdot J$

To avoid simulating the inner wiring system!!

Simulating AC DLL Measurements 1

Main challenges when simulating AC DLL measurements 1:

Governing equation

Variational formulation

DC

$$\nabla\cdot(\sigma\nabla\cdot u)=\nabla\cdot\mathbf{J}^{imp}$$

$$<\nabla v,\sigma\nabla u>_{L^2(\Omega)}=<v,\nabla\cdot\mathbf{J}^{imp}>_{L^2(\Omega)}+<v,g>_{L^2(\Gamma_N)}\quad\forall v\in H_D^1(\Omega)$$

AC

$$\begin{cases}\nabla\times\mathbf{H}=(\sigma+j\omega\varepsilon)\mathbf{E}+\mathbf{J}\\ \nabla\times\mathbf{E}=-j\omega\mathbf{H}\end{cases}$$

$$<\nabla\times\overline{\mathbf{F}},\mu^{-1}\nabla\times\mathbf{E}>_{L^2(\Omega)}-<\overline{\mathbf{F}},(\omega^2\varepsilon-j\omega\sigma)\mathbf{E}>_{L^2(\Omega)}-<\overline{\mathbf{F}},(\omega^2\varepsilon-j\omega\sigma)\nabla p>=$$
$$-j\omega\left\langle\overline{\mathbf{F}},\mathbf{J}^{imp}\right\rangle_{L^2(\Omega)}+j\omega\left\langle\overline{\mathbf{F}}_t,\mathbf{J}_S^{imp}\right\rangle_{L^2(\Gamma_H)}\ \ \forall\mathbf{F}\in H_{\Gamma_E}(\text{curl};\Omega)$$

0

Scalar potential eq.→

$$-<\nabla\overline{q},(\omega^2\varepsilon-j\omega\sigma)\mathbf{E}>_{L^2(\Omega)}=$$
$$-j\omega\left\langle\nabla\overline{q},\mathbf{J}^{imp}\right\rangle_{L^2(\Omega)}+j\omega\left\langle\nabla\overline{q},\mathbf{J}_S^{imp}\right\rangle_{L^2(\Gamma_H)}\ \ \forall q\in H_D^1$$

0

introducing ∇·J

$$j\omega<\overline{q},\nabla\cdot\mathbf{J}^{imp}>_{L^2(\Omega)}$$

$$\therefore-<\nabla\overline{q},(\omega^2\varepsilon-j\omega\sigma)\mathbf{E}>_{L^2(\Omega)}=j\omega<\overline{q},\nabla\cdot\mathbf{J}^{imp}>_{L^2(\Omega)}\quad\forall q\in H_D^1$$

Simulating AC DLL Measurements 1

Main challenges when simulating AC DLL measurements 1:

Governing equation

Variational formulation

DC

$$\nabla \cdot (\sigma \nabla \cdot u) = \nabla \cdot \mathbf{J}^{imp}$$

$$< \nabla v, \sigma \nabla u >_{L^2(\Omega)} = < v, \nabla \cdot \mathbf{J}^{imp} >_{L^2(\Omega)} + < v, g >_{L^2(\Gamma_N)} \quad \forall v \in H_D^1(\Omega)$$

AC

$$\begin{cases} \nabla \times \mathbf{H} = (\sigma + j\omega\varepsilon)\mathbf{E} + \mathbf{J} \\ \nabla \times \mathbf{E} = -j\omega \mathbf{H} \end{cases}$$

Final AC variational formulations we use:

$$< \nabla \times \overline{\mathbf{F}}, \mu^{-1} \nabla \times \mathbf{E} >_{L^2(\Omega)} - < \overline{\mathbf{F}}, (\omega^2 \varepsilon - j\omega\sigma)\mathbf{E} >_{L^2(\Omega)} - < \overline{\mathbf{F}}, (\omega^2 \varepsilon - j\omega\sigma)\nabla p > = 0 \quad \forall \mathbf{F} \in H_{\Gamma_E}(\text{curl};\Omega)$$

$$- < \nabla \overline{q}, (\omega^2 \varepsilon - j\omega\sigma)\mathbf{E} >_{L^2(\Omega)} = j\omega < \overline{q}, \nabla \cdot \mathbf{J}^{imp} >_{L^2(\Omega)} \quad \forall q \in H_D^1$$

Simulating AC DLL Measurements 2

Main challenges when simulating AC DLL measurements 2:

Simulation of current return at earth surface

1. No current return results in no Groningen effects.

(Numerical results will be shown)

2. We have to simulate the earth surface.

→ Our computing domain is larger than

2 km in the vertical direction.

Simulating AC DLL Measurements 2

Main challenges when simulating AC DLL measurements 2:

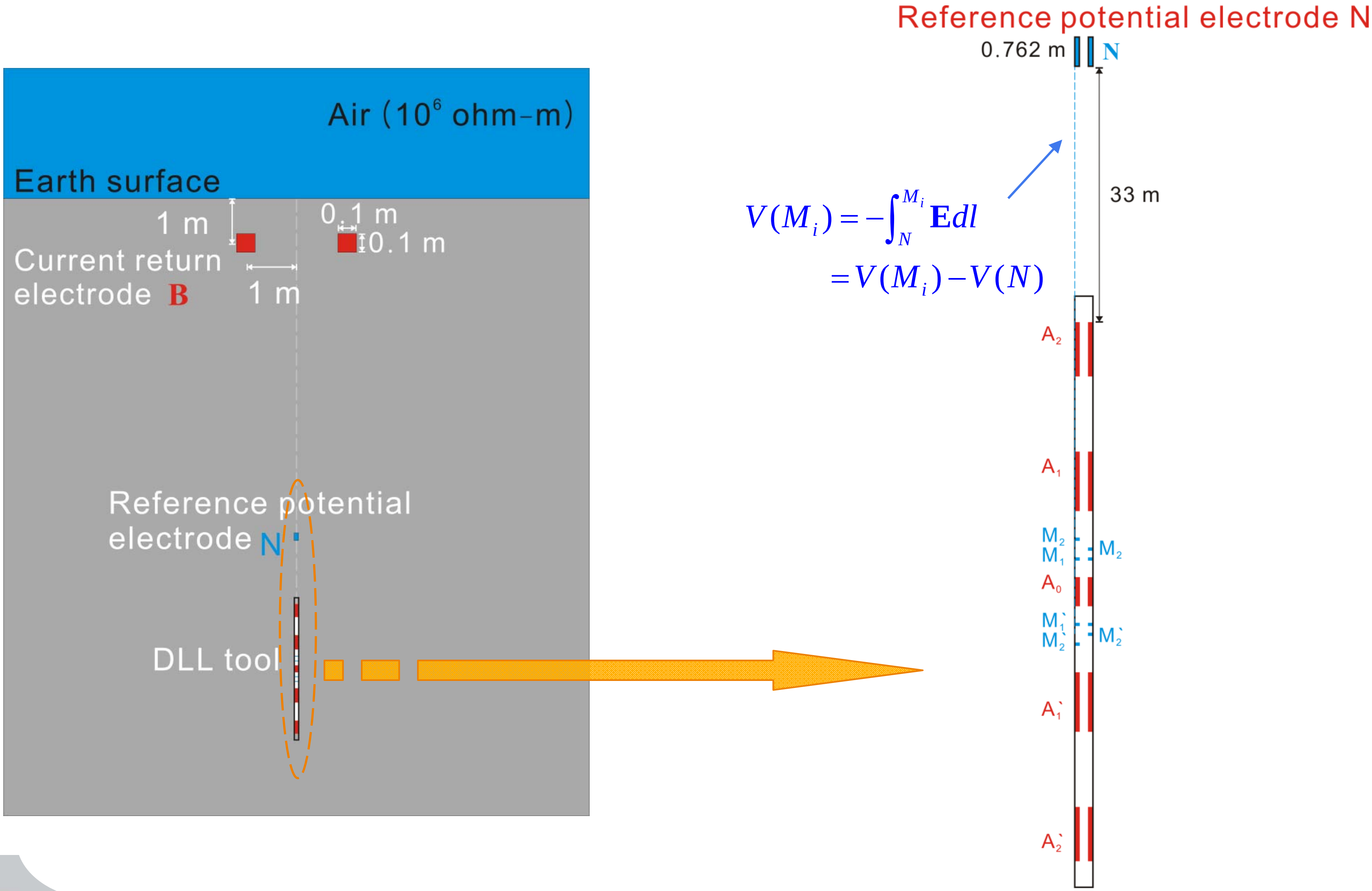

$$V(M_i) = -\int_N^{M_i} \mathbf{E}dl$$
$$= V(M_i) - V(N)$$

Groningen Effects on LLd at DC and AC

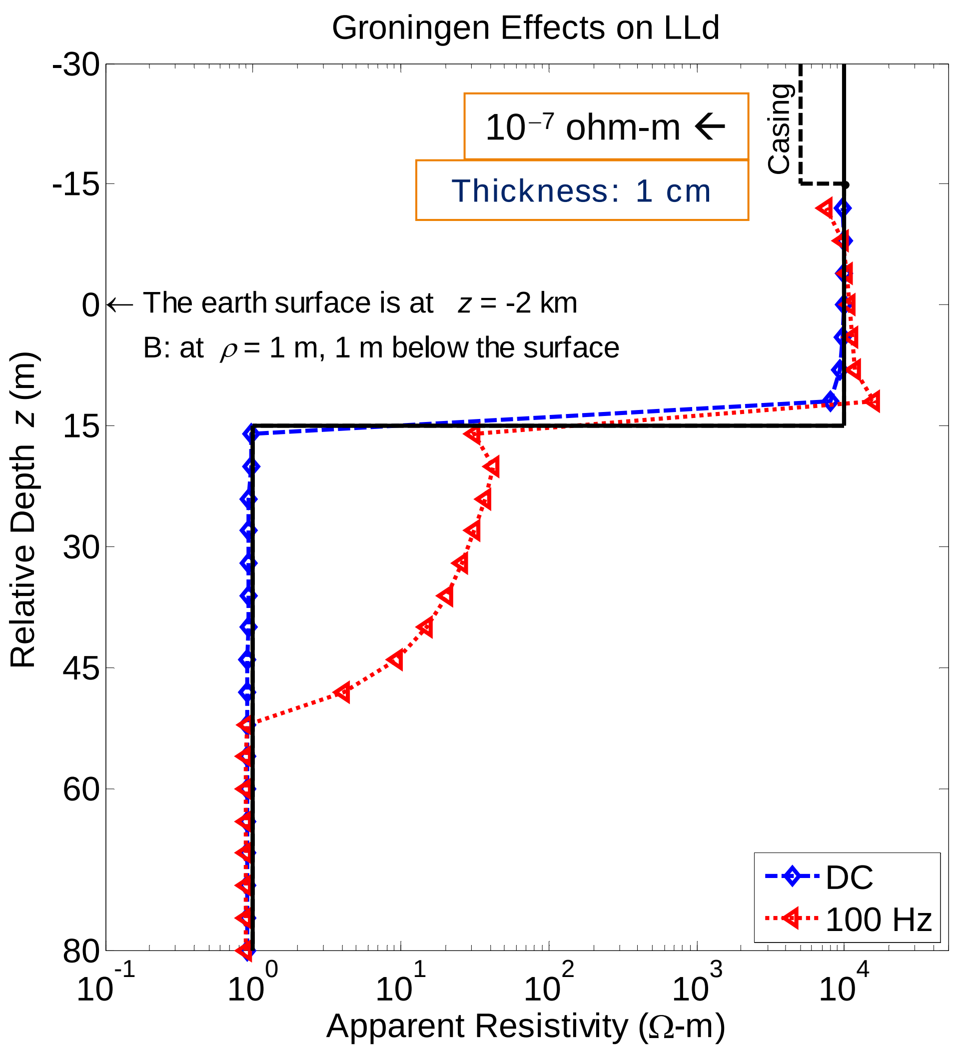

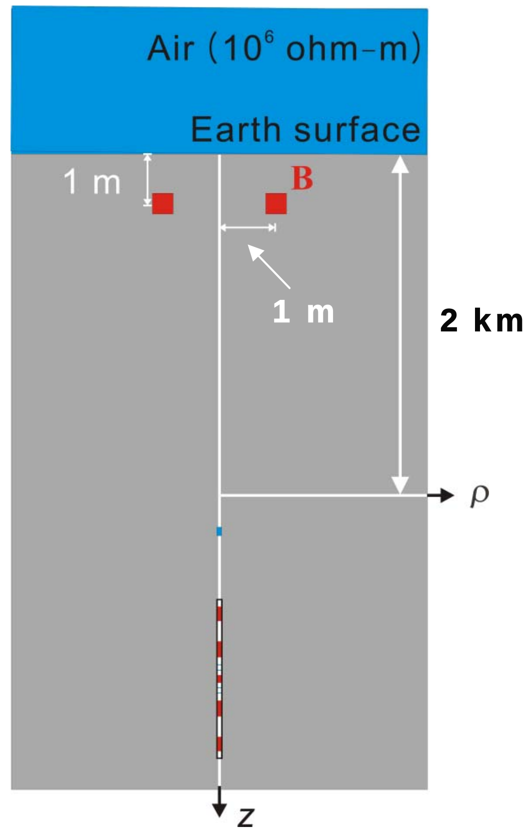

DC: No Groningen effects

AC: Groningen effects

Groningen Effects on LLd at 100 Hz (I)

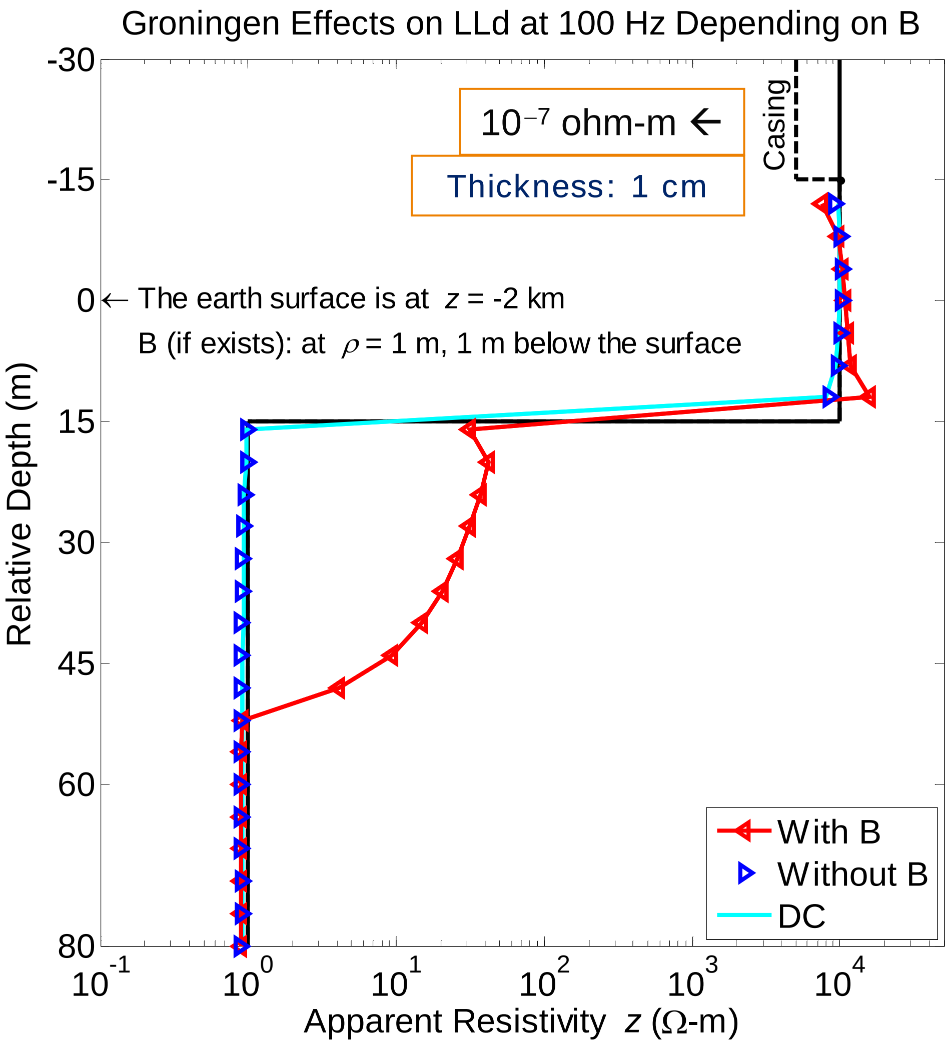

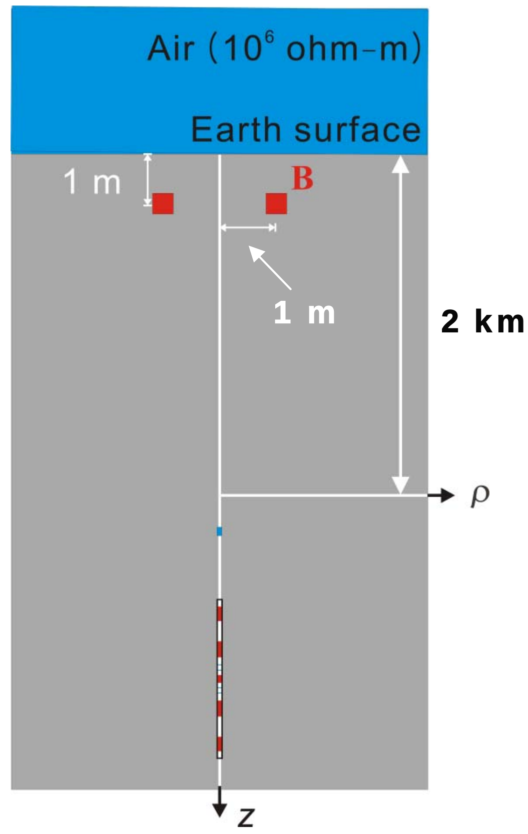

No B:

No Groningen effects

Groningen Effects on LLd at 100 Hz (II)

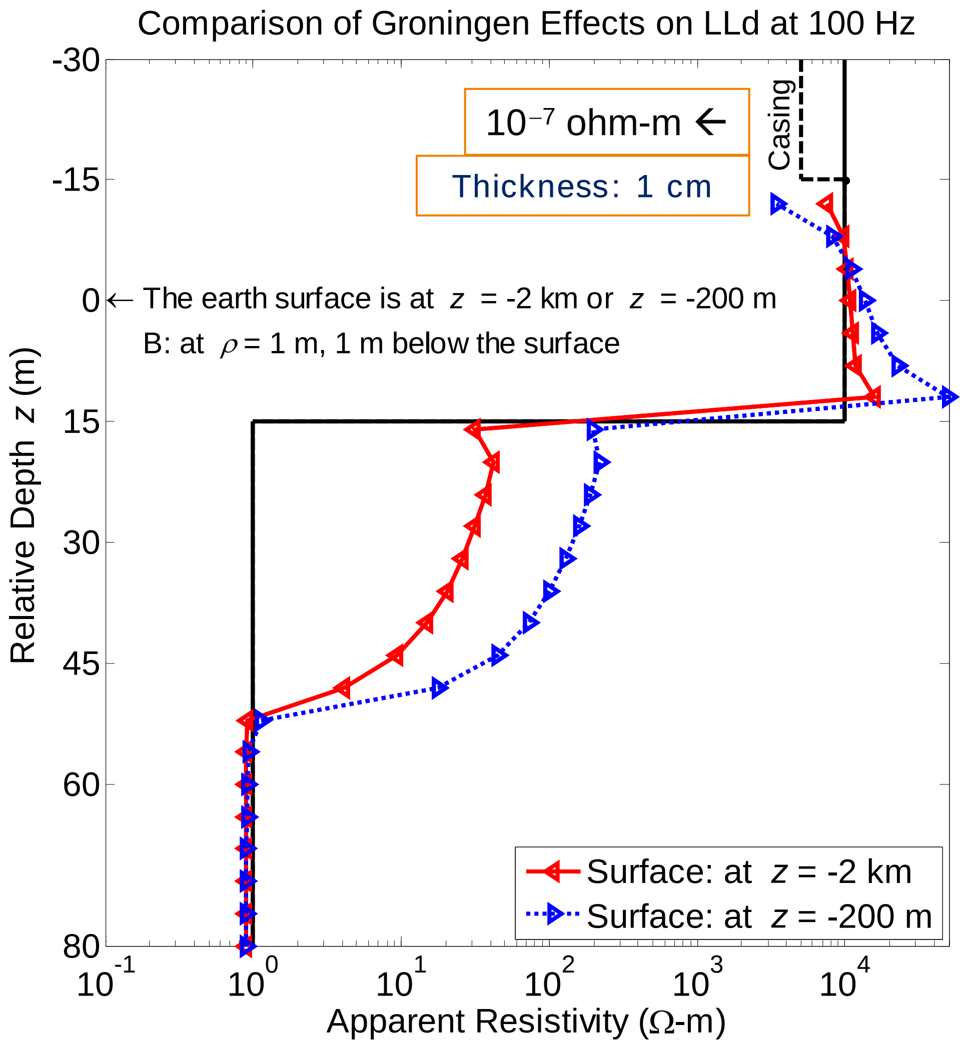

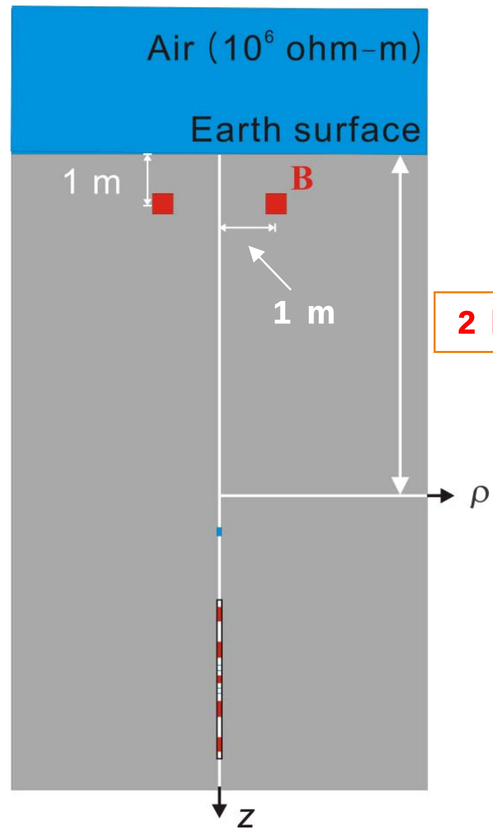

Further B in the *z* direction:

smaller Groningen effects

Groningen Effects on LLd at 100 Hz (III)

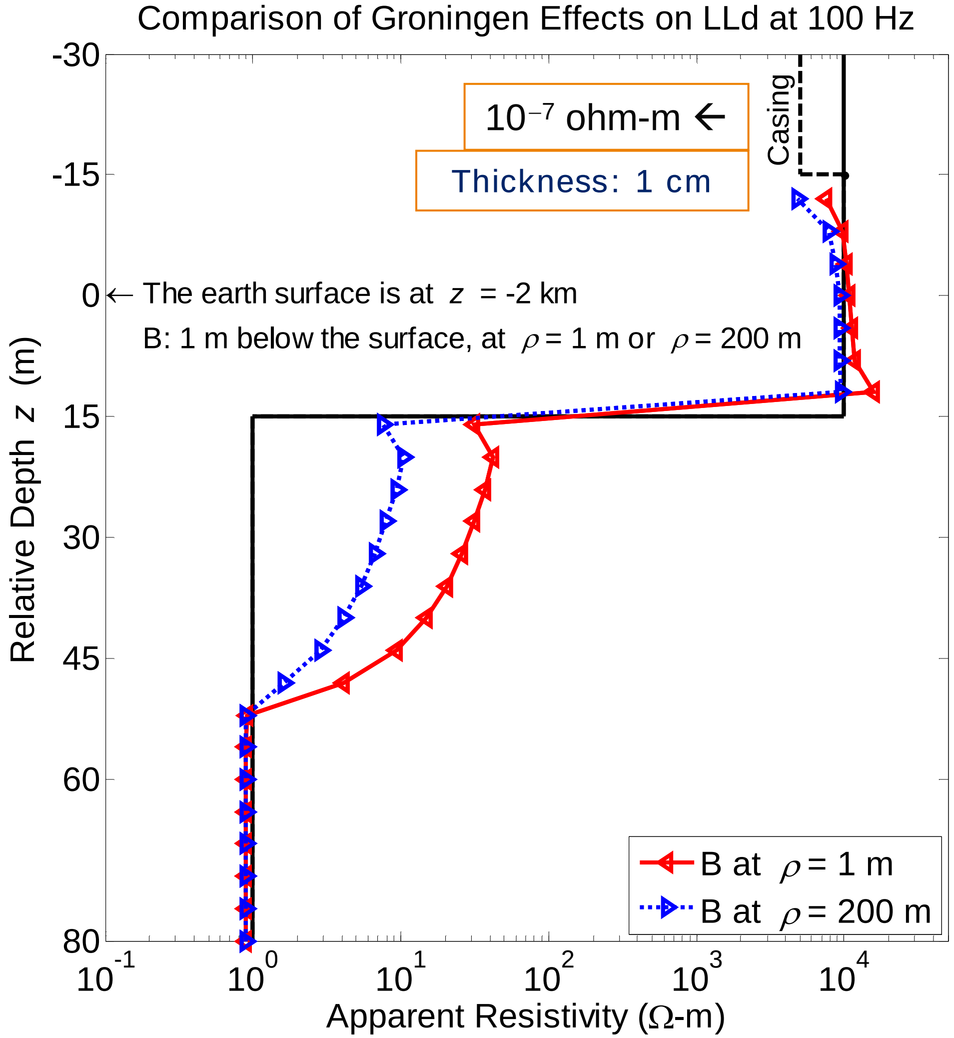

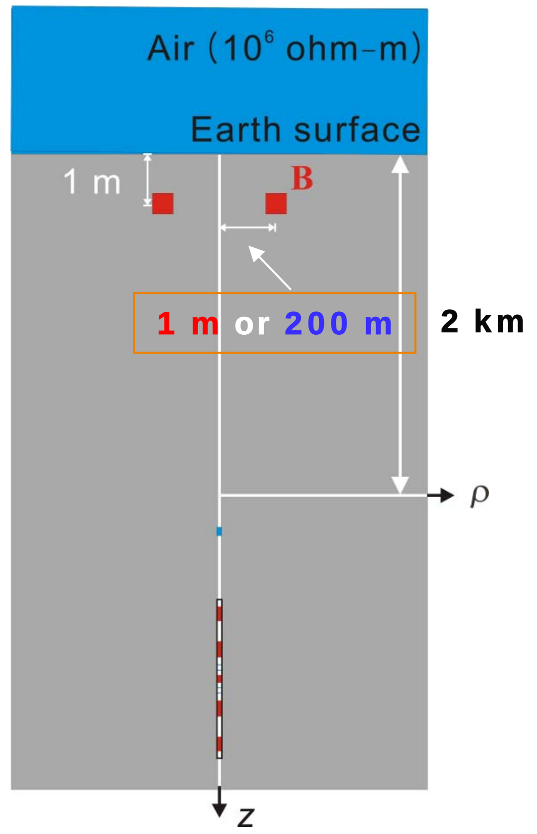

Further B in the ρ direction: smaller Groningen effects

Groningen Effects on LLd at 100 Hz (IV)

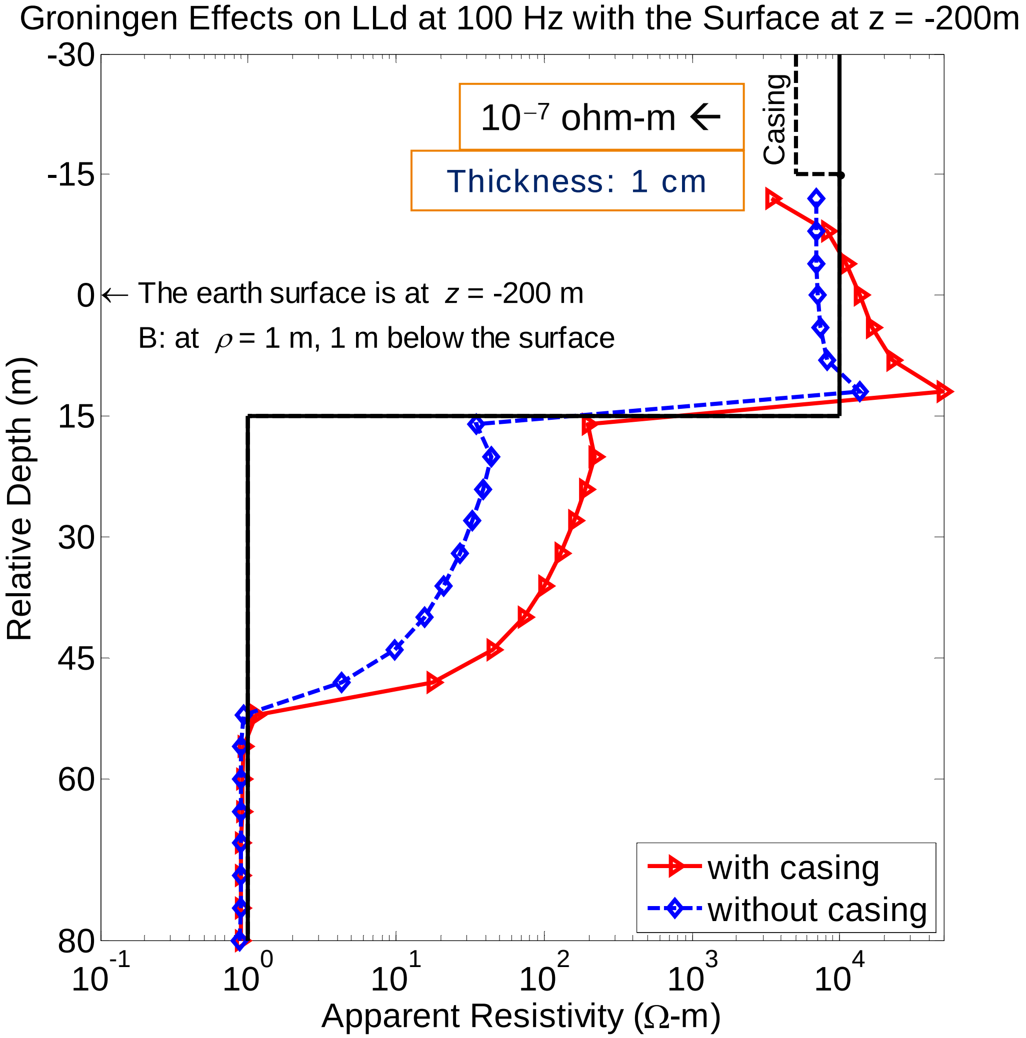

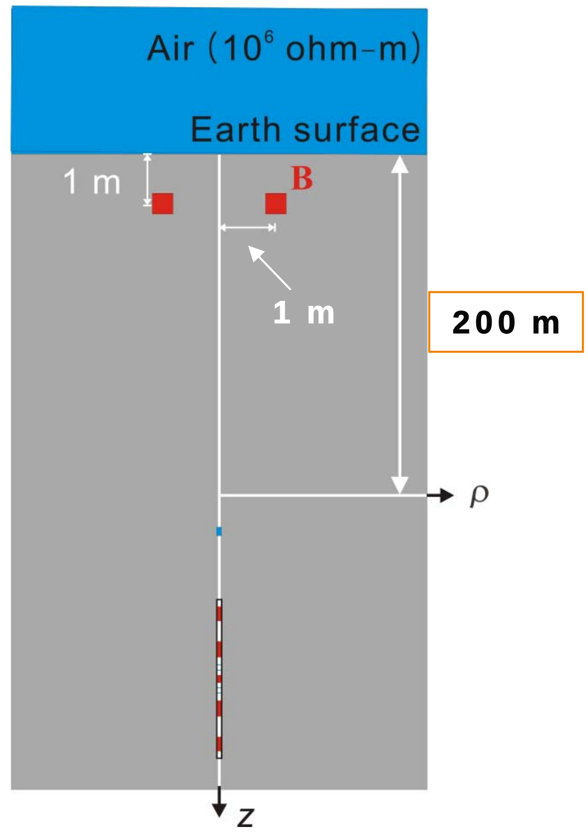

No casing with B 200 m apart: smaller Groningen effects

Groningen Effects on LLd at 100 Hz (V)

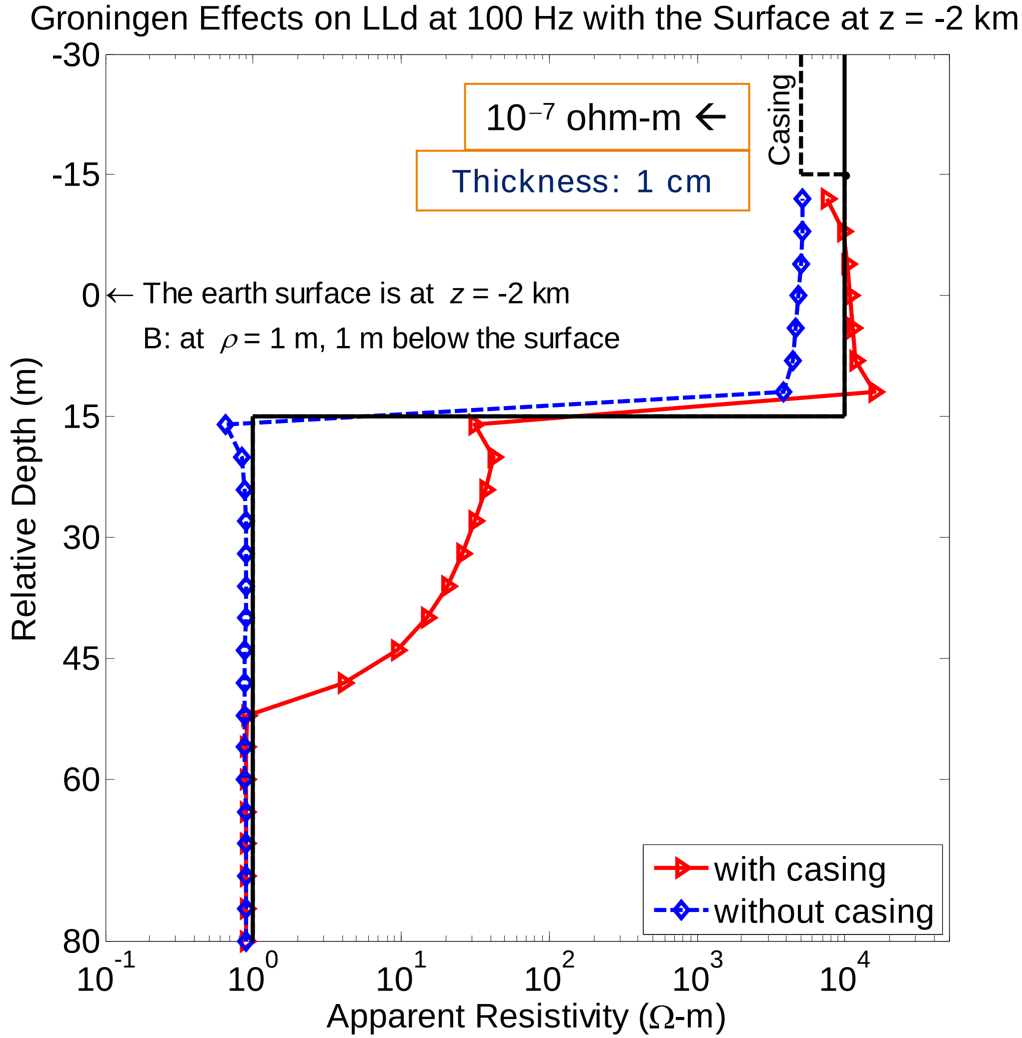

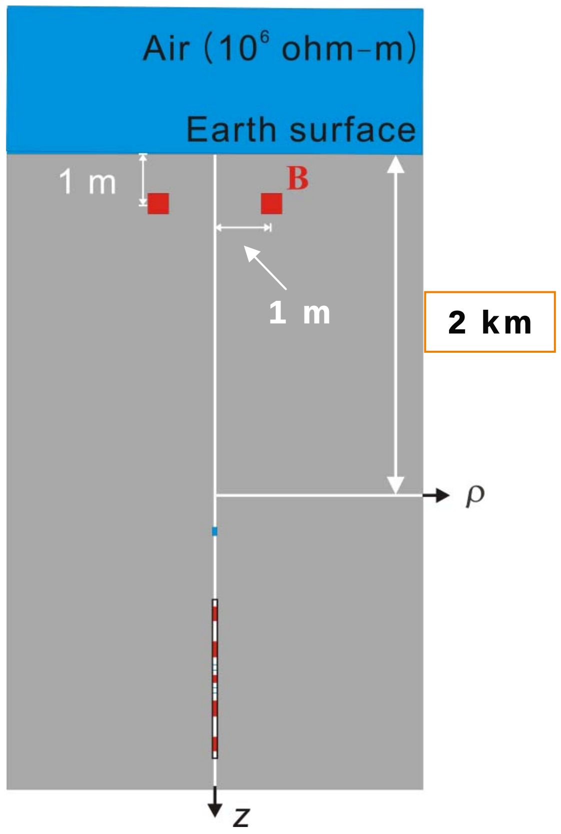

No casing with B 2 km apart:

No Groningen effects

A Middle East Formation Model

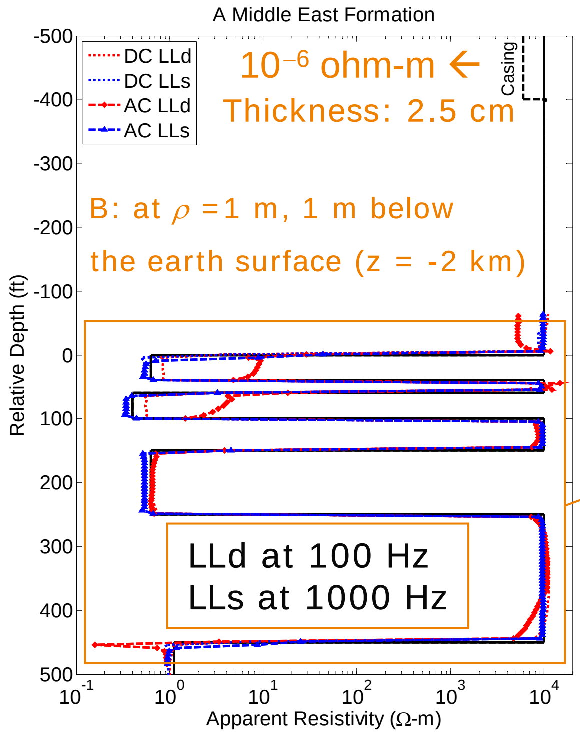

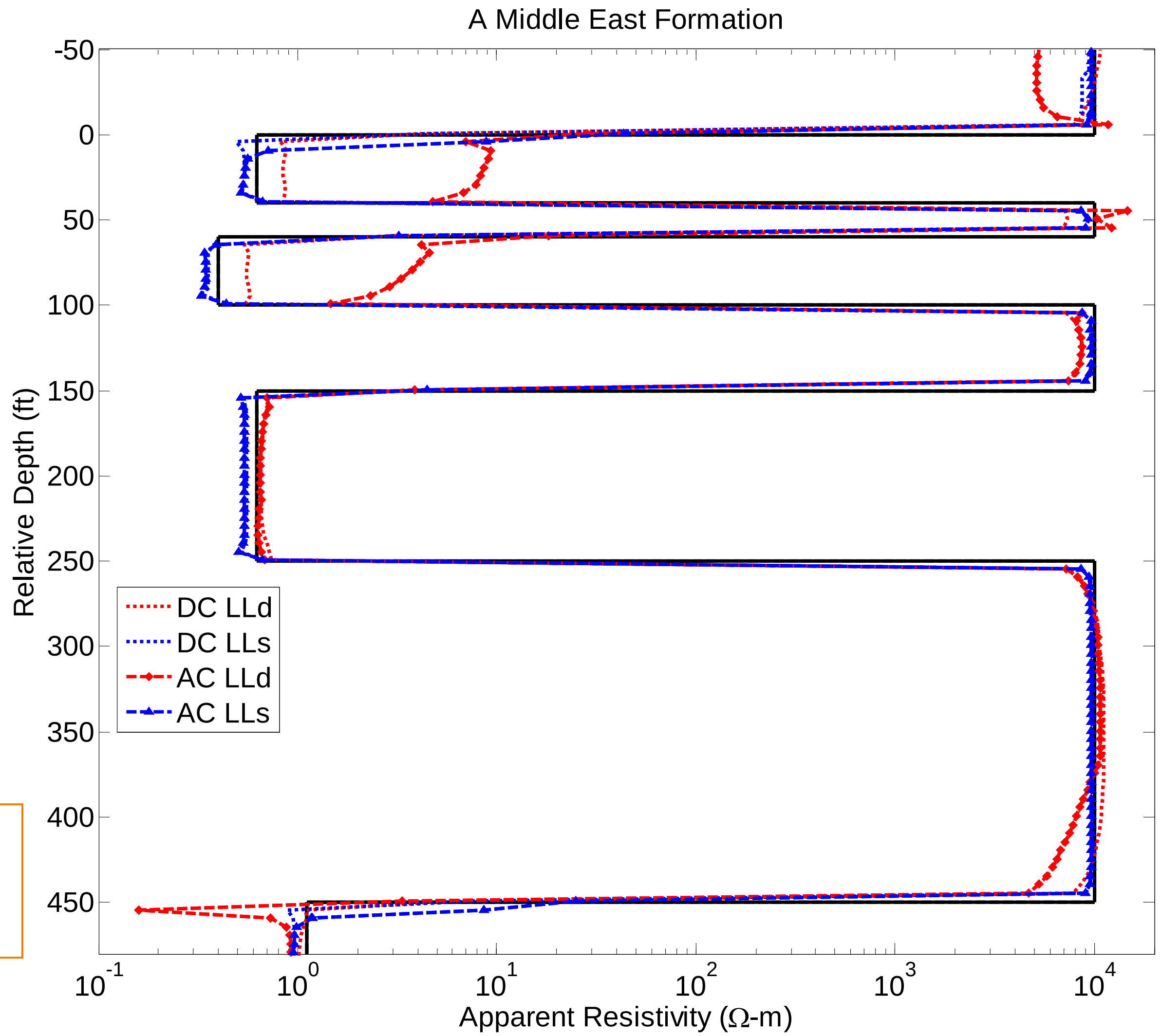

Frequency effects on AC DLL measurements

The resistivities of Layers: 10^4, 0.625, 10^4, 0.4, 10^4, and 0.625 ohm-m (from top to bottom)

Invaded Anisotropic Formation (DC DLL)

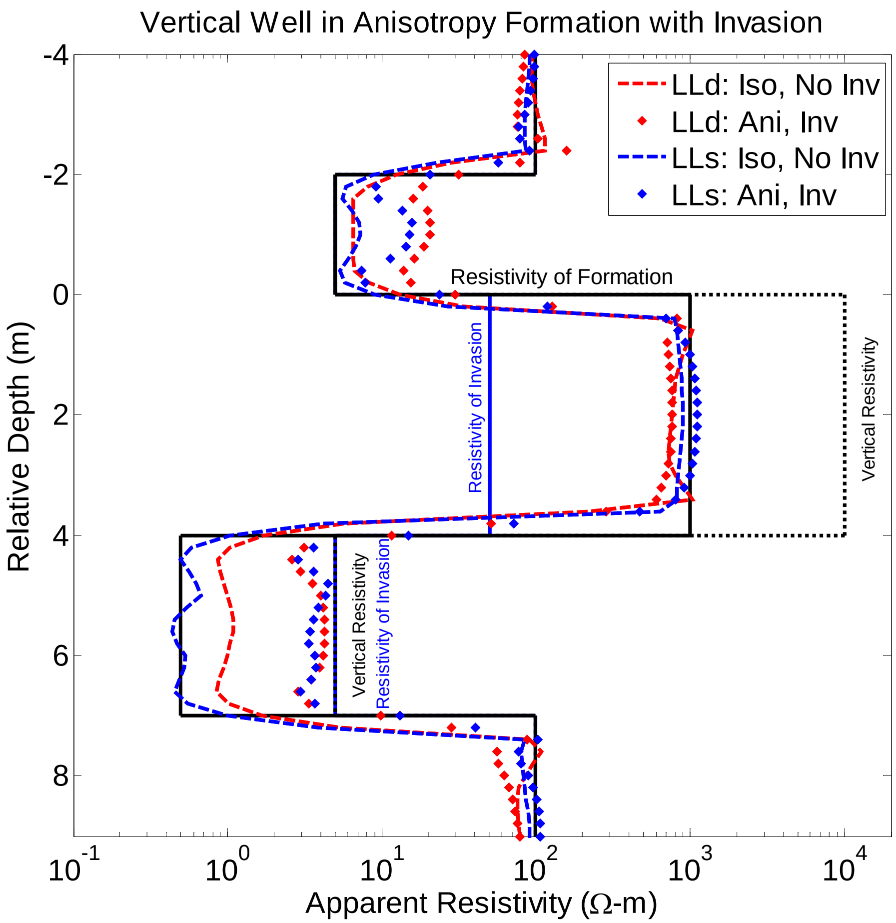

Vertical Well

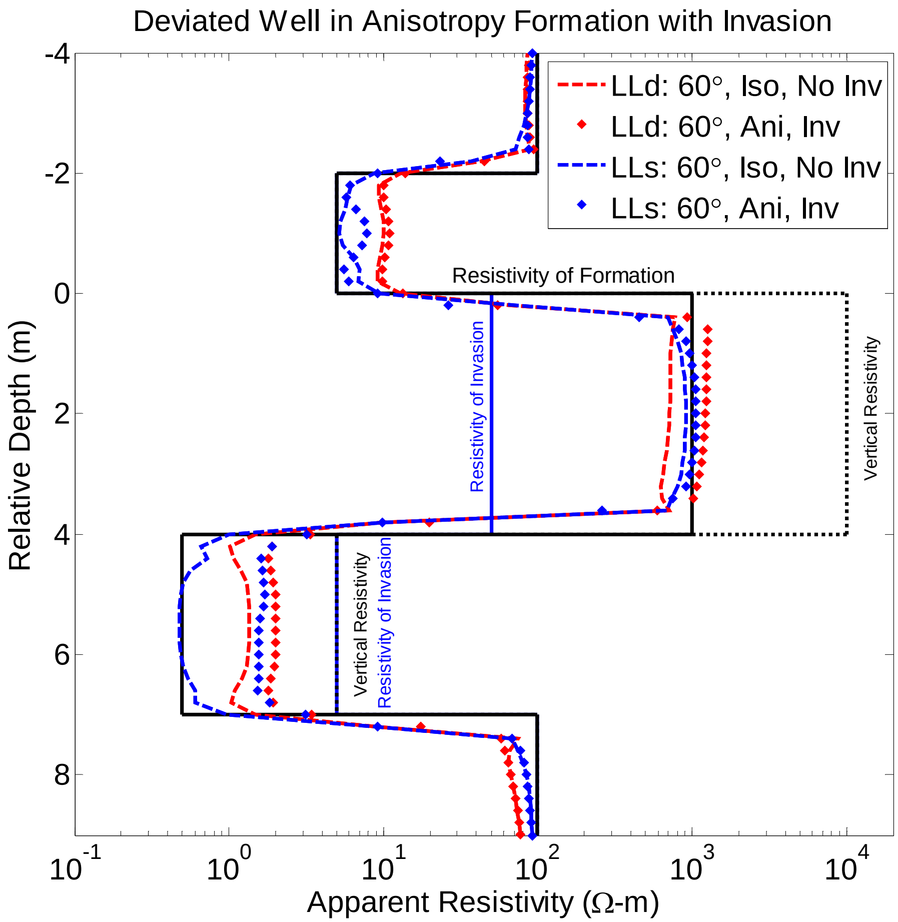

60 degree deviated Well

Eccentered Tool Effects (DC DLL)

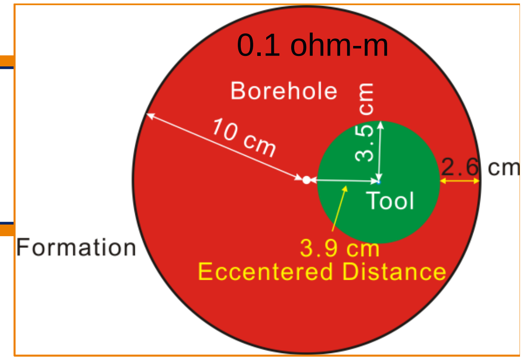

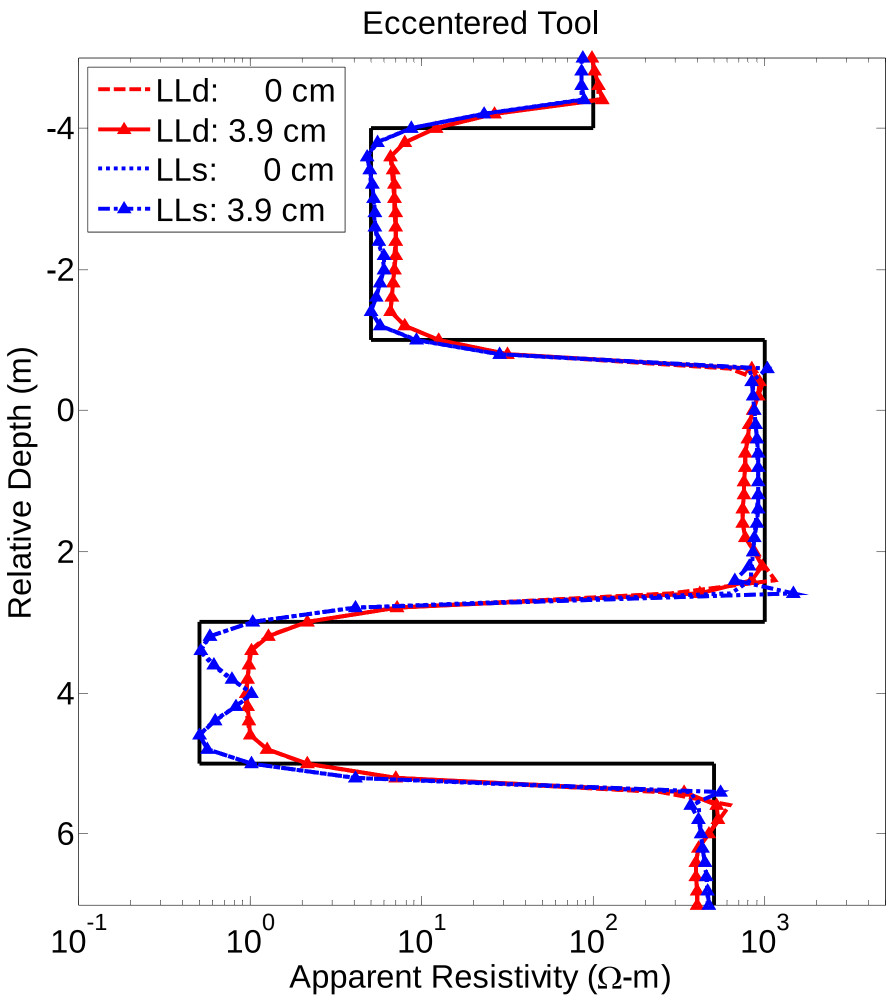

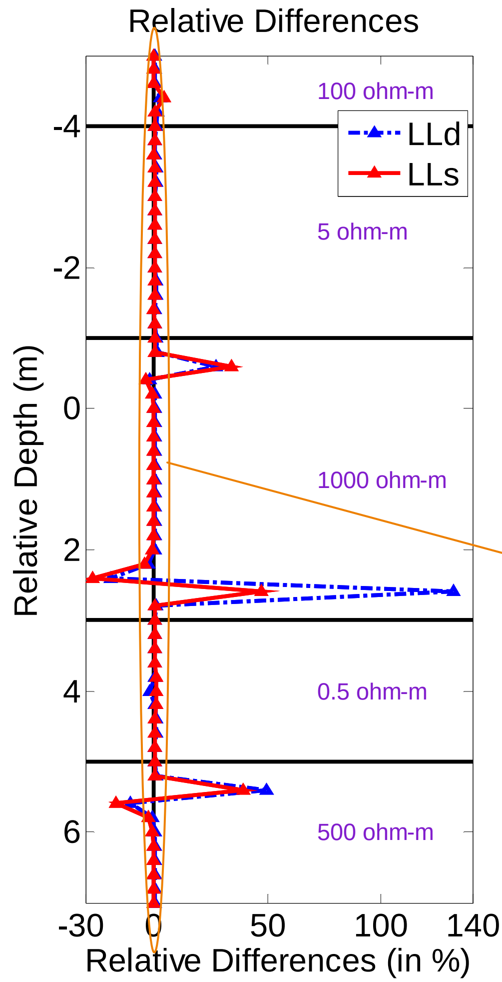

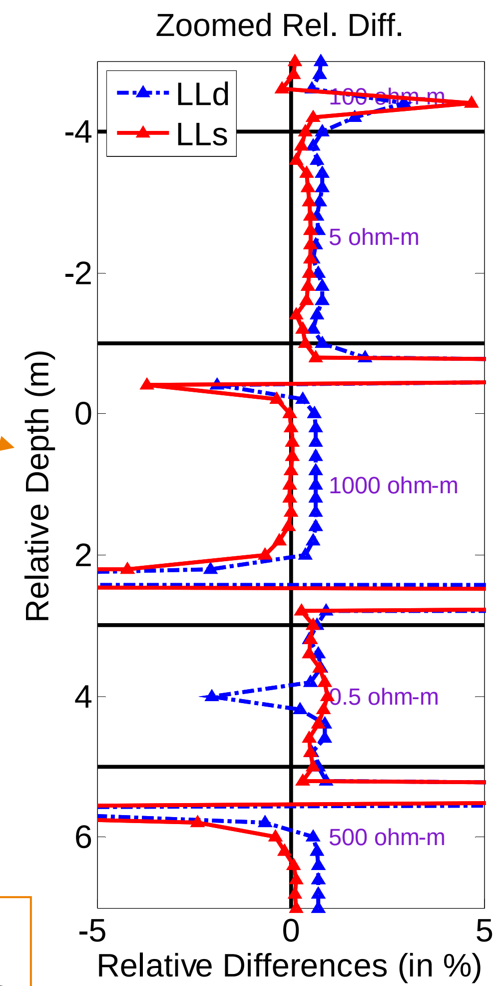

Eccentered-tool effects are larger
around layer boundaries in resistive layers

Conclusions

- We successfully simulated AC DLL measurements by explicitly incorporating the term $\nabla \cdot J$ for non-zero frequency Maxwell's equations.
- The simulation employed a high-order self-adaptive *hp* finite-element method with an embedded post-processing technique.
- Numerical experiments indicate that the inclusion of a current return electrode is critical to simulate Groningen effects.
- Groningen effects decrease as the current return is placed farther away from either the logging points or the borehole.

Acknowledgements

Sponsors of UT Austin's consortium on Formation Evaluation:

Anadarko Petroleum Corporation
ارامكو السعودية Saudi Aramco
Baker Hughes
Baker Atlas
bhpbilliton
bp
Chevron
ConocoPhillips
Agip
Eni
ExxonMobil
HALLIBURTON
IMP Innovar
INSTITUTO MEXICANO DEL PETRÓLEO
Marathon Oil Corporation
MARATHON
BR
PETROBRAS
Schlumberger
Shell
StatoilHydro
TOTAL
Weatherford